FROM GENOME SCAN TO DISEASE GENE IDENTIFICATION

by

Sibel Aylin Uğur İşeri

B.S., Molecular Biology and Genetics, Boğaziçi University, 2000

M.S., Molecular Biology and Genetics, Boğaziçi University, 2002

Submitted to the Institute for Graduate Studies in
Science and Engineering in partial fulfillment of
the requirements for the degree of
Doctor of Philosophy

Graduate Program in Molecular Biology and Genetics

Boğaziçi University

2008

ACKNOWLEDGMENTS

I would like to express my sincere gratitude to my thesis supervisor Dr. Aslı Tolun for her constructive criticism, guidance and encouragement throughout the study.

My appreciation is also extended to the members of my thesis committee, Dr. Hande Çağlayan, Dr. Arzu Çelik, Dr. Ahmet Gül and Dr. Eda Tahir Turanlı for allocating their time to evaluate this work.

I would like to thank Dr. Davut Gül for the initial blood samples, Dr. Ayşegül Bursalı for the clinical evaluation of limb malformations and Dr. Reha Tolun for interpretation of brain MRI. I thank all the families that participated in the study.

I convey my appreciation to all present and previous Kommagene laboratory members, especially Murat Çetinkaya for his help in lab work, Tarık Bozoğlu for data conversion, Nadire Duru for her great friendship and Çiğdem Köroğlu for everything. I would like to extend my thanks to all my dear friends in the department, among whom I would like to mention Birdal Bilir, Demet Candaş, İbrahim Barış, Cihan Erkut, Kader Çavuşoğlu, İnanç Fidancı, Tolga Aslan, Caroline Pirkevi, Duygu Altuntaş Dağlıkoca and Umut Dursun. My special thanks go to Ümit Bayraktar, Cenan Özbakır and Fatma Abla.

I wish to thank all of academic staff whose expertise added considerably to my graduate experience.

I have great pleasure in thanking my family for the support they provided through my entire life and in particular, I must acknowledge my husband and best friend, Alper, for his encouragement and critical assistance.

I gratefully acknowledge the genome scan performed by NHLBI Mammalian Genotyping Service (Contract Number HV48141). This work was supported by the State Planning Organization (97K120660). I was a fellow of the Scientific and Technological Research Council of Turkey from 2002 to 2006.

dedicated to my wise grandmother Alis

ABSTRACT

FROM GENOME SCAN TO DISEASE GENE IDENTIFICATION

Genetic linkage analysis is used to identify regions in the genome that contain genes associated with a particular disease. By genotyping with markers and observing allele segregation with the disease in families, it is possible to map disease loci. Advances in genotyping techniques together with the availability of densely spaced marker maps have facilitated such studies. Results of genetic linkage studies are statistically evaluated with lod score analysis by using computer programs developed for this purpose. In the framework of this study, genome wide linkage scans performed at the NHLBI Mammalian Genotyping service were evaluated with parametric linkage programs for the following five inherited disorders and suggestive loci were subsequently investigated with fine-mapping studies and candidate gene approach.

Split-Hand/Foot Malformation (SHFM) is a complex limb malformation affecting the central rays of the autopod. Twelve affected members of a consanguineous kindred had central feet reductions with or without hand involvement while the remaining one had the mildest phenotype and atypical SHFM. We identified a novel SHFM locus at 12q13.11-q13 and by subsequent candidate gene approach a homozygous missense *WNT10b* mutation (p.R332W) in all affected individuals but the atypical case plus in an asymptomatic female. We propose that either a second locus contributes to the manifestation of SHFM phenotype or a suppressor locus prevented trait manifestation in the non-penetrant female. This is the first reported *WNT10b* mutation on the pathogenesis of limb development and recessive mutation in SHFM.

Hypomyelination and congenital cataract (HCC) is a recently reported autosomal recessive white matter disorder characterized by hypomyelination of the central and peripheral nervous systems, progressive neurological impairment and congenital cataract and caused by mutations in gene *DRCTNNB1A*. Here we report a large intragenic deletion that does not lead to congenital cataract in all of the patients in an afflicted family.

A novel form of nonsyndromic autosomal recessive cone rod dystrophy was mapped to chromosome 17p13.2-p13.1 in a consanguineous kindred with six affected individuals, and the disease gene was identified as *GUCY2D* encoding the retinal guanylyl cyclase gene. The mutation (p.I949T) resided in the catalytic domain of the protein where other mutations had previously been associated with Leber congenital amaurosis, a common cause of childhood blindness. The milder phenotype observed in our patients implicate that either the mutation does not disturb the catalytic activity completely or modifier locus/loci interfere with the phenotype.

Lastly, an autosomal recessive form of *mental retardation* associated with hypertension and an autosomal dominant *arthrogryposis syndrome* Pseudoarthrogryposis-like Syndrome were mapped to chromosomes 7q21.3-q31.1 and 13q31.3-q32.1, respectively.

ÖZET

GENOM TARAMASINDAN HASTALIK GENİ TANIMLANMASINA

Genetik bağlantı analizi, genomda belirli bir hastalıkla ilişkilenen genleri içeren bölgeleri tespit etmek için kullanılır. Genetik belirteçlerle yapılan genotiplendirme ve aile içinde alel dağılımının hastalıkla takip edilmesi, hastalık bölgesinin haritalanmasına olanak sağlar. Son yıllarda genotiplendirme tekniklerinde yaşanan gelişmeler ve yoğun belirteç haritalarının varlığı bu tarz çalışmaların önünü açmıştır. Genetik bağlantı çalışmalarından elde edilen sonuçların istatistiksel değerlendirmesi bilgisayar destekli lod skor analizi ile yapılmaktadır. Bu çalışmada, aşağıda ismi geçen beş kalıtımsal hastalığın NHLBI Genotiplendirme Servisinde genom ölçeğinde gerçekleştirilmiş olan tarama sonuçları kullanılmıştır. Bu sonuçlar parametrik bağlantı programları ile değerlendirilmiş, anlamlı bölgeler ayrıntılı olarak haritalanarak aday gen incelemeleri yapılmıştır.

Yarık-El/Ayak Yapısal Bozukluğu (SHFM), el ve ayakların merkezi uzantılarını etkileyen karmaşık bir gelişimsel bozukluktur. İncelediğimiz ailede tümü akraba evliliği sonucu doğmuş olan bireylerin 12'sinde yapısal ayak bozukluğu gözlenmiş, bunların bazılarında bu duruma el bozukluğu da eşlik etmiştir. Bir tek bireyde ise fenotip en hafif şekilde atipik SHFM olarak izlenmiştir. Yaptığımız bağlantı analizi sonucunda bu bozukluktan etkilenen 12 birey ile 1 asemptomatik bireyde kromozom 12q13.11-q13'te ortak yeni bir SHFM bölgesi tanımladık. Daha sonra aday gen çalışması ile *WNT10b* geninde homozigot olarak seyreden p.R332W mutasyonunu bulduk. Atipik birey ise bu mutasyonu taşımıyordu. SHFM fenotipinin ortaya çıkmasında ikinci bir bölgenin katkıda bulunduğunu veya baskılayıcı bir gen varyantın asemptomatik bireyde hastalığın ortaya çıkmasını engellediğini düşünmekteyiz. Bu çalışmamız *WNT10b* gen mutasyonunun el ve ayak gelişimini etkilediğini ve SHFM fenotipinin çekinik bir mutasyonla ilişkilendirilebileceğini gösteren ilk çalışma olarak kaydedilmiştir.

Hipomiyelinizasyon ve Konjenital Katarakt (HCC), yeni bildirilmiş otozomal çekinik geçişli bir beyaz madde hastalığıdır. Hastalığın ayırıcı özellikleri merkezi ve çevresel sinir

sisteminde hipomiyelinizasyon, ilerleyici nörolojik hasar ve konjenital katarakt olarak sıralanır. Bu hastalığa *DRCTNNB1A* genindeki mutasyonların yol açtığı çalışmamız sürerken bildirildi. Çalışmamız kapsamında bulduğumuz bu gen içindeki büyük bir delesyonun ailedeki HCC hastalarının hepsinde katarakta neden olmadığını gösterdik.

Koni ve Çubuk Distrofisi hastalığının non-sendromik ve otozomal çekinik geçişli bir çeşidini çalıştık. Çalışmamızda bu hastalık altı hasta bireyi olan akraba evliliği yapmış bir ailede kromozom 17p13.2-p13.1'e haritalandı ve hastalık geninin retinaya özel Guanil Siklazı üreten *GUCY2D* geni olduğu gösterildi. Mutasyonun bulunduğu protein katalitik bölgesinde daha önce tanımlanan mutasyonlar çocukluk körlüğünün yaygın bir nedeni olan Leber'in konjenital amorozisi ile ilişkilendirilmişti. Çalıştığımız hastalarda gözlemlenen nispeten hafif fenotip, mutasyonun katalitik aktiviteyi tam olarak durdurmadığına veya fenotipin başka bölgeler tarafından da etkilendiğine işaret etmektedir.

Son olarak, hipertansiyonla seyreden otozomal çekinik gecişli bir *zeka geriliği* türü ile otozomal dominant bir *artrogriposis sendromu* sırasıyla kromozom 7q21.3-q31.1 ve 13q31.3-q32.1'ye haritalandı.

TABLE OF CONTENTS

LIST OF FIGURES

LIST OF TABLES

LIST OF SYMBOLS / ABBREVIATIONS

A	Adenine
C	Cytosine
G	Guanine
I	Isoleucine
R	Arginine
T	Thymine
W	Tryptophan
Z_{max}	Maximum Two-Point Lod Score
ΔNp63	N-Terminal-Truncated p63 Isotype
θ_{MLE}	Maximum Likelihood Estimate for Recombination Fraction (θ)
AD	Autosomal Dominant
AER	Apical Ectodermal Ridge
A-P	Antero-Posterior
AR	Autosomal Recessive
BMP	Bone Morphogenetic Protein
bp	Base Pair
cAMP	Cyclic Adenosine Monophosphate
CC2D1A	Coiled-Coil and C2 Domain Containing 1A
cGMP	Cyclic Guanosine Monophosphate
cM	Centi Morgan
CORD	Cone Rod Dystrophy
CRBN	Cerebron
CYCS	Cytochrome c
d.p.c.	Days Post Coitum
Dac	Dactylaplasia
DNA	Deoxyribonucleic Acid
DRCTNNB1A	Down-Regulated By B-Catenin, 1a

D-V	Dorso-Ventral
EDTA	Ethylenediaminetetraacetate
EEC	Ectrodactyly, Ectodermal Dysplasia, and Facial Cleft
EN1	Engrailed 1
ERG	Electroretinogram
FGF	Fibroblast Growth Factor
GRIK2	Glutamate Receptor, Ionotropic, Kainate 2
GUCY2D	Guanylate Cyclase 2D
GTP	Guanosine Triphosphate
HCC	Hypomyelination and Congenital Cataract
HIBADH	3-Hydroxyisobutyrate Dehydrogenase
HPRT1	Hypoxanthine Phosphoribosyltransferase 1
IBD	Identical by Descent
IQ	Intelligence Quotient
kb	Kilobase
LCA	Leber Congenital Amaurosis
Lod	Log of Odds
LRP	Low Density Lipoprotein Receptor-Related Protein
Mb	Mega Base
min	Minute
MLE	Maximum Likelihood Estimate
MLS	Maximum Lod Score
MR	Mental Retardation
MR-HT	Mental Retardation Associated With Hypertension
mRNA	Messenger Ribonucleic Acid
NA	Not Available
NCBI	National Center For Biotechnology Information
NHLBI	National Heart, Lung and Blood Institute
NS-ARMR	Nonsyndromic Autosomal Recessive Mental Retardation
p53	Tumor Protein 53
p63	Tumor Protein 63
PAG-L	Pseudoarthrogryposis-Like Syndrome
PAR1	Pseudoatosomal Region 1

PCR	Polymerase Chain Reaction
pLOD	Parametric Lod Score
Pr-D	Proximo-Distal
PRSS12	Protease, Serine, 12
PZ	Progress Zone
qRT-PCR	Quantitative Reverse Transcriptase-Polymerase Chain Reaction
retGC	Retinal Guanylate Cyclase
RPE	Retinal Pigmented Epithelium
Rpm	Revolution Per Minute
RT-PCR	Reverse Transcriptase-Polymerase Chain Reaction
SCAFUD	Scanning Fluorescence Detector
SDS	Sodium Dodecyl Sulphate
SHFM	Split-Hand/Foot Malformation
SHH	Sonic Hedgehog
SNP	Single Nucleotide Polymorphism
SSCP	Single Strand Conformational Polymorphism
TEMED	N, N, N, N'-Tetramethylethylenediamine
TP63	Tumor Protein 63, Gene
U	Unit
UTR	Untranslated Region
UV	Ultraviolet
WNT	Wingless-Type MMTV Integration Site Family Member
XLMR	X-Linked Mental Retardation
X-R	X-Recessive
ZPA	Zone Of Polarizing Activity

1. INTRODUCTION

In the context of this thesis, molecular studies were conducted with the purpose of mapping and subsequently identifying causative genes in four autosomal recessive disorders, namely, Split-Hand/Foot Malformation, Hypomyelination and Congenital Cataract, Cone Rod Dystrophy and Mental Retardation associated with Hypertension, and in one autosomal dominant disorder, namely, Pseudoarthrogryposis-like Syndrome. Causative genes for all were mapped and three of them identified.

1.1. Split-Hand/Foot Malformation (SHFM)

Split-Hand/Foot Malformation (SHFM) or ectrodactyly (from Greek "ektroma" meaning "abortion" and "daktylos" meaning "finger") is a limb malformation involving the central rays of the autopod (hand/foot). It presents with syndactyly, median clefts of the hands and feet, and aplasia and/or hypoplasia of the phalanges, metacarpals, and metatarsals.

SHFM is either sporadic or familial. When familial, the most common mode of inheritance is autosomal dominant with reduced penetrance, and variable expressivity and segregation distortion with excessive transmission from affected males to sons is a common feature. X-linked inheritance in a single family (Ahmad *et al.*, 1987) and rare autosomal-recessive inheritance (Zlotogora and Nubani, 1989; Gül and Öktenli, 2002) have also been reported. Linkage mapping and/or cytogenetic studies have shown that SHFM is genetically heterogenous. Four autosomal loci have been mapped, all with dominant inheritance: 7q21-22 (SHFM1; Scherer *et al.*, 1994), 10q24 (SHFM3; Roscioli *et al.*, 2004), 3q27 (SHFM4; Ianakiev *et al.*, 2000), and 2q31 (SHFM5; Goodman *et al.*, 2002). Also, for the single X-linked family, a locus with semi-recessive effect at Xq26 has been reported (SHFM2; Faiyaz ul Haque *et al.*, 1993). The gene responsible has been identified only in SHFM4, as *TP63* (Ianakiev *et al.*, 2000), encoding a homologue of the tumor suppressor p53. Despite the homology, p63 plays a key role in embryonic development, rather than tumor suppression. Additionally, genomic rearrangements characterized in SHFM1, SHFM3 and SHFM5 cases have led to identification of candidate

genes (Table 1.1, reviewed in Basel *et al.*, 2006). In general, genomic deletions in SHFM1 and SHFM5 and genomic duplications in SHFM3 possibly resulting in haploinsufficiency and/or overexpression of certain genes have been proposed to underlie the pathogenesis of these loci.

Table 1.1. Candidate genes in human loci mapped for SHFM

Designation	MIM	Locus	Candidate Genes
Autosomal Dominant SHFM			
SHFM1	103600	7q21	*DLX5, DLX6,DSS1*
SHFM3	600095	10q24	*DAC, FGF8, SUFU, BTRC*
SHFM4	605289	3q27	***TP63*** (causative gene)
SHFM5	606708	2q31	*DLX1, DLX2*
X-linked SHFM			
SHFM2	606708	Xq26	*FGF13, VGLL1*

Gene name	Encoded Protein and Potential Function
BTRC (**b**eta-**t**ransducin **r**epeat **c**ontaining)	F-box/WD40 adaptor protein involved in ubiquitination Machinery
DAC (**dac**tylin)	F-box/WD40 adaptor protein involved in ubiquitination Machinery
DLX (**d**istal-**l**ess homeobo**x**)	Homeobox-containing protein involved in forebrain and craniofacial development
DSS (**d**osage-**s**ensitive **s**ex reversal)	Proposed to function in ovarian development
FGF (**f**ibroblast **g**rowth **f**actor)	Growth factor involved in a variety of biological processes, including embryonic development, cell growth, morphogenesis, tissue repair, tumor growth and invasion
SUFU (**su**ppressor of **fu**sed homolog)	Component of sonic hedgehog (SHH)/patched (PTCH) signaling pathway
TP63 (**t**umor **p**rotein 63)	p53 homologue involved in embryonic development
VGLL1 (**v**esti**g**ia**l** **l**ike 1)	Specific coactivator for the mammalian transcription factor thyrotrophic embryonic factor (TEF)

1.1.1. Phenotypic features

The severity of SHFM phenotype is highly variable, grading from syndactyly in mildly affected patients to lobster claw-like appearance of the autopod in severe cases. Basically, the core SHFM phenotype is categorized in three distinct classes: (1) Monodactyly, (2) Bidactyly in which two digital elements are present with a median cleft, as in lobster-claw appearance, and (3) Oligodactyly (most common form) in which three or more digits are present and associated with syndactyly and median cleft. The noncore phenotypic features include clinodactyly, campodactyly, triphalangeal thumb and ulnar

deviation (Basel *et al.*, 2006). Elliott *et al.*, 2005 performed a literature review of 153 SHFM cases and suggested that preaxial involvement in the hands is a strong locus discriminator for SHFM3. They also hypothesized that a differential developmental pattern exists between hands and feet, as the feet of SHFM3 patients generally have central longitudinal deficiency without a preaxial component.

1.1.2. The Developing Limb

Limb development relies on interplay of spatially and temporally controlled processes of cellular differentiation, pattern formation, and tissue morphogenesis. Most common human congenital anomalies include limb defects, since mutations and teratogens can cause severe malformations on the structure of the limb morphology without affecting survival and reproduction. This has led to a wide-ranging set of limb variations throughout the human population.

Vertebrate limb development is in three phases: limb bud initiation, early limb patterning, and late limb morphogenesis (Yang, 2003). In the limb bud initiation phase, the limb protrudes from the flank of embryo from the lateral plate mesoderm as a small bud that consists of morphologically homogenous mesenchyme cells covered by a layer of ectoderm (Niswander, 2003). In humans, limb buds appear on day 26-28 for arms and 2 days later for legs (Manouvrier-Hanu *et al.*, 1999). In the early patterning phase, proper modeling of the limb bud is coordinated by both spatial and temporal expression of a variety of signaling molecules and transcription factors including fibroblast growth factors (FGFs), bone morphogenetic proteins (BMPs), WNT and hedgehog signaling molecules, and homeobox proteins (Figure 1.1, Tickle, 2006). At the apex of the limb bud, ectodermal cells differentiate into apical ectodermal ridge (AER) by inductive signals originating from the underlying mesenchyme. AER expresses and secretes FGFs to the sub-adjacent mesenchyme -the progress zone (PZ)- in order to keep those cells undifferentiated and proliferating. Interplay between AER and PZ determines the proximo-distal polarity (Pr-D, shoulder-finger) of the limb. FGF signaling from AER also maintains sonic hedgehog (SHH) expression from zone of polarizing activity (ZPA, also known as polarizing region) at the posterior mesenchyme, which controls antero-posterior polarity (A-P, thumb-little finger) (Ingham and Placzek, 2006). Retinoic acid is likely to play a key role in the

induction of ZPA. Dorso-ventral polarity (D-V, back-palm) is maintained by the non-AER ectoderm signaling: BMPs and Engrailed 1 from the ventral ectoderm and WNT7a from the dorsal ectoderm. In the late limb morphogenesis phase, the limb matures into a functional organ as the skeletal elements, muscles, tendons, vessels etc., emerge.

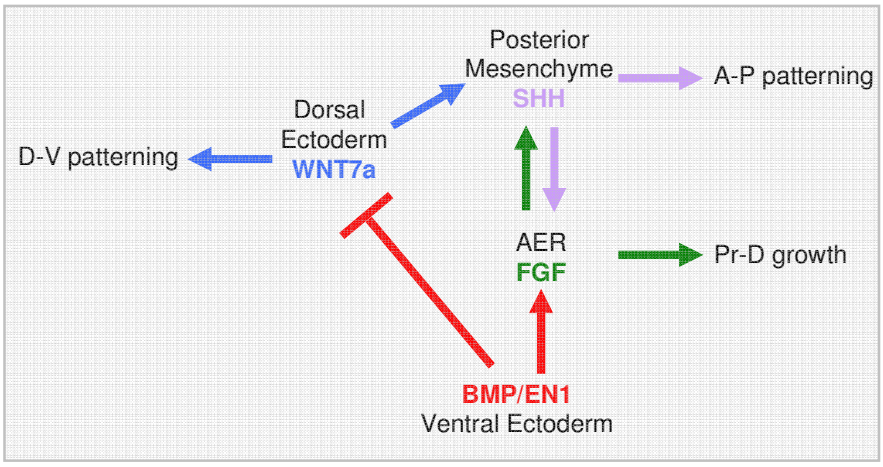

Figure 1.1. Molecular interactions that govern the early limb patterning phase along the three limb axes. Pr–D axis is under the control of FGFs (green) from AER, the A–P axis is under the control of SHH (purple) from the posterior mesenchyme, and the D–V axis is under the control of BMPs and EN1 (both in red) from the ventral ectoderm and WNT7a (blue) from the dorsal ectoderm (modified from Niswander, 2003).

The skeletons of vertebrate limbs consist of three basic elements: stylopod (upper arm or thigh), zeugopod (forearm or shank), and autopod (hand or foot) (Figure 1.2). This segmentation is coordinated in a Pr-D fashion: the mesenchymal cells exiting from the PZ initiate formation of limb elements fated to be closest to the body followed successively by ones furthest from the body. In this sense, the stylopod is patterned first, followed by the zeugopod and finally the autopod, digits being the last specified structures. The Pr-D positional information of the mesenchymal cells has been proposed to be determined by the length of time cells spend in the PZ under the influence of signals derived from the AER and ZPA (Progress zone model, Figure 1.3, a). More recently, Dudley *et al.*, 2002 propose that all Pr–D fates are specified within the early limb bud (Figure 1.3, b). Mesenchymal cells at their final destination condense and enter the chondrocyte differentiation pathway to form the cartilage elements. An endochondral ossification process replaces the cartilage elements with bone.

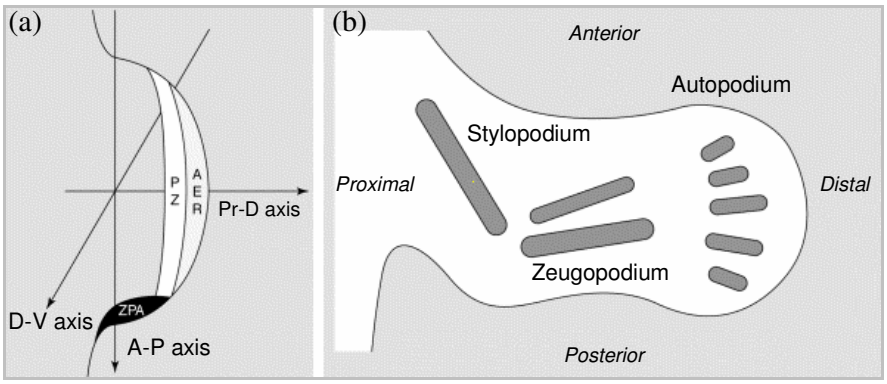

Figure 1.2. Spatial directions of development in the limb. (a), and three basic elements of the limb skeleton (b) (modified from Manouvrier-Hanu *et al.*, 1999).

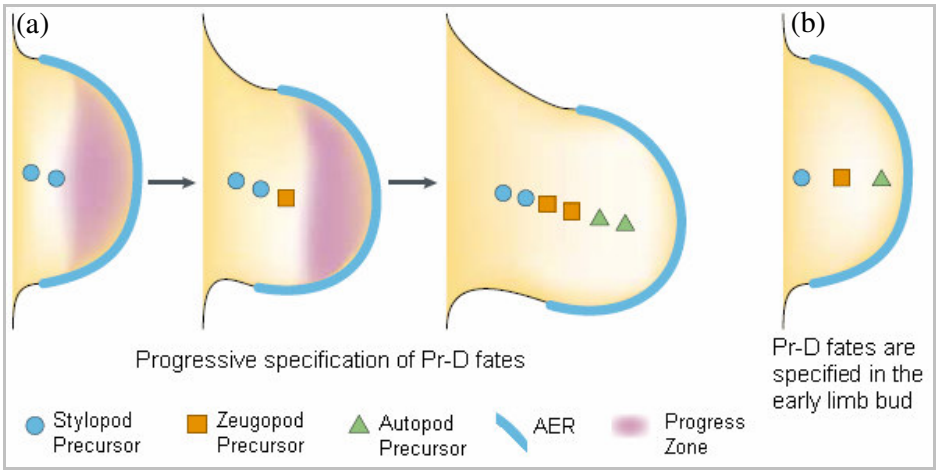

Figure 1.3. Schematic comparison of progress zone (a), and early limb bud (b) models in the Pr–D limb patterning (modified from Niswander, 2003)

The digits at the tip of limb development are established along the A-P axis and separated eventually by interdigital spaces. Initially in the autopod, the regions that will progress into condensations (digital rays) or interdigital tissue are defined. The direction of condensations is common in most organisms: it starts from the most posterior digit followed by a posterior to anterior progression. It is an important developmental phenomenon, since these two regions will determine the differential fate of cells; condensations will progress into cartilage, while cells in the interdigital tissue will be removed by apoptosis. Mesenchymal apoptosis at the interdigital tissue allows separation of digits on about day 51-53 in humans (Manouvrier-Hanu *et al.*, 1999). If this process fails, syndactyly occurs, most probably due to defects in BMP signaling. It has been shown

that blocking BMP signaling in chicken embryonic hind limbs resulted in a webbed feet phenotype. Interestingly, BMPs are shown not to be expressed in the duck interdigit, which has naturally occurring webbed feet (Zou and Niswander, 1996). The variable developmental mechanisms leading to differential fates in fore and hindlimbs have maybe best implicated in bats. It has been reported that bat forelimb and hindlimb interdigital tissues express BMP signaling components, but that only bat hindlimbs undergo interdigital apoptosis. Expression of *Fgf8* together with BMP inhibitor *gremlin* accompanies maintenance of interdigital webbing in the bat forelimb (Weatherbee *et al.*, 2006).

An AER driven model for segmentation within a digit is shown in Figure 1.4. AER has both activator and inhibitor roles: it promotes the growth of the digital ray in the distal direction by FGF signaling while inhibiting joint formation distally, and its presence holds back tip formation. A joint can only be formed when cells escape both this inhibition and the one exerted by the previously formed proximal joint. Once both inhibitions are overcome, joint markers are expressed, probably induced by Wnt14. Upon ceasing of FGF signaling from the AER, the final joint is formed in the distal region, and the molecular program to establish the last phalange or the tip is induced (Casanova and Sanz-Ezquerro, 2007).

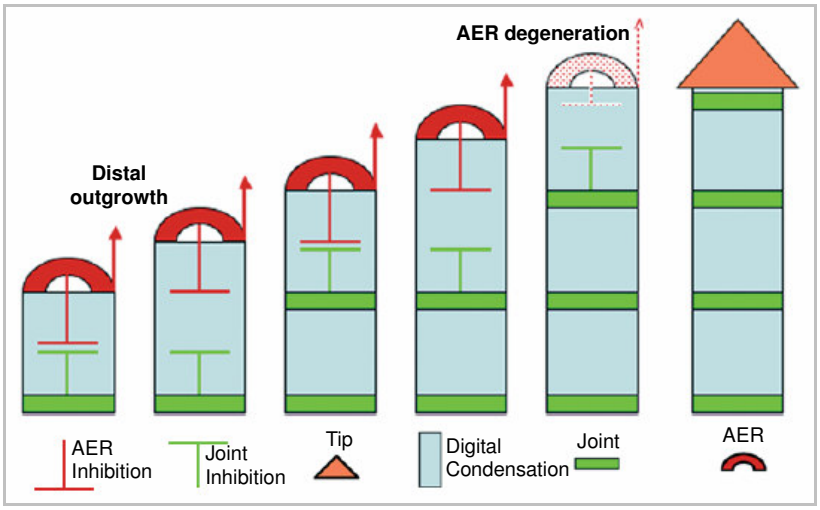

Figure 1.4. Model for growth and segmentation in digits (modified from Casanova and Sanz-Ezquerro, 2007)

1.1.3. Genetic Modifiers in SHFM

SHFM occurs in one in 8,500-25,000 newborns and accounts for 10-17 per cent of all limb reduction defects (Calzolari *et al.*, 1990). The condition is clinically heterogeneous; it may occur either as an isolated entity (non-syndromic SHFM) or part of a syndrome (syndromic SHFM). More than 50 syndromes and associations for syndromic SHFM have been identified (Duijf *et al.*, 2003), which could have resulted from either single gene defects or chromosomal rearrangements involving two or more genes. The best known example for the former case is *TP63* gene. Different *TP63* mutations are found to be associated with one non-syndomic (Ianakiev *et al.*, 2000) and four syndromic SHFM disorders (Celli *et al.*, 1999; Bokhoven *et al.*, 2001). Two mutations at the same residue are of particular interest: p.R280C and p.R280H give rise to either EEC (**e**ctrodactyly, **e**ctodermal dysplasia, and facial **c**left) syndrome or to non-syndromic SHFM (SHFM4). The situation is even further complicated by the reduced penetrance of mutations at residue p.R280 in SHFM4 patients. These observations suggest the involvement of other genes in the pathogenesis of SHFM.

The role of genetic modifiers is also implicated in the semidominant mouse mutant *Dactylaplasia* (Chai, 1981). Heterozygous animals display an isolated limb defect characterized by missing phlanges in the central digits, and homozygous animals are characterized by monodactyly. The dactylaplasia phenotype depends not only on the genotype at the mutated locus, *Dac*, but also on homozygosity at another unlinked locus, *mdac* (**m**odifier of **dac**), that is polymorphic among inbred strains (Chai, 1981; Johnson *et al.*, 1995). *Dac*/+ and *Dac/Dac* mice display the phenotype only if they are also homozygous for a particular permissive allele at mdac locus (*mdac/mdac*) - if they are *Mdac/Mdac* or *Mdac/mdac*, their limbs are normal. The *Dactylaplasia* mouse is a model for human SHFM3. SHFM3 locus at 10q24 is syntenic to mouse chromosome 19 where the mouse *Dac* locus has been mapped (Johnson *et al.*, 1995) and mutations in mouse dactylin gene was identified (Sidow *et al.*, 1999). *Mdac*, which modulates the expression level of dactylin, resides on mouse chromosome 13 in an area syntenic to human chromosome 5q.

1.1.4. Pathogenesis of SHFM

Pathogenesis of SHFM has been attributed to defects in maintenance of median AER activity (Figure 1.5, a) in studies with *Dac* mice. The primary *Dac* phenotype has shown to be a failure to maintain cell proliferation in the anterior and central AER with abnormally low levels of fgf4, fgf8, bmp2, and bmp4, which eliminates the AER prematurely (Crackower *et al.*, 1998). Sidow *et al.*, 1999 proposed the existence of a suppressor, which would be degraded by dac to allow an appropriate level of cell proliferation in the AER. The structure of dactylin suggests it as a member of the F-Box/WD40 family of proteins, which recruit specific target proteins through their WD-40 protein-protein binding domains for ubiquitin mediated degradation. In *Dac* mice this suppressor would not be degraded and cell proliferation would weaken, thus shifting the balance between cell proliferation and cell death, resulting in the premature elimination of the AER (Sidow *et al.*, 1999).

Genetic as well as environmental factors may cause this condition by interfering with AER. *TP63* was shown to be highly expressed in AER (Yang *et al.*, 1999; Yasue *et al.*, 2001). Proteins encoded by candidate SHFM genes (Table 1.1) implicated in signaling pathways in developing limb are shown in (Figure 1.5, b).

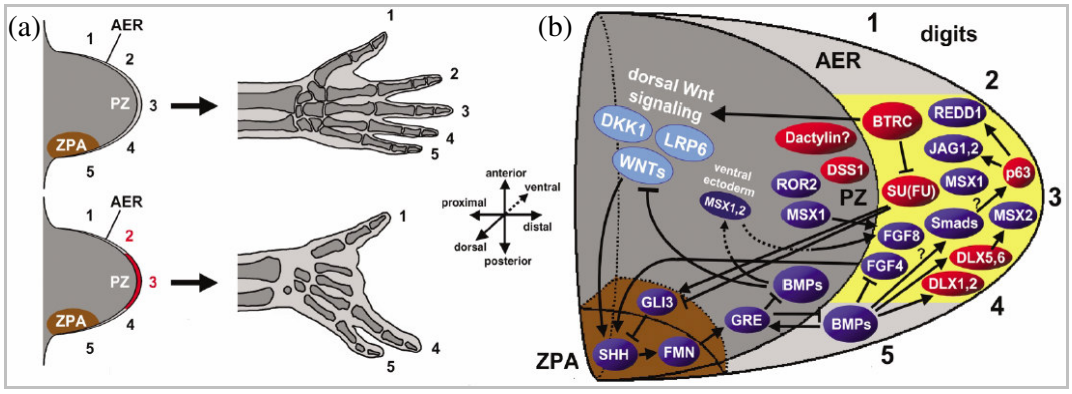

Figure 1.5. Pathogenesis of SHFM and signaling pathways implicated in SHFM. (a) Normal development of the autopod (top) and oligodactylic SHFM (bottom). Defects in median AER activity (red) lead to an absence of the central rays (right). (b) Positions of AER (light grey and yellow), PZ (dark grey), and ZPA (brown) are indicated. Numbers 1-5 refer to the future positions of digits 1-5. Proteins encoded by the candidate genes on Table 1.2 are highlighted here in red. Dorsally and ventrally expressed proteins are represented in lighter and darker blue, respectively (modified from Duijf *et al.*, 2003).

1.1.5. WNT Signaling

WNT signaling plays a role in vertebrate limb development (reviewed in Yang, 2003). WNTs are secreted glycoproteins that are implicated in cell fate determination and cell growth, acting as short-range ligands in a variety of signaling pathways. Among those pathways, canonical Wnt/β-catenin is the best defined. Upon WNT binding to cell surface receptor Frizzled and co-receptor LRP5/6, cytoplasmic β-catenin is stabilized, which then enters the nucleus and forms a transcriptional complex with TCF/LEF DNA binding proteins in order to induce the expression of downstream target genes (Miller *et al.*, 1999). β-catenin independent noncanonical Wnt pathway signals through activating Ca^{2+} flux, JNK activation, and both small and heterotrimeric G proteins, and induces changes in gene expression, cell adhesion, migration, and polarity. The noncanonical Wnt pathways also require Frizzled as receptor, but the coreceptor is the proteoglycan protein Knypek (Kikuchi *et al.*, 2007). Canonical and noncanonical Wnt pathways are summarized in Figure 1.6.

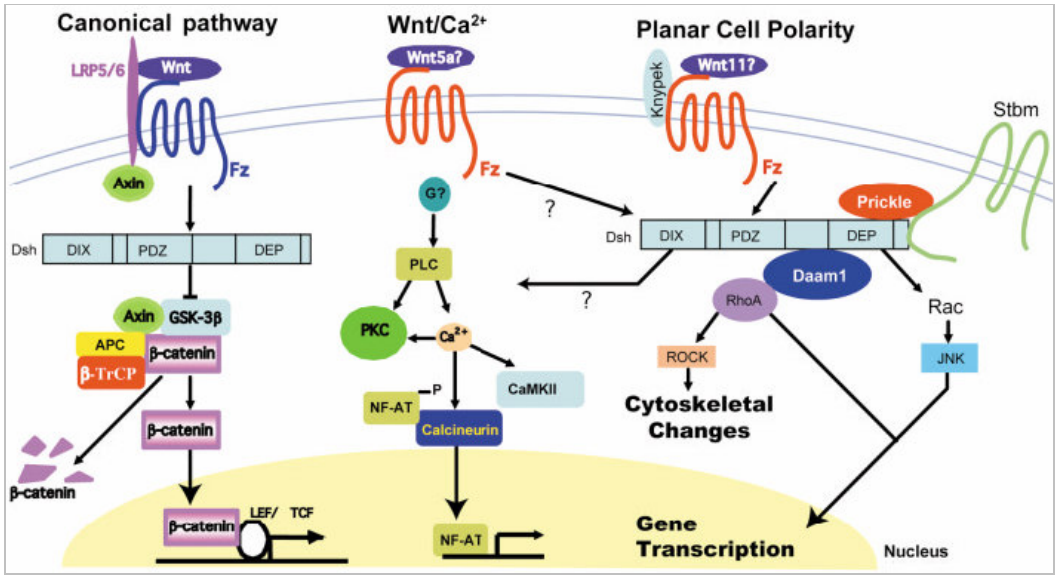

Figure 1.6. Three intracellular signaling pathways activated by Wnt proteins (modified from Yang, 2003)

WNTs are found throughout the animal kingdom, and 19 mammalian homologues several of which encode additional alternatively spliced isoforms have been identified (The WNT homepage). WNTs contain a highly conserved distribution of cysteines. It has been

difficult to purify and biochemically characterize WNTs, even though they are secreted proteins. Currently, only Wnt-3a and Wnt-5a could be purified from cultured cells in active form as tested for their ability to stabilize cytosolic β-catenin (Willert *et al.*, 2003; Mikels and Nusse, 2006). The difficulty in purification arises from insolubility of WNTs due to high hydrophobicity. It is shown that WNTs, at least Wnt-3a and Wnt-5a, are even further lipidified by post-translational palmotylation. Accordingly, structural data for WNTs could not be established. It has been suggested that lipidification is crucial for WNT activity, since either the enzymatic removal of the palmitate or the site-directed mutagenesis of the palmotylated cysteine in Wnt-3a resulted in loss of activity (Willert *et al.*, 2003).

1.1.6. Gene *WNT10b*

WNT10b is a member of the WNT gene family. It was first isolated by Bui *et al.*, 1997 from human genomic DNA and cDNA libraries, using degenerate primers. The gene is clustered with another family member *WNT1*, on chromosome 12q13, a region frequently rearranged in human tumors. Expression of *WNT10b* is found to be elevated in some breast carcinomas, despite no expression in normal breast tissue or its benign tumors (Bui *et al.*, 1997)

Wang and Schackleford, 1996 performed an extensive study on expression patterns of murine *Wnt10b* in adult and embryonic tissues, via Northern blot analysis. Expression of *Wnt10b* was highest in adult lung and uterus. In the developing embryo, *Wnt10b* expression peaked at about 15.5 days post coitum (d.p.c.) and was strongest in face, limbs and skin. The expression of *Wnt10b* in limbs was consistent with the finding of Christiansen *et al.*, 1995, who showed that *Wnt10b* was expressed in the AER starting from 10.5 d.p.c.

WNT10b -the human homolog of murine *Wnt10b*- encodes a 389-amino acid protein with 96.6 per cent sequence identity to murine Wnt10b protein. The gene is composed of five exons, the first one non-coding. WNT10b major transcript (NM003394) is 2288 nucleotides long and databases report one smaller alternatively spliced isoform (AI332374). *WNT10b* is also shown to be expressed in most adult tissues, but the highest

levels are found in heart and skeletal muscles, while the lowest levels are in brain (Hardiman *et al.*, 1997).

Activation of WNT signaling by Wnt10b has been implicated in osteoblastogenesis. Wnt10b acts as a molecular switch that governs commitment of mesenchymal cells to adipocytes or osteoblastocytes (Figure 1.7). *In vitro* studies with bipotential cells showed that ectopic expression of *Wnt10b* maintains preadipocytes in an undifferentiated state through inhibition of the adipogenic transcription factors C/EBPα and PPARγ and activation of osteoblastogenetic transcription factors Runx2, Dlx5 and osterix (Ross *et al.*, 2000; Kang *et al.*, 2007). When WNT signaling in preadipocytes is prevented by overexpression of either axin or dominant-negative TCF4, the cells differentiate into adipocytes. Disruption of WNT signaling also causes transdifferentiation of myoblasts into adipocytes (Ross *et al.*, 2000). *In vivo* studies with mice expressing Wnt10b transgene in marrow have further emphasized the role of *Wnt10b* as a regulator of osteoblastogenesis (Bennett *et al.*, 2005). Those mice had decreased to about half in whole body fat and increased four fold in trabecular bone mass and strength. Wnt10b-/- mice, on the other hand, had decreased trabecular bone.

It was recently shown that autosomal recessive SHFM is associated with homozygous *WNT10b* gene mutation (Uğur and Tolun, 2008a).

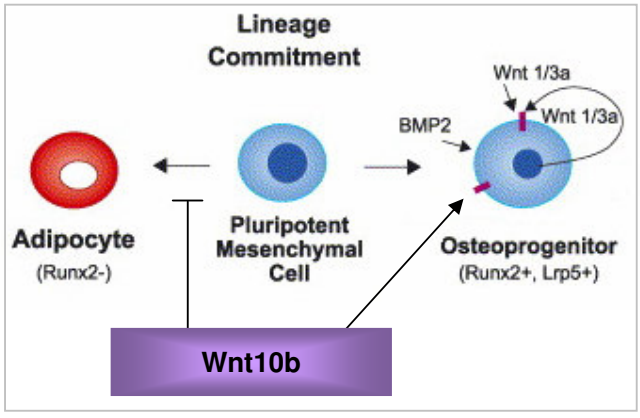

Figure 1.7. Effect of Wnt10b on lineage commitment of pluripotent mesenchymal cells (modified from Westerndorf *et al.*, 2004)

1.2. Hypomyelination and Congenital Cataract

Leukodystrophies are a group of genetically determined progressive disorders that primarily affect the central nervous system and in some cases the peripheral nerves as well. They are characterized by progressive deterioration of the white matter of the brain due to imperfect growth or development of the myelin sheath. In general, clinical features include progressive visual failure, mental deterioration, and pyramidal and cerebellar symptoms and signs (Kaye, 2001; Schiffmann and Knaap, 2004). The genes responsible for such inherited metabolic defects have been cloned for a variety of leukodystrophy syndromes: (1) Lysosomal storage diseases with myelin lipidosis: Metachromatic Leukodystrophy, Krabbe Disease, Canavan Disease, Cerebrotendinous Xanthomatosis and Sjögren-Larsson Syndrome; (2) Peroxisomal storage diseases: Adrenoleukodystrophy, neonatal Adrenoleukodystrophy and Zellweger Syndrome; (3) Myelin protein related disorders: Pelizaeus-Merzbacher Disease; and (4) Dysfunction of glia leading to abnormal myelination: Alexander Disease and Vanishing White Matter disease. These syndromes are usually inherited in an autosomal or X-linked recessive fashion; however, rare autosomal dominant forms of leukodystrophy have also been reported (Itoh *et al.*, 2006; Stumpf *et al.*, 2003).

Hypomyelination and congenital cataract (HCC) is a new leukodystrophy characterized by hypomyelination of the central and peripheral nervous systems, progressive neurological impairment and congenital cataract. This disease was reported recently by Zara *et al.*, 2006 who also identified the gene responsible as *DRCTNNB1A* (down-regulated by by β-catenin, 1a) and referred the protein product as hyccin. Shortly after, a large intragenic deletion in *DRCTNNB1A* that does not lead to congenital cataract in all of the patients in an afflicted family was reported (Uğur and Tolun, 2008b).

DRCTNNB1A encodes a 521 amino acid membrane protein whose expression was shown to be downregulated by β-catenin (Kawasoe *et al.*, 2001). RNA blot analysis demonstrated that *DRCTNNB1A* is expressed in several adult tissues including heart, kidney, placenta and brain. RT-PCR analysis showed that the gene is expressed in the lens as well (Zara *et al.*, 2006). It was suggested that hyccin has membrane localization, as two putative transmembrane segments were uncovered by a transmembrane prediction

program. However, database searches did not result in any known functional domains or motifs (Zara *et al.*, 2006).

1.3. Retinal Dystrophies Associated with Retinal Guanylate Cyclase 2D Mutations

The retina is a light-sensitive multi-layered sensory tissue that lines the posterior eye and acts at the border of input light and visual perception (Figure 1.8). Its function involves capturing photons and converting them into electrical impulses that reach to the brain through the optic nerve. Various cell types comprise the retina, of which neural cells predominate: rod and cone photoreceptors and amacrine, bipolar, horizontal, and ganglion cells. Defects in any of these cells can lead to a variety of retinal diseases, resulting in impaired vision.

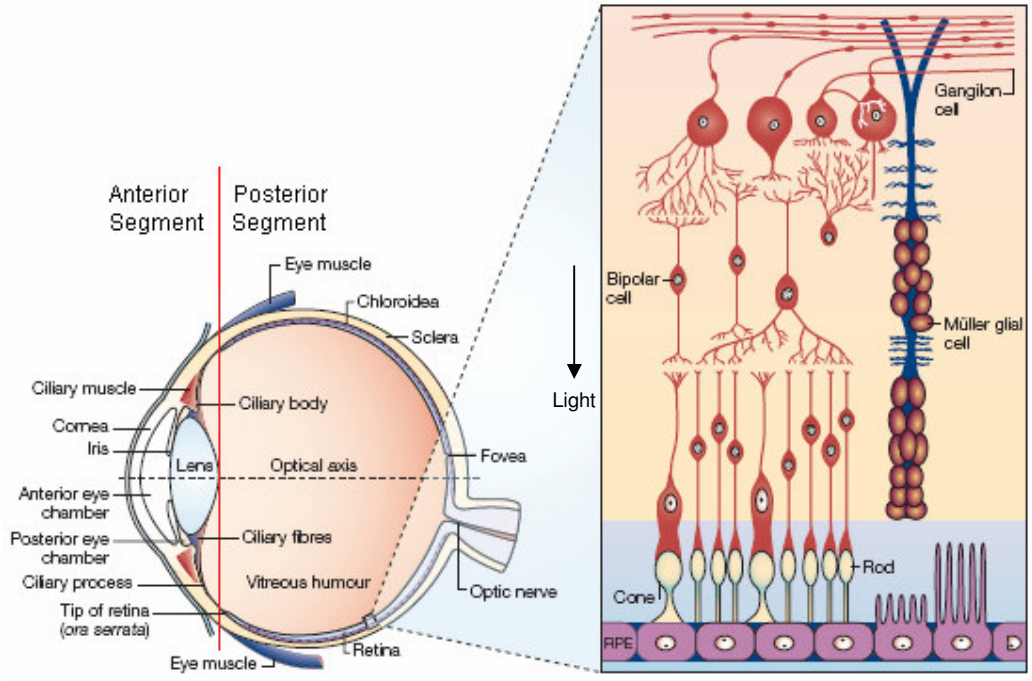

Figure 1.8. The structures of the human eye and retina. The eye is shown on the left side, and components of the retina are illustrated in the enlarged view. The vertical line divides the anterior segment of the eye from the posterior segment. Light enters the eye through the cornea, the anterior chamber and the lens. Light passes through the vitreous humour before reaching the retina. Components of the retina (from the outside to the inside of the retina) are the retinal pigmented epithelium (RPE), rod and cone photoreceptor cells, Müller glial cells, bipolar cells and ganglion cells (modified from Graw, 2003).

Guanylate cyclases, either soluble or membrane bound, catalyze the production of cGMP from GTP. The membrane guanylate cyclases comprise a family of cell-surface receptors having similar structures: an extracellular ligand-binding domain, a single membrane-spanning domain, and an intracellular region that contains both a protein kinase-like domain and a cyclase catalytic domain. cGMP produced binds and activates a cGMP-dependent serine-threonine protein kinase.

Retinal guanylate cyclase (retGC) encoded by the Guanylate Cyclase 2D gene (*GUCY2D*) is an important component in the recovery process of phototransduction in the vertebrate retina. In both rod and cone photoreceptor cells, light activated rhodopsin which is a G-protein linked receptor stimulates cGMP phosphodiesterase activity via GTP/GDP exchange on the G protein transducin followed by hydrolysis of cGMP and the closure of cGMP-gated cation channels on photoreceptors, causing membrane hyperpolarization. In the recovery phase, a decrease in the free intracellular calcium due to closed cation channels stimulates retinal Guanylate Cyclase via a calcium sensor protein. This contributes to photoreceptor recovery and light adaptation as cGMP level is restored and cGMP gated channels are re-opened. At the same time rhodopsin-specific kinase phosphorylates cytosolic tail of active rhodopsin to inhibit rhodopsin activation of transducin. Also, arrestin binds and inactivates phosphorylated rhodopsin (Figure 1.9).

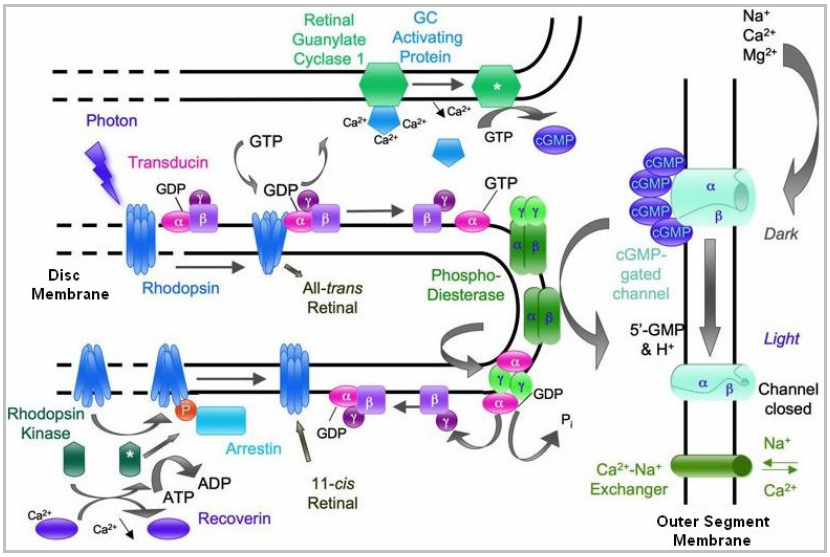

Figure 1.9. Phototransduction cascade in the vertebrate retina (Koenekoop, 2004). The illustration is freely available at www.eyegene.eu.

Two isoforms of guanylate cyclase, namely retGC and GC-F encoded by separate genes, have been identified in the mammalian retina (Yang *et al.*, 1995). Although expressed in the same photoreceptors, these cyclases are active as homodimers like other members of the receptor guanyl cyclase family (Yang and Garbes, 1997). retGC expression is confined to the eye (Yang *et al.*, 1995), showing a higher expression in cone than rod cells (Dizhoor *et al.*, 1994). It is unlikely that GC-F can compensate for defective retGC, since in humans recessive mutations in *GUCY2D* encoding retGC are responsible for congenital blindness as in Leber congenital amaurosis (LCA) and impaired vision as in cone-rod dystrophy. Ten to twenty per cent of all LCA types and at least seven per cent of all dominant cone rod dystrophies are caused by *GUCY2D* mutations (Retinal Information Network).

1.3.1. Leber Congenital Amaurosis

Leber congenital amaurosis (LCA) is the earliest and most severe form of inherited retinopathies first described almost 150 years ago. Its prevalence is 1:50,000-100,000 in newborns, and about twenty per cent of children in schools for blind have LCA. LCA is generally diagnosed immediately after birth as total blindness or greatly impaired vision, infantile nystagmus, normal fundus and a non-detectable electroretinogram (ERG). (clinical symptoms reviewed in Allikmets, 2008). LCA accounts for more than five per cent of all retinopathies, and this estimate may even rise in countries with high rate of consanguineous marriages, since LCA is typically a recessive condition (Perrault *et al.*, 2000).

Molecular genetic studies explain only about one in three of all LCA; to date eleven genetic loci have been identified and in ten causative genes have been identified (Table 1.2). This heterogeneity in the etiopathology of LCA lead to the classification of the disease in three categories: aplasia with abnormal embryological development, degeneration with early photoreceptor death (predominance either in rods or cones or both), and dysfunction with normal retinal anatomy but defective biochemical pathways (Ahmed and Loewenstein, 2008).

Table 1.2. Loci and genes for autosomal recessive LCA

LCA#	Locus	Gene	Description	MIM
LCA1	17p13.1	*GUCY2D*	retinal guanylate cyclase	204000
LCA2	1p31	*RPE65*	retinal pigment epithelium-specific protein 65 involved in the production of 11-cis retinal and in visual pigment regeneration	204100
LCA3	14q24.1	*RDH12*	retinol dehydrogenase 12 with dual activity towards all-*trans*-retinols and *cis*-retinols	604232
LCA4	17p13.1	*AIPL1*	aryl hydrocarbon receptor interacting protein-like 1 possibly involved in nuclear transport or chaperone activity and localizes to rods only	604393
LCA5	6q14.1	*LCA5*	protein hypothesized to be involved in centrosomal or ciliary functions	604537
LCA6	14q11	*RPGRIP1*	retinitis pigmentosa GTPase regulator (RPGR) interacting protein 1, functions in disc morphogenesis and anchors RPGR to the photoreceptor cilium	605446
LCA7	19q13.3	*CRX*	cone-rod homeobox, photoreceptor-specific transcription factor	602225
LCA8	1q31.3	*CRB1*	crumbs homolog 1 (Drosophila), localizes to the inner segment of mammalian photoreceptors, may be a component of the molecular scaffold that controls proper development of polarity in the eye	604210
LCA9	1p36	-	-	608553
LCA10	12q21.32	*CEP290*	centrosomal protein 290kDa, associates with microtubule proteins in centrosomes and cilia, including the rod connecting cilium	611755
LCA11	7q32.1	*IMPDH1*	inosine monophosphate dehydrogenase 1, the rate-limiting enzyme in the de novo synthesis of guanine nucleotides	146690
LCA12	1q32.3	RD3	retinal degeneration 3, retinopathy-associated subnuclear protein	610612

Although LCA is a severe and early-onset disease, its overlapping phenotype with other causes of early retinal blindness makes the differential diagnosis of LCA complex. LCA is sometimes misdiagnosed as early onset retinitis pigmentosa, since the two conditions represent a spectrum of phenotypes often caused by mutations in the same genes. Nevertheless, with careful ophthalmologic examination and testing together with molecular genetic analysis, the correct diagnosis can be made.

1.3.2. Cone and Cone-Rod Dystrophy

Rod and cone photoreceptors are delicately designed for vertebrate vision. Rods are specialized for low-light vision. They are extremely sensitive and can signal the absorption of single photons. Cones mediate color vision in bright light. They are much less sensitive

to light than rods, but have higher temporal resolution. The presence of typically more than one type of cones in the retina mediates color vision. Cone dystrophies (COD) are inherited, progressive retinal dystrophies that are characterized by an initial degeneration of cones, causing an early decrease of visual activity and color vision in adolescence or early adult life. The condition is followed by rod degeneration which is now called cone-rod dystrophy (CORD) leading to progressive nyctalopia (night blindness) and peripheral visual field loss (Moore, 1992). Differential diagnosis of early onset CORD from LCA is sometimes difficult because both diseases share the same clinical signs. The presence of a time delay of several years before dramatic worsening of the visual impairment allows the classification of the disease as CORD rather than LCA (Hamel, 2007). Inherited maculopathies affect the macula, an area of the central retina that involves cones only. Therefore, it may also be difficult to differentiate large, extended maculopathies from end stage CORD. The full field ERG is the key test (Hamel, 2007).

COD and CORD are genetically heterogeneous; various loci with dominant, recessive and X-linked inheritance have been reported (Table 1.3). Autosomal dominant CORD6 is caused by mutations in gene *GUCY2D*. Interestingly, all dominant CORD6 mutations are confined to the exons encoding the dimerization domain of retGC (Duda and Koch, 2002). Recently, novel mutation P575L was found in exon 8 of the *GUCY2D* gene, encoding a part of the kinase-like domain (Small *et al.*, 2008). Recessive *GUCY2D* mutations causing LCA1 is distributed throughout the remaining exons (Perrault *et al.*, 2000). Exon structure of *GUCY2D* together with encoded domains is shown in Figure 1.10.

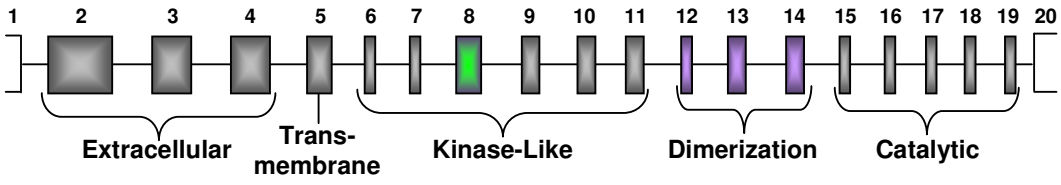

Figure 1.10. Schematic representation of *GUCY2D* exon structure and encoded domains. Untranslated regions are indicated with open boxes. Exons with mutations identified only for LCA and for CORD are shown in grey and purple, respectively. Exon 8 found to be mutated in both conditions is shown in green.

Table 1.3. Loci and genes for COD and CORDs

CORD#	Locus	Gene	Description	Inheritance	MIM
CORD1	18q21.1-q21.3	-	-	AD	600624
CORD2	19q13.3	*CRX*	see Table 1.2	AD	120970
CORD3	1p21-p13	*ABCA4*	ATP-binding cassette, sub-family A (ABC1), member 4, retina-specific transporter	AR	604116
CORD4	17q	-	-	AD	-
CORD5	17p13-p12	-	may be same as CORD6, genetic testing not performed	AD	600977
CORD6	17p13.1	*GUCY2D*	see Table 1.2	AD	601777
CORD7	6q12-q13	*RIMS1*	regulating synaptic membrane exocytosis 1	AD	603649
CORD8	1q12-q24	-	-	AR	605549
CORD9	14q11	*RPGRIP1*	see Table 1.2	AR	608194
CORD10	1q22	*SEMA4A*	a transmembrane semaphorin (also called semaphorin B) which enhances T-cell activation; homozygous knockout mice have severe retinal degeneration	AD	610283
CORD11	19p13.3	*RAXL1*	retina and anterior neural fold homeobox-like-1	AD	610381
CORDX1	Xp21.1	*RPGR*	retinitis pigmentosa GTPase regulator, functions in disc morphogenesis, intracellular trafficking and nucleocytoplasmic transport	X-linked	304020
CORDX2	Xq28	-	-	X-linked	300085
CORDX3	Xp11.23	*CACNA1F*	calcium channel, voltage-dependent, L type, alpha 1F subunit	X-linked	300476

1.4. Nonsyndromic Mental Retardation

Mental retardation (MR) refers to substantial limitations in mental functioning that affects from one to three per cent of human population. It is characterized by significantly sub-average cognitive functioning, existing concurrently with related limitations in two or more of the adaptive skill areas: communication, self-care, home living, social skills, community use, self-direction, health and safety, functional academics, leisure and work (Castellivi-Bel and Mila, 2001). The term ‘intellectual disability’ is increasingly being used instead of MR. The widely used classification system for MR distinguishes the several degrees of retardation relative to the intelligence quotient (IQ) scores of the affected: “mild” (IQ of 50–55 to 70), “moderate” (35-40 to 50-55), “severe” (20-25 to 35-40), and “profound” (20-25 and below) (Toniolo and D’Adamo, 2000).

MR associated with mild to severe learning and behavioral defects may be the only manifestation of the disease (nonsyndromic MR) or may be accompanied by other somatic, neurological, behavioral, or metabolic findings (syndromic MR). Therefore, MR is an extremely heterogeneous condition that may result from both genetic and non-genetic factors that overall affect cognitive functioning. Well-established genetic causes of MR include chromosomal anomalies and monogenic diseases, while the environmental factors that may contribute to MR include alcohol exposure, malnutrition and infectious diseases during pregnancy, premature birth, perinatal anoxia, and trauma. OMIM database contains almost 1,000 entries that contain the term "MR" as a clinical feature. However, 40 per cent of cases with moderate to severe MR and most mild MR cases (about 70 per cent) remain unexplained. Most of the mild cases probably result from a combination of multigenic and environmental causes (Chelly and Mandel, 2001).

Nonsyndromic MR is the diagnosis of exclusion in mentally retarded individuals who do not display apparently abnormal brain development or other clinical features. Although it represents the most common cognitive dysfunction, it remains poorly understood. The broad genetic heterogeneity and scarcity of large pedigrees have hindered linkage analysis in nonsyndromic MR.

1.4.1. X-Linked Mental Retardation

X-linked mental retardation (XLMR) is a common cause of inherited intellectual disability with a prevalence of 1:1000 in males. The inheritance of XLMR is generally X-linked recessive, but it is not uncommon for female carriers to manifest milder symptoms due to skewed X-chromosome inactivation.

The breakthrough on XLMR syndromes was the identification of the fragile X syndrome as a clinically distinct entity in the late 1970s. The syndrome is associated with a fragile site at Xq27.3. The causative mutation is the expansion of a CGG trinucleotide repeat that disturbs the expression of fragile X mental retardation 1 (*FRM1*) gene (Bardoni *et al.*, 2000). The FRM1 protein is an RNA-binding factor that is thought to regulate the transport or translation of specific mRNAs. This syndrome accounts for two to three per

cent of MR in males and about one per cent in females, who are less severely affected than males.

In a recent literature review, 215 distinct XLMR conditions have been listed, and clinically subdivided into two major groups: 149 syndromic and 66 nonsyndomic (MRX) forms. Eighty-two XLMR genes have been cloned to date, and 97 additional genetic loci have been identified by linkage analysis or cytogenetic breakpoint determination (Chiurazzi *et al.*, 2008).

1.4.2. Nonsyndromic Autosomal Recessive Mental Retardation (NS-ARMR)

Autosomal recessive mode of inheritance accounts for nearly twenty-five per cent of all nonsyndromic MR cases. Eleven loci for nonsyndromic autosomal recessive MR (NS-ARMR) have been mapped to date, but only four genes have been found to be directly associated with the condition: *PRSS12* (neurotrypsin at 4q25) encoding an extracellular trypsin-like serine protease suggested to act in synaptic proteolysis in brain, *CRBN* (cerebron at 3p26.2) encoding an ATP-dependent Lon protease, *CC2D1A* (coiled-coil and C2 domain containing 1A at 19p13) encoding a putative signal transducer that participates in the positive regulation of the I-kB kinase/NF-kB cascade, and *GRIK2* (glutamate receptor, ionotropic, kainate 2 at 6q21) encoding an ionotropic glutamate receptor (Molinari, *et al.*, 2002; Higgins *et al.*, 2004; Basel-Vanagaite *et al.*, 2006; Motazacker *et al.*, 2007).

Najmabadi *et al.*, 2007 mapped 8 novel gene loci by homozygosity mapping in 78 consanguineous Iranian families with NS-ARMR on chromosomes 1p34-p33, 5p15-p14, 6q21, 8p12, 10q22, 14q11.2-q12, 16p12-q12, and 19q13.2-q13.3, but the causative mutations have only been identified for *GRIK2* at 6q21.

1.4.3. Cytogenetic Abnormalities in Mental Retardation

Cytogenically visible chromosomal aberrations account for approximately 15 per cent of all MR cases, but recent studies suggest that cytogenetically invisible submicroscopic chromosomal rearrangements especially in the subtelomeric regions are a

significant cause of mental retardation (Knight *et al.*, 1999). However, conventional karyotyping allows genome-wide detection of chromosomal abnormalities at a limited resolution (5–10 Mb). The development of array-based comparative genomic hybridization techniques has proven to be an effective tool to evaluate DNA copy-number alterations across the whole-genome at a much higher resolution. Different studies with numerous patients with idiopathic mental retardation and normal karyotype using genome-wide microarray platforms have detected chromosome abnormalities in up to seventeen per cent of the cases (Zhang *et al.*, 2008).

1.5. Distal Arthrogryposis Syndromes

Arthrogryposis (from Greek "arthro" meaning "joint" and "gryposis" meaning "abnormal curvature") is a term describing the presence of multiple contractures at birth. A contracture is a limitation in the range of motion of a joint. A child with an isolated congenital contracture is born once in every 200-500 live births, and one of every 3000 children is born with two or more body areas affected by arthrogyroposis.

The etiology and pathogenesis of arthrogyroposis in neurologically normal children, most of which are sporadic (about 95 per cent), usually remain unclear. Nevertheless, autosomal dominant segregation of contractures has been well documented. Bamshat *et al.*, 1996 have classified a group of heritable disorders called the "distal arthrogryposes" (DAs). In general, DAs are characterized by nonprogressive, congenital contractures of two or more different body areas without primary neurological and/or muscle disease that affect limb function. Features common to all DAs include a consistent pattern of distal joint involvement, limited proximal joint involvement, an autosomal dominant inheritance pattern, and widely variable expressivity. On Table 1.4, 11 distinct DA classes with identified loci and genes and the prominent clinical features are listed. Five genes encoding major components of contractile apparatus of fast-twitch myofibers have been identified to cause DA syndromes: Troponin T and Troponin I isoforms encoded by *TNNT3* and *TNNI2*, respectively, β-tropomyosin encoded by *TPM2*, and myosin heavy chains encoded by *MYH3* and *MYH8*. The contraction of striated muscles is initiated by the binding of intracellular calcium to the troponin complex composed of troponin C, troponin T, and troponin I and located in the thin filaments.

Table 1.4. Distal arthrogryposis syndromes

Class[1]	Alternative titles	*Inheritance*	Locus	*Gene(s) involved*	Prominent Features	*MIM*
DA1	Arthrogryposis Multiplex Congenita, Distal, Type I	AD[2]	9p13.2-p13.1	*TPM2*	○ prototypic DA ○ camptodactyly and clubfoot	108120
DA2A	Freeman-Sheldon Syndrome (FSS), Whistling Face-Windmill Vane Hand Syndrome	AD, AR[3]	17p13.1	*MYH3*	○ very similar to DA1 ○ also includes scoliosis, small oral orifice, H-shaped dimpling of the chin, deep nasolabial folds and blepharophimosis	193700
DA2B	Freeman-Sheldon Variant (FSSV)	AD	11p15.5, 17p13.1	*TNNT3* *TNNI2, MYH3*	○ similar to DA1 and FSS ○ also includes triangular face, downward slanting palpebral fissures, prominent nasolabial folds, small mouth and mandible, cervical webbing and ulnar deviation	601680
DA3	Gordon syndrome	AD	-	-	○ camptodactyly, clubfoot, short stature, ptosis, vertebral abnormalities, pterygium colli and ± cleft palate	114300
DA4	DA with scoliosis	AD	-	-	○ short stature and neck, ptosis, immobile facial expression, camptodactyly with absent flexion creases on hands	609128
DA5	DA with oculomotor limitation & electroretinal abnormalities	AD	-	-	○ rigid trunk with limb contractures and hunched shoulders, deep set eyes with ocular movement limitation and macular pigmentation; limb muscle aplasia, and pyloric stenosis	108145
DA6	DA with sensorineural hearing loss	AD	-	- -	○ sensorineural hearing loss, camptodactyly, and microcephaly	108200
DA7	Trismus-Pseudocamptodactyly Syndrome	AD	17p13.1	*MYH8*	○ short finger-flexor tendons, and short leg muscles resulting in foot deformity	158300
DA8	Pterygium Syndrome, Multiple	AD, AR, X-linked	-	- -	○ distal limb contractures, multiple pterygia, ptosis and severe scoliosis due to hemivertebrae, short stature, atrophy in muscles	178110
DA9	Contractural Arachnodactyly, Congenital	AD	5q23-q31	Fibrillin-2	○ marfanoid habitus, severe kyphoscoliosis, generalized osteopenia, common proximal contractures, crumpled ears and muscular hypoplasia	121050
DA10	Tendo Calcaneus, Short	AD	-	-	○ plantar flexion contractures ○ milder contractures of hips, elbows, wrists, and fingers	187370

[1]Distal arthrogryposis. [2]Autosomal dominant. [3]Autosomal recessive.

This causes an allosteric change, transmitted as uncovering the actin binding sites occupied by tropomyosin and in turn allowing the cross bridges to bind the actin in thin filaments. Cross bridges are globular myosin heads which are composed of heavy and light chains with an ATPase site and an actin binding site. Myosin acts as a contractile protein that converts chemical energy into mechanical energy through the hydrolysis of ATP (Figure 1.11).

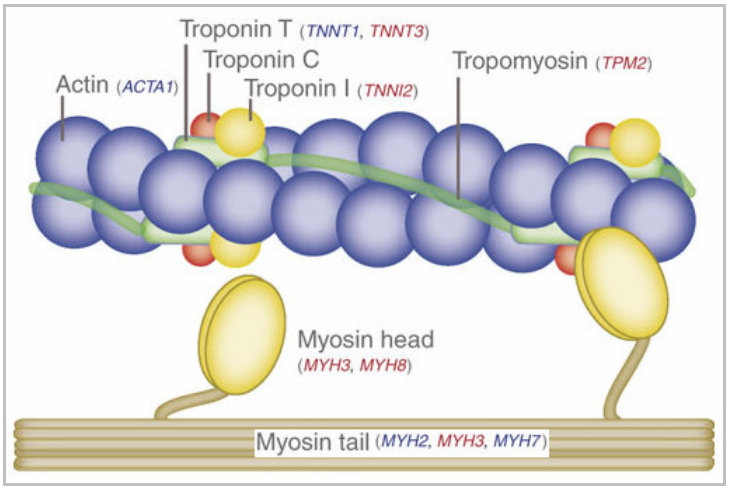

Figure 1.11. Schematic illustration of muscle contractile complex. Mutations in genes that can cause congenital contractures in DA syndromes and myopathies are shown in red and blue, respectively (modified from Toydemir *et al.*, 2006).

1.5.1. Arthrogryposis Like Syndromes

1.5.1.1. Arthrogryposis-Like Disorder (MIM 208200). An autosomal recessive form of arthrogryposis-like syndrome has been described in the Eskimo and named Kuskokwim disease after the Kuskokwim Delta area where it was observed. Arthrogryposis in patients affected predominantly the knees and ankles with atrophy and compensatory hypertrophy of associated muscle groups. No locus or gene was identified.

1.5.1.2. Pseudoarthrogryposis (MIM 177300). Pseudoarthrogryposis confined only to females had been described in two unrelated families. The syndrome manifests with rigidity of the elbows and/or knees, ankylosis at the elbows, proximal fusion of the tibia

and fibula, and bilateral fusion of the humerus, radius and ulna. No locus or gene was identified.

1.5.1.3. Pseudoarthrogryposis-like Syndrome (PAG-L). Pseudoarthrogryposis-like syndrome (PAG-L), a novel disorder, has been observed in a large Turkish kinship. Manifesting multiple contractures in patients and displaying an autosomal dominant mode of inheritance, the syndrome may be classified as a new form of DA. However, PAG-L is progressive with a preadolescence age of onset, which makes it distinct from DA syndromes. This is the family genetically analyzed in this study.

1.6. Linkage Analysis

Genetic linkage reflects the fact that two loci close to each other on the same chromosome tend to be inherited together. However, if the loci are some distance apart, crossing over or recombination between homologous chromosomes in meiosis creates new combination of alleles. The frequency with which recombination occurs, namely recombination fraction denoted by θ, increases with the distance between loci. If the loci are far apart, the probabilities of recombinant and parental chromosomes are equal, that is $\theta = 0.5$, just as when loci are on different chromosomes. Recombination events along a chromosome that harbors closely spaced genetic markers can be used to localize or link a disease gene within a relatively short genetic distance flanked by markers.

The availability of numerous genetic markers, including restriction fragment length polymorphisms, variable number tandem repeats, microsattelites and single nucleotide polymorphisms (SNPs) together with databases that store, integrate and distribute that information has made linkage analysis more feasible. Recent completion of the HapMap Project (The International HapMap Consortium, 2007) together with technical advances in microarray technology has allowed cost and time effective large scale SNP genotyping for linkage analysis. Commonly used SNP panels varying from 10K (10,000 SNPs) to 1000K (1,000,000 SNPs) can interrogate many SNP loci in a single chip experiment and allow genome resolution as low as ten kilo bases (kb) (Li *et al.*, 2008).

1.7. Lod Score Analysis

Linkage analysis approaches can be classified in two groups: parametric (model-based) and nonparametric (model-free). The former case requires specification of genetic parameters such as penetrance, disease-allele frequency, and phenocopy and mutation rates in one or more families in order to describe the mode of inheritance, in other words 'the model'. The statistical method to evaluate parametric linkage analysis is lod (**l**ogarithm of **od**ds) score analysis.

Lod score analysis introduced by Morton (1955) discriminates between two hypotheses: the null hypothesis of no linkage ($\theta = 0.5$) and the alternative hypothesis of linkage ($\theta < 0.5$). The statistical criterion for concluding linkage between two traits is based on an observed odds ratio "L", which is the ratio of the probability of observing the distributional pattern of the two traits in a given family with linkage at θ to the same probability under the hypothesis of no linkage at $\theta = 0.5$ (Risch, 1992). This is a likelihood-based method that originated from the Neymann-Pearson lemma, which states that if there is a best test for a given hypothesis, it takes the form of a likelihood ratio test. The decimal logarithm of L, namely the lod score, denoted by the function $Z(\theta)$ is calculated at several values of θ, and the maximum test statistics of Z-maximum likelihood lod score (MLS) is reported. The θ value, which gives the MLS, is the maximum likelihood estimate (MLE) of θ. A lod score of 3 is the threshold used in human linkage analysis to accept linkage (Terwilliger and Ott, 1994).

A lod score analysis between two loci, namely two-point lod score analysis, calculates lod scores by evaluating cosegregation of one marker at a time with disease locus. The analysis is based on determination of the recombinant and nonrecombinant individuals in phase-known meioses, i.e., parental origin of a particular allele of a sibling can be traced in the pedigree. In order to determine the phases and obtain information for linkage, the parents should be heterozygous for both loci. When more than two loci are analyzed simultaneously, namely multi-point lod score analysis, linkage analysis can be more efficient, but far more complex. Multipoint analysis calculates lod scores for each possible location along a map of genetic markers. Moreover, it can overcome the limited

informativeness of markers, which is critical for SNPs where only two alleles are present. In fact, the maximum lod score obtained via multi-point analysis would exactly be the same as the maximum two-point lod score between the disease locus and a particular marker locus, if all meioses were informative. Thus, multi-point mapping extracts the full information from a linkage study.

Homozygosity mapping is an application of parametric linkage analysis in consanguineous families and inbred or isolated populations. It is based on the idea that affected individuals for an autosomal recessive trait whose parents are related most likely have received a common haplotype without recombination and in the homozygous state from a single ancestor (Lander and Botstein, 1987). Inbreeding increases the incidence of autosomal recessive disorders. Most of the time, the frequency of a trait is so low that the disease can only arise due to parental consanguinity. In such cases, it is highly likely that the affected individuals in the population are homozygous by descent. Inbred families are of great value for linkage studies, as a single family can produce a significantly high lod score.

The inheritance patterns for complex traits are not straightforward. In contrast to Mendelian traits, complex traits are rather common and most probably are due to multiple interacting genes and environmental factors, thus complicating the genetic analysis. Therefore, nonparametric methods (model free) are often preferred to search for susceptibility genes underlying complex traits. The rationale is that, between affected relatives excess sharing of haplotypes that are identical by descent (IBD) in the region of a susceptibility gene would be expected, irrespective of the mode of inheritance. Various methods test whether IBD sharing at a locus is greater than the expected null hypothesis of no linkage (reviewed in Teare and Barrett, 2005).

Various computer programs have been developed and distributed free of charge for the application of statistical tests for linkage analysis (Dudbridge, 2003). There is also much effort in creating user friendly software platforms, where various linkage programs are integrated with standardized input data formats and results are presented in graphic outputs. ALOHOMORA (Rüschendorf and Nürnberg, 2005) specially designed for SNP

panels and easyLINKAGE (Hoffmann and Lindner, 2005) applicable both to SNP and microsatellite panels are such software tools widely used for linkage analysis.

1.8. Candidate Gene Approach

A genetic locus identified with genome scans and fine-mapped with further genotyping studies is evaluated for candidate genes whenever computer programs and visual inspection of haplotypes support linkage to that locus. A candidate gene for a particular disease is selected upon various criteria: (i) the gene is located within the minimal critical gene region, (ii) the gene product is presumably involved in the mechanisms leading to disease pathogenesis, (iii) animal models of the gene matches to the disease phenotype, (iv) spatial and temporal expression of the gene is compatible with the disease phenotype. Extensive database mining together with proper clinical evaluation of the patients is crucial in the assessment of the candidate genes.

2. PURPOSE

In the first part of this study, the purpose was to map the gene loci for five rare inherited disorders in single families using the genome scan data for the families and subsequent fine-mapping studies and statistical analyses. The disorders were Split Hand Foot Malformation (SHFM), Hypomyelination and Congenital Cataract (HCC), Cone Rod Dystrophy (CORD), Mental Retardation associated with Hypertension (MR-HT), and Pseudoarthrogryposis-like Syndrome (PAG-L). Additionally, we intended to investigate any loci possibly modulating the expressivity and/or penetrance in SHFM.

In the second part of the study, we performed candidate gene approach with the aim of identifying genes responsible for SHFM, HCC and CORD.

3. MATERIALS

3.1. Subjects

Informed consent was obtained from/for all subjects participated in this study. The study was approved by the Committee on Research with Human Participants at Boğaziçi University.

3.1.1. SHFM

A large kindred from Eastern Turkey with thirteen members afflicted with an autosomal recessive form of SHFM was investigated in this study (Figure 3.1). All affected individuals were born to consanguineous parents. Clinical findings for nine of the cases have been described (Gül and Öktenli, 2002). The clinical evaluation for the cases is compiled in Table 3.1, and examples are presented in Figure 3.2.

All affected members except individual 407 had central feet reductions with or without hand involvement. Individual 407 can best be described as atypical SHFM (Elliott *et al.*, 2005), having just unilateral hand syndactyly with no foot involvement. In general, females were less severely affected than the males, and hands were affected much less than the feet. The trait exhibited a great degree of variable expressivity among affected subjects. Blood samples for 21 individuals were supplied by Dr. Davut Gül at the Military Academy of Medicine in Ankara and processed thereafter for the initial genome scan. Blood samples for additional twelve individuals were obtained by myself and Dr. Aslı Tolun at the Department of Molecular Biology and Genetics, Boğaziçi University and employed for mutation analysis and fine mapping studies.

Radiographs were evaluated by Dr. Ayşegül Bursalı at Metin Sabancı Baltalimanı Hospital for Research and Education, Istanbul.

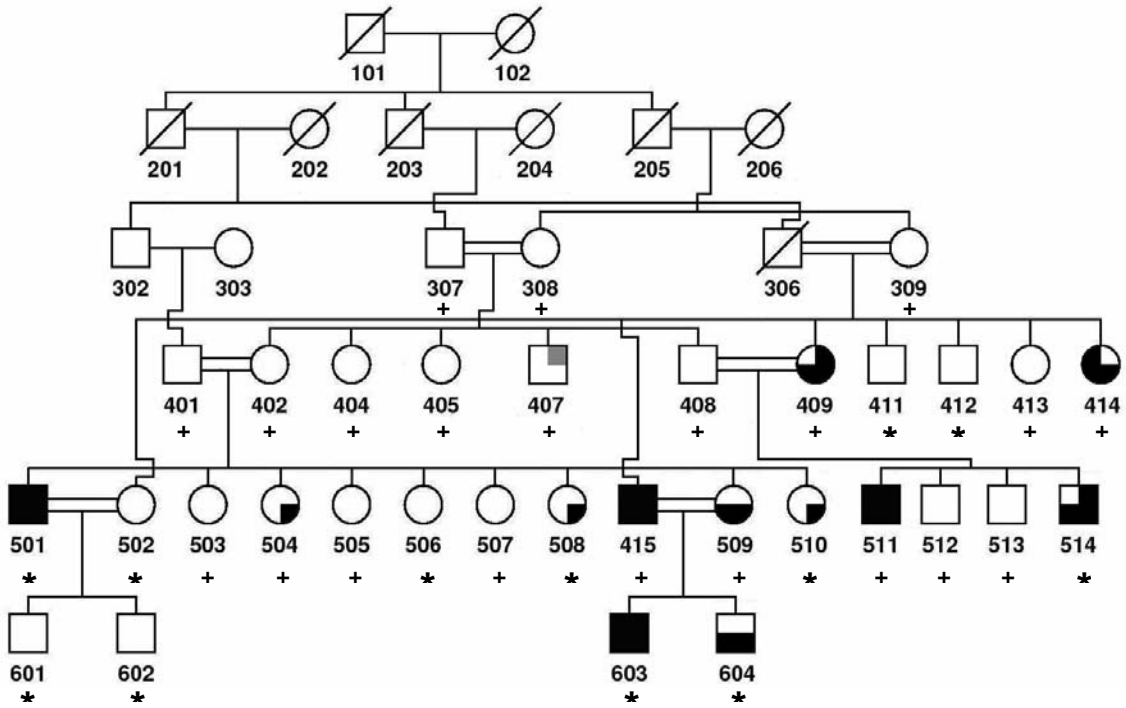

Figure 3.1. Pedigree diagram for the SHFM kindred. The first three generations are partial. DNA available for the genome scan is marked with a plus sign, and DNA available later is marked with an asterisk. Symbols for affected individuals are shown in four quadrants according to upper and lower extremity involvement. Upper left quadrant represents the left hand and so forth. Individual 407 is shaded uniquely, since he had atypical SHFM (Ugur and Tolun, 2008a).

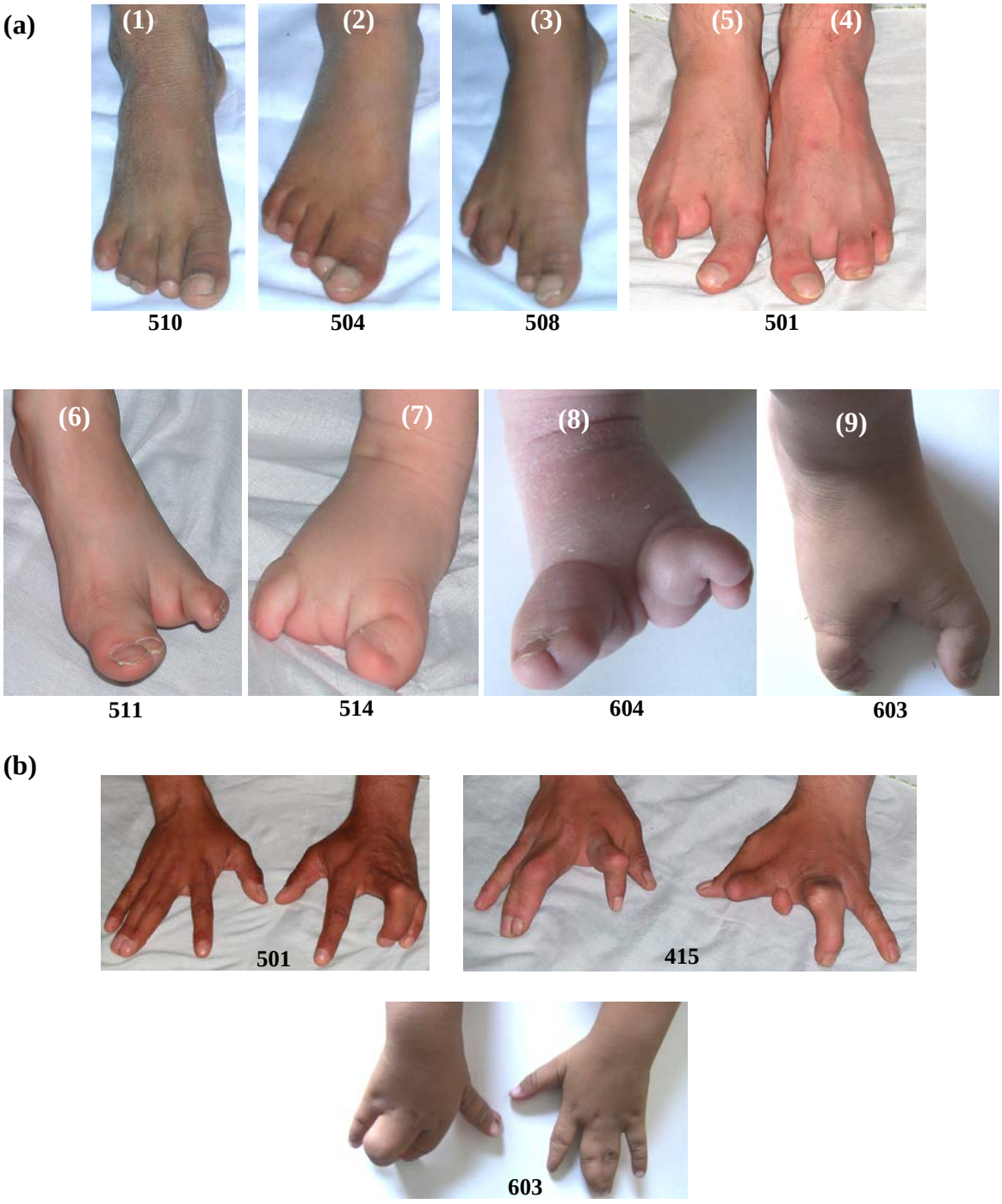

Figure 3.2. Examples for autopod malformations in the kindred. (a) Foot phenotypes are demonstrated roughly in increasing severity: (**1**) postaxial syndactyly of toes 3-4, (**2**) preaxial syndactyly of toes 1-2, (**3**) conditions (1) and (2) together, (**4**) (3) together with loss of toe 2 and no clefting (**5**) (3) together with loss of toe 2 and clefting, (**6**) loss of toe 3 with syndactyly of remaining toes in both pre-and post axial direction with clefting, (**7**) (6) together with loss of toe 2 and no clefting, (**8**) (6) together with loss of toe 2 with clefting, (**9**) classical cleft foot. (b) Hand malformations in three males (Ugur and Tolun, 2008a).

Table 3.1. Review of the autopod malformations in the kindred. The degree of severity in foot malformations are numbered from 1 to 9 according to Figure 3.2. Photographs and/or radiographs for individuals with a plus sign are available (Ugur and Tolun, 2008a).

			Autopod Malformations					
ID	Case[1]	Sex	Left hand	Right hand	Left foot	Right foot	Photographs	Radiographs
407	5	M	None	Syndactyly type I (operated)	None	None	-	+
409	6	F	None	Postaxial partial syndactyly (fingers 3-4)	3	2	+	+
414	7	F	Postaxial partial syndactyly (fingers 3-4)	None	9	8	-	-
415	8	M	Postaxial syndactyly (fingers 3-4) with bone deformity, extra rudimentary bone, hypoplastic finger 2	Postaxial syndactyly (fingers 3-4) with bone deformity, flexion deformity of finger 2	9	9	+	+
501	1	M	Postaxial syndactyly (fingers 3-4) with bone deformity	Postaxial syndactyly (fingers 3-4) with almost fused nail beds	4	5	+	-
504	4	F	None	None	None	3	+	-
507	-	F	None	None	None	None	+	+
508	3	F	None	None	None	3	+	-
509	2	F	None	None	7	6, but toe 3 rudimentary	-	-
510	-	F	None	None	None	1	+	+
511	9	M	Finger 5 clinodactyly	Finger 5 clinodactyly	6	6	+	-
514	-	M	None	Postaxial partial syndactyly (fingers 3-4)	9	7	+	-
603	-	M	Postaxial syndactyly (fingers 3-4) with bone deformity	Postaxial syndactyly (fingers 3-4) with bone deformity, preaxial polydactyly type 1	9	9	+	-
604	-	M	None	None	8	9	+	-

[1]Case numbering (Gül and Öktenli, 2002)

3.1.2. HCC

A large consanguineous family afflicted with a novel form of autosomal recessive leukodystrophy was investigated in this study. (Figure 3.3). Blood samples for 16 individuals were obtained by Dr. Aslı Tolun at the Department of Molecular Biology and Genetics, Boğaziçi University. The condition was later diagnosed as hypomyelination and congenital cataract (HCC) (Zara *et al.*, 2006). The clinical and neurological findings in patients are summarized in Table 3.2.

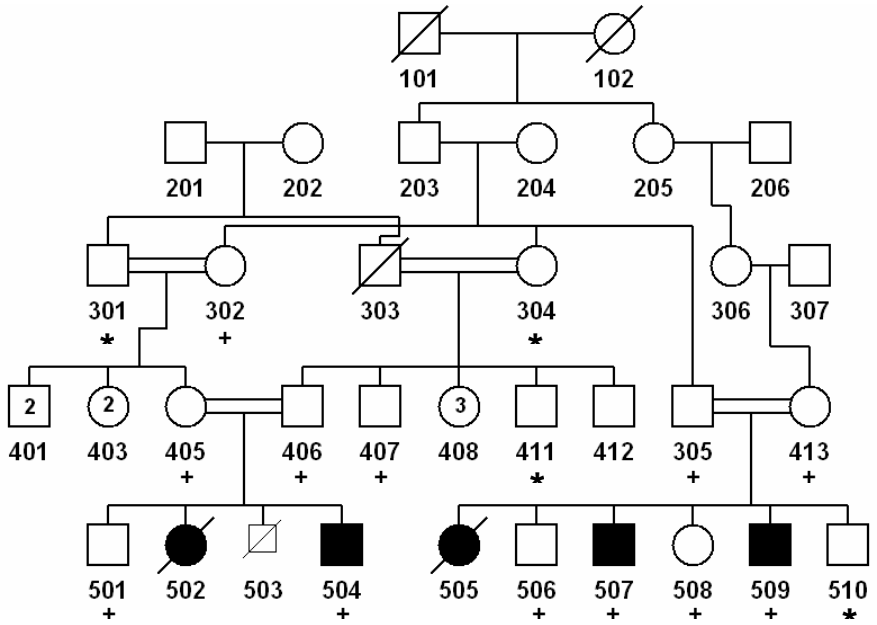

Figure 3.3. Pedigree diagram for the HCC family. DNA available for the genome scan is marked with a plus sign, and DNA available later is marked with an asterisk.

Table 3.2. Clinical and neurological findings in patients (Ugur and Tolun, 2008b)

ID	Sex	Present Age	Cataract		Loss of ability to walk with support	Seizures	Mental Retardation
			Acquisition (age)	Uni/ Bilateral			
502	F	died at 2 y	congenital	bilateral	-	NA	NA
504	M	10 y	congenital	bilateral	never walked	-	moderate
505	F	died at 12 y	congenital	unilateral	2 y	NA	moderate
507	M	16 y	congenital	bilateral	6 y	-	mild
509	M	13 y	9 y	bilateral	6 y	-	mild

NA: data not available

3.1.3. CORD

A large consanguineous family afflicted with cone rod dystrophy (CORD) was investigated in this study (Figure 3.3). Retinitis pigmentosa, Leber's congenital amaurosis and Best dystrofy were excluded by differential diagnosis. Initial blood samples for 14 individuals were supplied by Dr. Davut Gül at the Military Academy of Medicine in Ankara and and repeated samples for affected individuals 409, 507 and 509 were obtained by Dr. Aslı Tolun at the Department of Molecular Biology and Genetics, Boğaziçi University .

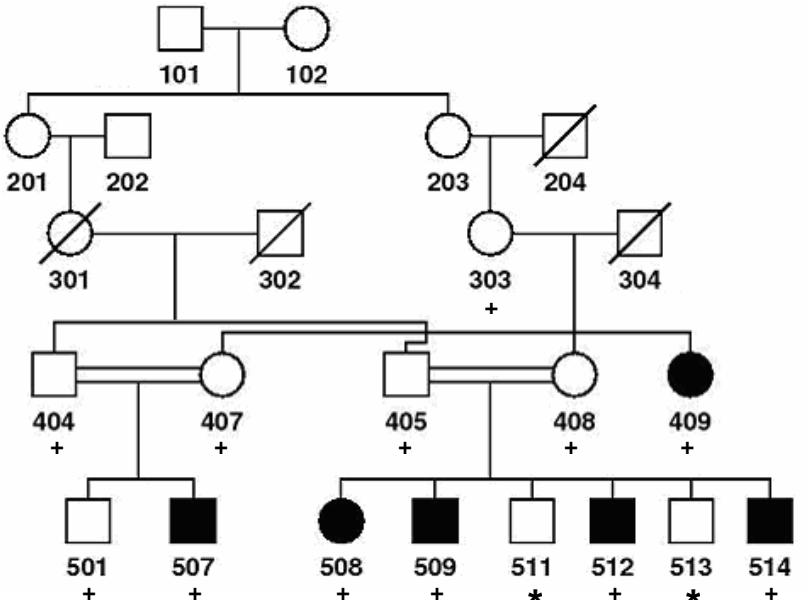

Figure 3.4. Pedigree diagram for the CORD family. DNA available for the genome scan is marked with a plus sign, and DNA available later is marked with an asterisk.

3.1.4. MR-HT

Peripheral blood samples from MR-HT patients and their family members used in this study were provided by Dr. Davut Gül at the Military Academy of Medicine in Ankara. Detailed clinical findings were available for patient 504 only. He had mental and growth retardation and facial dysmorphism, including bifrontal depression, down slanting palpebral fissures, microphthalmic appearance, photophobia, prominent nose and low set ears. Karyotype analysis was normal. Ophthalmologic examination revealed retinal

degeneration and normal cornea. Widened subarachnoid spaces and interhemispheric fissures and sulcus were notable in the computer tomography of the brain. All patients, including 502 had elevated blood tension levels; 141/93 mmHg for 502 by November 2006, and 134/98 mmHg for 503, 146/86 mmHg for 504 and 135/96 mmHg for 505 by June 2006. However, recently obtained familial history and some new clinical findings complicated the mode of inheritance in the family. Individuals 406, 407, 409 and 306 had sight problems, particularly night blindness. Mental statute for 406 and 407 were moderate. A detailed clinical examination had not been conducted for 502, including karyotype analysis. His facial appearance did not match those of the other patients.

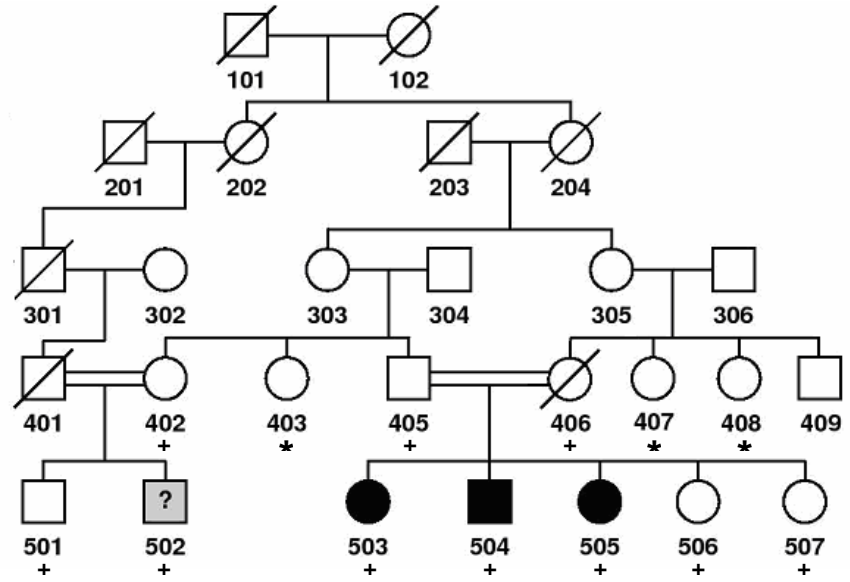

Figure 3.5. Pedigree diagram for the MR-HT family. DNA available for the genome scan is marked with a plus sign, and DNA available later is marked with an asterisk.

3.1.5. PAG-L

Peripheral blood samples from 28 PAG-L patients and their family members used in the initial genome-wide linkage study were obtained by Dr. Aslı Tolun at the Department of Molecular Biology and Genetics, Boğaziçi University. Twenty additional samples were obtained by me, Dr. Aslı Tolun and Dr. Davut Gül at the Military Academy of Medicine in Ankara. DNA of affected individuals 315 and 416 did not amplify well in the genome

scan, so new blood samples were obtained and further genotyping studies were performed with these samples in our laboratory (Figure 3.6).

All of the patients have similar clinical manifestations, so only patient 445 (Figure 3.6) is described here. A normal gestational history and birth were reported for the proband. The disease onset was early childhood. He was a high school graduate with normal mental status. At age 20, his OFC (occipital-frontal circumference), height and limb ratios were recorded (Table 3.3). He had multiple pigmented nevi. Upper extremities exhibited bilateral rhizomelic shortening, multiple joint stiffness (elbow, interphalangeal), and brachydactyly. Lower extremities exhibited stiffness in the knees, bilateral cutaneous syndactyly (2-3), and venous varicosities.

Neurological examination revealed moderate weakness and atrophy in limb muscles, weaker proximal muscles than distal muscles, hypoactive deep tendon reflexes, and hypertrophy in the distal muscles of the lower extremities. Gower's sign was present. Results of abdominal ultrasonography, electrocardiogram, and echocardiogram were all normal. X-ray examination of all long bones, hands, and patella revealed short humeri; otherwise, all bones were normal. EMG showed myopathy. He had normal karyotype.

Table 3.3. OFC and ratios of height to arm span and hand to middle finger

	OFC	**Height /Arm Span**	**Hand / Middle Finger**
Normal	56-59 cm	~ 1	~ 1
Patient 445	53.5 cm	169 cm / 150 cm = 1.13	9.5 cm / 6.5 cm = 1.46

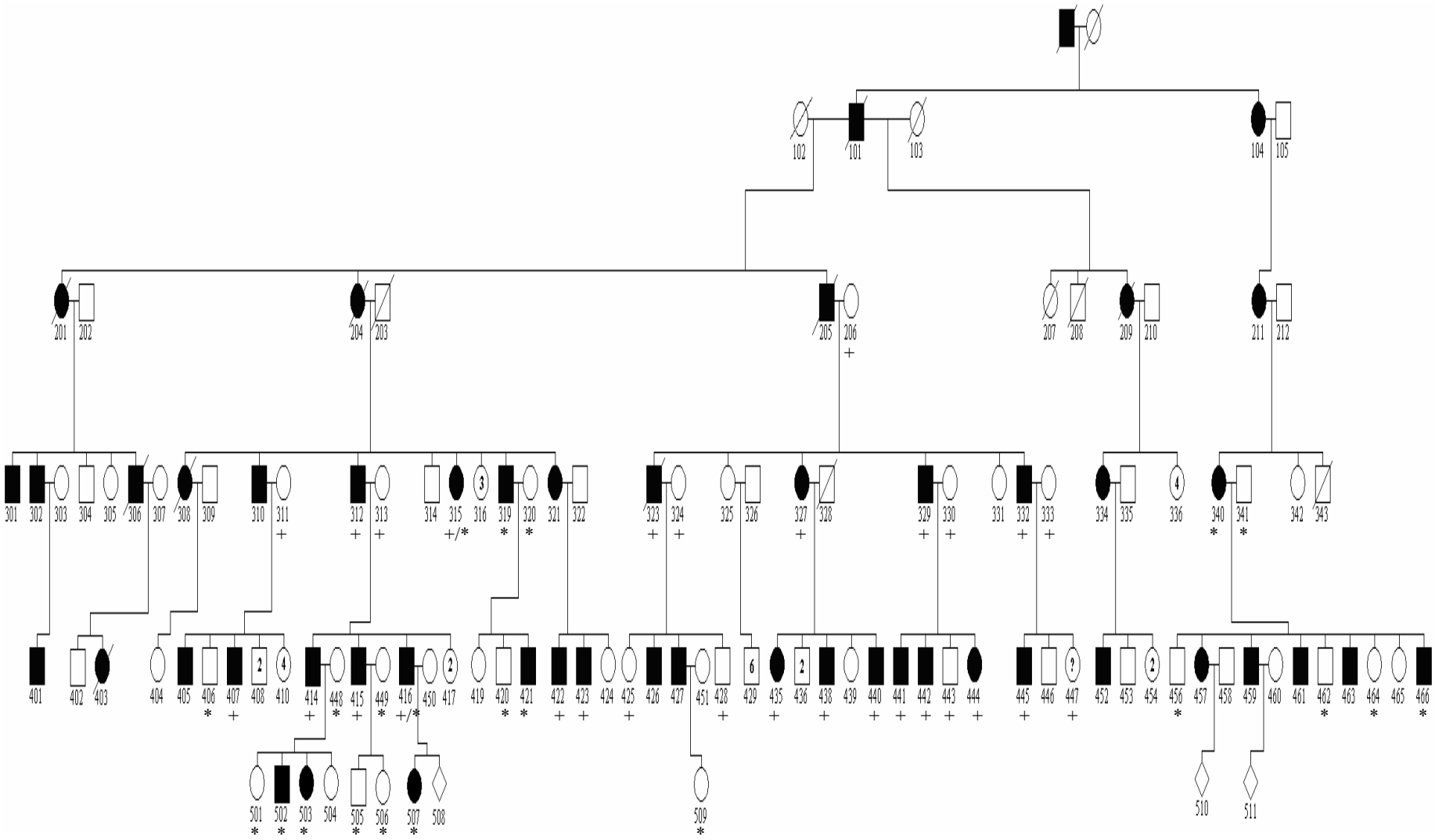

Figure 3.6. Pedigree diagram for the PAG-L kindred. A plus sign indicates that DNA was available before and an asterisk after the genome-scan.

3.2. Chemicals

All solid and liquid chemicals used in this study were purchased from Merck (Germany), Sigma (USA), Riedel de-Häen (Germany), Carlo Erba (Italy) and Biochrom (Germany) unless stated otherwise in the text.

3.3. Buffers And Solutions

3.3.1. DNA Extraction from Whole Blood

Cell Lysis Buffer	:	155 mM NH_4Cl, 10 mM $KHCO_3$ 0.1 mM Na_2EDTA (pH 7.4)
Nucleus Lysis Buffer	:	400 mM NaCl, 2 mM Na_2EDTA, 10 mM Tris (pH 8.2)
Proteinase K	:	20 mg/ml Proteinase K in dH_2O (Sigma, USA)
Sodiumdodecylsulfate (SDS)	:	10 per cent SDS (w/v) in dH_2O
Ammonium Acetate	:	7.5 M CH_3COONH_4 in dH_2O
Ethanol	:	Absolute Ethanol
TE buffer	:	1 mM EDTA, 20 mM Tris-HCl, pH 8.0

3.3.2. Polymerase Chain Reaction (PCR)

10 X PCR Buffer A	:	20 mM $MgCl_2$, 500 mM KCl, 100 mM Tris-HCl (pH 8.3)

10 X PCR Buffer B	:	20 mM $MgSO_4$, 100 mM KCl, 200 mM Tris-HCl (pH 8.8), 100 mM $(NH_4)_2SO_4$, 1 per cent Triton X-100, 1 mg/ml BSA
$MgCl_2$	:	25 mM $MgCl_2$ (Roche, Germany)
dNTP	:	12.5 mM each of dATP, dCTP, dGTP and dTTP in dH_2O (Roche, Germany)
Betaine	:	5 M Betaine (Promega, USA)

3.3.3. Agarose Gel Electrophoresis

Agarose	:	2 per cent Agarose in 0.5 X TBE buffer
NuSieve	:	2 per cent Agarose-NuSieve (2:1) in 0.5 X TBE buffer
10 X TBE Buffer	:	20 mM EDTA, 0.89 M Boric Acid, 0.89 M Trizma base (pH 8.3)
6 X Loading Buffer	:	10 mM Tris-HCl (pH 7.6), 50 per cent Glycerol, 60 mM EDTA, 2.5 mg/ml Bromophenol Blue and/or 2.5 mg/ml Xylene Cyanol
Ethidium Bromide	:	10 mg/ml in dH_2O

3.3.4 Polyacrylamide Gel Electrophoresis (PAGE)

40 per cent Acrylamide (Stock)	:	40 per cent Acrylamide-bisacrylamide (19:1) in dH_2O

8 per cent Instagel (Denaturing)	:	8 per cent Acrylamide-bisacrylamide (19:1), 8.3 M urea in 1 X TBE buffer
APS	:	10 per cent Ammonium Peroxidisulfate
TEMED	:	N,N,N,N-tetramethylethylenediamine
10 X Sample Buffer	:	95 per cent formamide, 20 mM EDTA, 0.05 per cent xylene cyanol, 0.05 per cent bromophenol blue

3.3.5. Single Strand Conformational Polymorphism (SSCP) Gel Electrophoresis

40 per cent Acrylamide (Stock)	:	40 per cent Acrylamide-bisacrylamide (37.5:1 or 50:1) in dH_2O
8 or 10 per cent Acrylamide (37.5:1, non-denaturing)	:	8 or 10 per cent Acrylamide-bisacrylamide in 0.6 X TBE buffer
Glycerol	:	5 per cent Glycerol in gel solution

3.3.6. Silver Staining

Staining Buffer	:	0.1 per cent $AgNO_3$ in dH_2O
Developing Buffer	:	1.5 per cent NaOH, 0.01 per cent $NaBH_4$, 0.015 per cent formaldehyde in dH_2O
Stop Buffer	:	0.75 per cent $NaCO_3$ in dH_2O

3.4. Kits

A list of commercial kits utilized in this study is given in Table 3.4.

Table 3.4. List of kits used in this study with their description and manufacturing company

Name	Used for	Company
Qiagen Taq PCR Core Kit with Q-solution	Amplification of difficult templates	Qiagen, USA
Expand Long Range, dNTPack	Amplification of long templates	Roche, Germany
GC-Rich PCR System	Amplification of templates rich in GC nucleotides	Roche, Germany
M-MLV Reverse Transcriptase Kit	RT-PCR	Promega, USA
Agarose Gel DNA Extraction Kit	Elution of DNA fragments run in agarose gels	Roche, Germany
QIAquick PCR Purification Kit	PCR Clean-up	Qiagen, USA
High Pure PCR Template Preparation Kit	DNA extraction from whole blood	Roche, Germany
PAXgene Blood RNA Kit	Isolation of cellular RNA from whole blood stabilized in PAXgene Blood RNA tubes	Qiagen, USA
LightCycler 480 High Resolution Melting Kit	Heteroduplex analysis on LightCycler 480	Roche, Germany
LightCycler 480 ProbeMaster Kit	Relative quantification on LightCycler 480	Roche, Germany

3.5. Enzymes

Taq DNA polymerase was purchased from Roche, Germany or Qiagen, USA (supplied with Q-solution). The restriction enzymes and their appropriate buffers were from New England Biolabs (USA).

3.6. Oligonucleotide Primers and Probes

The oligonuclotide primers used in this study were purchased from Iontek (Turkey) or Massachusetts General Hospital (MGH) DNA Synthesis Core (USA). Lyophilized primers were dissolved in 1000 µl dH_2O, and 10 µM dilutions were used for PCR assays.

Intron-spanning TaqMan assays for genes *WNT10b* and *HPRT1* were designed at Universal Probe Library (Roche, Germany) by the software ProbeFinder version 2.35.

Relevant primers were purchased from MGH DNA Synthesis Core (USA) and the probes from Universal Probe Library (Roche, Germany).

3.7. DNA Molecular Weight Markers

Lambda DNA/*Hind*III and pUC19 DNA/*Msp*I markers were purchased from Fermentas (Lithuania), and 50 bp DNA ladder was purchased from Roche (Germany).

3.8. Equipment

Autoclave	:	Midas 55 (Prior Clave, UK) AMB430T (Astell, UK)
Balance	:	Electronic Balance (Precisa, Switzerland)
Centrifuges	:	MiniSpin Plus (Eppendorf, Germany) Universal 16R (Hettich, Germany) Allegra X-22R (Beckman Coulter, USA) J2-MC (Beckman Coulter, USA)
Deep Freezers	:	-20^{o}C (Bosch, Germany) -20^{o}C (AEG, Turkey) -80^{o}C Ultra Freezer (Thermo Scientific, USA)
Documentation System	:	GelDoc Documentation System with Quantity One 1-D Analysis Software (BioRad, USA)
Electrophoretic Equipment	:	Horizontal DNA Electrophoresis Gel Box (Bio-Rad, USA) Primo Minicell Horizontal Gel Sytem (Thermo Scientific, USA) Sequi-Gen Sequencing Cell (Bio-Rad, USA)

		DCode Universal Mutation Detection System (Bio-Rad, USA)
Incubator	:	Orbital (Gallenkamp, Germany)
Magnetic Stirrer	:	MR3001 (Heidolph, Germany)
Micropipettes	:	Pipetman (Gilson, France)
Minishaker	:	Rotamax 120 (Heidolph, Germany)
Ovens	:	Heraus (Germany) EN 400 (Nüve, Turkey)
Power Supplies	:	Power Pac Model 3000 (Bio-Rad, USA) Fotoforce 250 Electrophoresis Power Supply (Fotodyne, USA) P250A Power Supply (Sigma-Aldrich, USA)
Refrigerator	:	4^{o}C (Arçelik, Turkey)
Spectrophotometers	:	8453 UV-Visible Spectrophotometer (Agilent, USA) NanoDrop 1000 (Thermo Scientific, USA)
Thermal Cyclers	:	MyCycler (Bio-Rad, USA) PTC-200 (MJ Research, USA) Techne (Progene, UK) LightCycler 480 (Roche, Germany)
Transilluminator	:	Fluorescent Table (Consort, Belgium)
Vortex	:	Reax vortexmixer (Heidolph, Germany)

		Lab Dancer Vario (Roth, Germany)
Waterbath	:	Grant LTD 6G Thermostatic Water Bath (Grant, Germany)
Water Purification System	:	Ultra Pure Water Purification system (Watech, Germany)

3.9. Electronic Databases

A list of electronic databases utilized in this study is given in Table.3.5.

Table 3.5. List of electronic databases

Name	Description
Databases	
Ensembl http://www.ensembl.org/	Software system which produces and maintains automatic annotation on selected eukaryotic genomes
EXPOLDB http://expoldb.igib.res.in/expol/expol.html/	Expression data of human blood leukocytes
NCBI genome resorces http://www.ncbi.nlm.nih.gov/genome/guide/human/	Supplies reference sequence and working draft assemblies for a large collection of genomes
Online Mendelian Inheritance in Man http://www.ncbi.nlm.nih.gov/Omim/	A guide to human genes and inherited disorders
RCSB Protein Databank http://www.rcsb.org/pdb/home/home.do/	Tools (including Protein Workbench software) and resources for studying the structures of biological macromolecules
UCSC Genome Browser http://genome.ucsc.edu/	Reference sequence and working draft assemblies for a large collection of genomes
Amino Acid Substitution Prediction Tools	
Molecular Modelling and Bioinformatics (MMB) http://mmb2.pcb.ub.es:8080/PMut/	Annotation and prediction of pathological mutations. Output prediction score of > 0.5 is pathological otherwise neutral
MutDB http://www.mutdb.org/	Interactive structural analysis of mutation data
*Poly*morphism *Phe*otyping (PolyPhen) http://genetics.bwh.harvard.edu/pph/	Uses sequence conservation and structure to model position of amino acid substitution. Output score ranges from 0 to a positive number, where 0 is neutral and a high positive number is damaging
SIFT http://blocks.fhcrc.org/sift/SIFT.html/	Calculates position-specific scores for amino acids, using sequence homology to Output score ranges from 0 to 1, where 0 is damaging and 1 is neutral

Table 3.5. List of electronic databases (continued)

Name	Description
SNPs3D http://snps3d.org/	Assigns functional effects of non-synonymous SNPs based on structure and sequence analysis. Output scores of <0 is damaging. Mutation on protein structure can be visualized.
Tools for detection of particular patterns in sequences	
Biology WorkBench http:// workbench.sdsc. edu/	Web-based package of tools for storing and analyzing input sequences. Includes Primer3, restriction analysis, etc.
Tandem Repeats Finder http://tandem.bu.edu/trf/trf.html/	Locates and displays tandem repeats in a given DNA sequence.
Others	
Alternative Splicing Structural Genomics Project http://moult.umbi.umd.edu/human2004/	Modeling alternative splicing and its effects on protein folds
Laboratory of Statistical Genetics at Rockefeller University http://linkage.rockefeller.edu/	List of statistical tools for genetic linkage analysis
Mammalian Genotyping Service http://research.marshfieldclinic.org/genetics/	Genotyping maps and statistics
Retina International Mutation Database http://www.retina-international.com/sci-news/gcmut.htm/	List of *GUCY2D* mutations
RetNet http://www.sph.uth.tmc.edu/retnet/	Retinal Information Network
Rutgers map http://compgen.rutgers.edu/maps/	Second generation combined linkage and physical map
The WNT Homepage http://www.stanford.edu/~rnusse/wntwindow.html/	Up to date information on WNT signaling

4. METHODS

4.1. DNA Extraction from Peripheral Blood Samples

Genomic DNA from patients and their family members were isolated from peripheral blood samples that had been collected into sterile vacutainer tubes containing K_2EDTA as anticoagulant. Thirty ml of cell lysis buffer was added to every 10 ml of blood sample and kept for 15 minutes (min) at 4°C to lyse the plasma membrane. The samples were centrifuged at 5000 revolution per minute (rpm) and 4°C for 10 min. The supernatant was discarded, and the pellet of leukocyte nuclei was washed by suspending in 10 ml of cell lysis buffer and centrifugation for 10 min. The supernatant was discarded, and the nuclei were suspended in 5 ml of nucleus lysis buffer by extensive vortexing. After the entire pellet had been dissolved, 50 µl of Proteinase K (20 mg/ml) and 80 µl of 10 per cent SDS were added and mixed gently. The sample was incubated either at 37°C overnight or at 56°C for 3 hours (hr) to digest the nuclear proteins. In order to precipitate the protein residues, the sample was shaken vigorously to salt out the proteins after the addition of 2.8 ml 9.5 M NH_4Ac and was centrifuged at 10,000 rpm and room temperature for 25 min. The supernatant was transferred to a 50 ml tube. Two volumes of ethanol was added to it to precipitate out DNA. DNA was fished out carefully with a micropipette tip and transferred into a 1.5 ml tube. DNA was air-dried, dissolved in 500 µl of TE buffer, and stored at -20^{o}C. If the starting blood amount was low, DNA was extracted by High Pure PCR Template Purification Kit instead.

4.2. Linkage Analysis

A whole-genome scan has been conducted to localize the genes responsible for SHFM, HCC, CORD, MR-HT and PAG-L at the National Heart, Lung and Blood Institute (NHLBI) Mammalian Genotyping Service (Contract Number HV48141, Weber and Bronnan, 2001). Marshfield Screening Set 13 was used for SHFM, HCC and PAG-L, and Set 16 for CORD and MR-HT. Screening sets used for the genome scan contained 411 and 402 microsatellite markers, respectively that both spanned autosomes and sex

chromosomes with an average spacing of 10 cM. The genotyping error rate of the service was 0.50 per cent, as estimated by blindly typing some control DNA samples.

The genotyping service required 15-30 µg of DNA from each individual for amplification of microsatellite loci with fluorescently labeled primers. The amplified products were then genotyped on a custom-built **sca**nning **flu**orescence **d**etector (SCAFUD) using software developed to automatically process the SCAFUD output and assign allele sizes. The results were submitted to us in the LINKAGE file format.

The raw data obtained from NHLBI Mammalian Genotyping Service was reformatted for the software package easyLINKAGE by an Microsoft Excel macro created in our laboratory in order to detect genotyping errors (PedCheck), calculating two (SuperLink v1.6) and multipoint (SimWalk v2.91) lod scores, and constructing haplotypes (Genehunter v2.1 with split families). The updated physical and genetic positions of the markers were obtained from the sequence tagged site (STS) map of GenBank (NCBI Build 36.3) and the Rutgers second generation combined linkage and physical map of the human genome. Rutgers map was also used to estimate genetic positions of markers whenever not known. The candidate loci deduced after computer analyses were fine-mapped by typing additional microsatellite markers flanking and/or within those loci using silver stained polyacrylamide gels. All of the statistical analyses were performed under a parametric model: dominant or recessive inheritance either with full or reduced penetrance.

Microsatellite markers that were reported in the databases were primarily selected for the analyses (Table 4.1). Sequences for primers used for amplification of those repeats were obtained from GenBank; their properties and PCR conditions employed were available at http://mp.invitrogen.com/mappairs.php3. For regions where no repeats were reported, the relevant DNA sequence was introduced to Tandem Repeats Finder program and primer pairs were designed to amplify the repeats revealed by this program (Table 4.2). Nevertheless, some genomic regions did not contain any repetitive elements. We then amplified groups of SNPs in those regions and checked their inheritance on SSCP gels. These variants could also be resolved with PAGE, if the sequence variants contained IN-DELs (insertion-deletion variants) (Table 4.3).

PCR for each marker was carried out in a total volume of 11 µl, consisting of 1 X PCR buffer, 0.3 µl of each primer pair, 0.2 mM of each dNTP, 20-100 ng of genomic DNA, 0.15 U Taq DNA polymerase and sufficient dH_2O to adjust the volume. The PCR conditions were as follows: an initial denaturation step at 95°C for 2 min, followed by 30 cycles of 45 sec denaturation at 94°C, 45 sec annealing at appropriate temperature and 1 min elongation at 72°C, and a final extension step for 10 min at 72°C. In order to avoid shadow banding in dinucleotide repeats, Betaine together with DMSO were included to the PCR with final concentrations of 1.3 M and 1.3 per cent, respectively. Buffer B was preferred for amplification of tri-and tetranucleotide repeats but was mostly not used for amplification of dinucleotide repeats, as it enhances shadow generation. Genotypes of microsatellite markers were determined by PCR amplification and subsequent analysis by PAGE and were visualized by silver staining. Examples for gels showing marker genotypes are given in Figure 4.1. Noninformative markers were left out when constructing haplotypes.

Table 4.1. List of microsatellite markers used in this study

SHFM				
Chromosome 1				
D1S496	D1S2131	D1S2733	D1S386	D1S2137
D1S1190	D1S2743	D1S451	D1S200	D1S2139
D1S1157	D1S2632	D1S2874	D1S1150	D1S3736
D1S2892	GATA129H04	D1S197	D1S3728	D1S2137
MYCL1	D1S193	D1S1661	D1S3467	
Chromosome 4				
D4S1533	D4S1650	D4S2305	D4S1091	D4S2397
Chromosome 7				
D7S531	D7S517	D7S493	D7S673	GGAA3F06
Chromosome 11				
D11S1334	D11S4114	D11S4967	D11S929	D11S2001
D11S1901	D11S1359	D11S4163	D11S2364	D11S1393
D11S4190				
Chromosome 12				
D12S1053	D12S1687	D12S1661	D12S339	D12S1620
GATA167C012	D12S85	D12S2196n	D12S1590	D12S1635
D12S2194	D12S1701	D12S1290n	D12S1627	D12S398
D12S1296				
Chromosome 14				
D14S1280	D14S607	D14S63	D14S603	D14S555
D14S306	D14S994	D14S125	D14S251	D14S606
D14S976	D14S586	D14S119	D14S268	D14S128
D14S562	ATA19H08	D14S540	D14S77	GATA168F06

Table 4.1. List of microsatellite markers used in this study (continued)

D14S745	D14S997	GGAA4A12	D14S1025	
Chromosome 17				
GTAT1A05	GATA8C04	D17S749	D17S966	D17S902
D17S960	GATA185H04	D17S1841	D17S1181	D17S2180
D17S1353	D17S689	GGAA9D03	D17S1814	D17S1302
D17S1791	D17S691	D17S2194	GATA25A04	AAT245
D17S804				
Chromosome X				
GATA31F01	DXS8063	GATA172D05	ATCT003	DXS8094
DXS6799	DXS6797	GATA48H04	DXS1047	DXS1062
DXS8020	DXS1059	GATA165B12	DXS8033	GATA31E08
HCC				
Chromosome 7				
D7S493	D7S673	D7S1808	D7S617	D7S2492
D7S2510	D7S2440	D7S2515	D7S2496	D7S632
D7S1810				
CORD				
Chromosome 17				
GTAT1A05	D17S1828	D17S906	GATA7B03	D17S1791
D17S919	D17S559	D17S1353	D17S1844	D17S945
MR-HT				
Chromosome 7				
GATA118G10	D7S627	D7S1796	D7S796	D7S692
GATA73D10	D7S1820	D7S1522	GATA23F05	D7S1817
GATA3F01	GATA5D08	D7S515	D7S501	D7S2214
D7S2555				
Chromosome 17				
GGAA9D03	D17S964	095TC5ZP	AAT245	D17S2182
D17S1293	GATA25A04	D17S1306	GATA49C09N	TTCA006M
D17S1872	D17S965	D17S2188	300xa5P	044xg3
D17S1181	D17S934			
PARp (Major Pseudoautosomal Region)				
DXYS233	DXYS228	DXYS234		
PAG-L				
Chromosome 13				
D13S787	D13S765	D13S318	D13S628	D13S631
ATA5a09	D13S325	D13S800	D13S767	D13S793
D13S893	D13S788	D13S1804	D13S795	D13S770
D13S1493	D13S784	D13S170	D13S1811	D13S1284
D13S894	D13S801	D13S317	D13S762	D13S1267
D13S779	D13S796	L18097	D13S783	D13S895

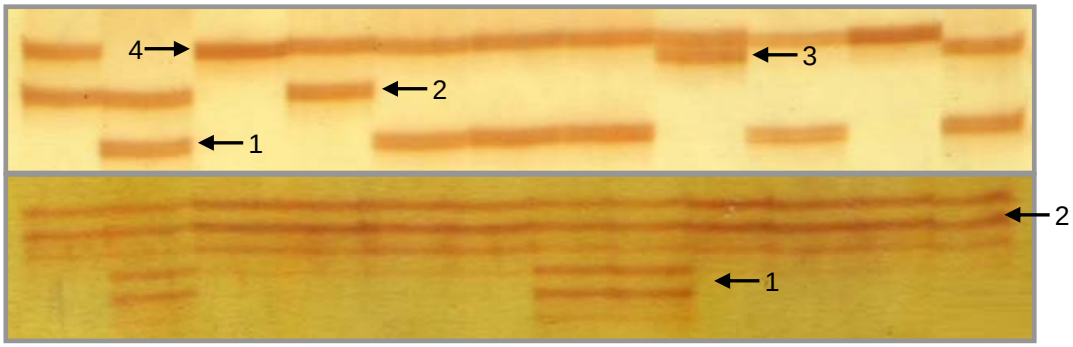

Figure 4.1. Examples for silver stained denaturing PAGE gels. Alleles resolved for a tetra repeat marker (upper panel, D14S562) and for a di repeat marker (lower panel, D1S193) are shown. Arrows indicate allele numbers scored manually according to ascending allele length.

Table 4.2. Primer sequences, properties and PCR conditions for microsatellite repeats designed in this study

Marker	Primer Sequence (5' → 3')	Size (bp)	Repeat Type	Buffer Choice	Annealing Temperature (°C)
SHFM					
D1S_39.89Mb	TTCCTCCTCCTCTTCCCTGT GGCCTGGTAACATGGACATT	177	$(CA)_{24}$	Buffer A + 8 % DMSO	TouchDown 65→55
D1S_39.90Mb	GGAACCCCCAGAGCTACACT GTGATGGTCCGTTGTAACCC	177	$(CA)_{10}$	Buffer A + 8 % DMSO	TouchDown 58→48
$D1SAAAG^{x32}$	AGATCTTGCCACTGCACTCC CTTAACATGCCTGTGCCTTG	220	$(AAAG)_{32}$	Buffer A + 8 % DMSO	TouchDown 65→55
$D1STTAT^{x12}$	TGTGCCCACATGTTCTGTTT GAATCGCTTGAACCCAGAAG	270	$(TTAT)_{12}$	Buffer A + 8 % DMSO	TouchDown 65→55
D3S190.88	GGACTTGGTCCTAAGGGGAA TGCAGAATAATGGTGAAAGACC	189	$(AT)_{21}$	Buffer A + 6 % DMSO	TouchDown 65→55
D4S26.1	CAAGGCATCTGCAATGAGAA TTTGCCCCTTTACCACTGAC	130	$(CT)_{17}$	Buffer A + 8 % DMSO	TouchDown 64→54
D4S26.4	CACACCTGGCTTTCCTTCTC CATGGTGAAACCCCATCTTT	213	$(CTTT)_{22}$	Buffer A + 8 % DMSO	TouchDown 64→54
D12S48_196	CCTGGCAACAGAGCAAGACT ACATGTAGCACATGACCCCA	127	$(AT)_{21}$	Buffer A + 10 % glycerol	52.5
D12S48_286	CATGTTCACGCCACTACACC TTTAGCATTATGGGATGTTCCTC	120	$(CA)_{24}$	Buffer A + Betaine	54.5
$D12SAAGG^{x18}$	CCACTTATGCACTGGAGCCT GATCGTGTCACTGCACTCCA	270	$(AAGG)_{18}$	Buffer A + 8 % DMSO	TouchDown 65→55
$D12SAAAG^{x47}$	GGGTGCAGGGAAAGAGAGAG TTTTTCCTTCTTTCCTCCCG	285	$(AAAG)_{47}$	Buffer A	53
MR-HT					
DXYS1	CCTTAGAATCATGGCCTCCA CCTGGGGAACAAGAGTGAGA	244	$(TTA)_{14}$	Buffer A + BSA(0.2µg/ml)	54

Table 4.2. Primer sequences, properties and PCR conditions for microsatellite repeats designed in this study (continued)

Marker	Primer Sequence (5' → 3')	Size (bp)	Repeat Type	Buffer Choice	Annealing Temperature (°C)
DXYS2	CAGAGCTGCTCAACTGAACG GATTGCTGTCTGCATCTTGG	238	$(CT)_{24}$	Buffer A	56
DXYS3	ATCCAGTGAGTGGGATGAGG GTGGTGCATGCCTGTAATCC	293	$(GT)_{24}$	Buffer A	56
DXYS4	GCCCTGTGATTAAATCCGAA TTCTCAGGGACCTTCTGTGG	141	$(AG)_{19}$	Buffer A+ 6 % DMSO	TouchDown 67→57
DXYS5	TGTGGAAGGGAAACCTCATC CCTTGAGAGGAAACAGGTGC	116	$(GT)_{25}$	Buffer A+ 6 % DMSO	TouchDown 67→57
DXYS6	CTTTGGTAGGGGTTGGGAG TGACAGAGCAAGACCCTGAA	140	$(CCCT)_{20}$	Buffer A+ 8 % DMSO	54
DXYS7	GGGCTGATAAAGAATGGGCT ACTCAGATCTTCCCTGCTGC	106	$(CCCT)_7$	Buffer A+ 6 % DMSO	TouchDown 67→57
DXYS8	TGCCTCTGTCTCTCCTTCTCA CACAAACACCTCCACACCTG	113	$(CA)_{17}$	Buffer A	57
DXYS9	GTATTCCCTTTCTTGCCTGC ATATGGGCTACATTCACGGC	180	$(CCTT)_{24}$	Buffer A	55
PAG-L					
D13S91-7	CAGAGCGAGACTCCATCTCA TCTGGATGTTTTTCCCATCA	115	$(CA)_{23}$	Buffer A	53

Table 4.3. Primer sequences designed, properties and PCR conditions for SNPs analyzed in this study

Primer Sequence (5' → 3')	Size (bp)	Included SNPs	Buffer Choice	Annealing Temperature (° C)
BMP-G1 TTAACATGGGTGAGTGCGG CAGGTGGGCAAAGACATCA	300	rs230329, rs4068800, rs2745519, rs230328, rs11585053, rs11581134, rs11585039, rs2463261	Buffer A + 8 % DMSO	56
BMP-G2 AGCACTTTGGGAGGCCAAG CTTATTGAGCAGTGCCAGACA	303	rs12756902, rs7518937, rs498734, rs230323, rs230322, rs6678976, rs3062778, rs5773675, rs2311563	Buffer A + 8 % DMSO	56
BMP-G3 GACTTCAAAAGACACCCTTGG AGTGCCTTCCCCAAAACC	322	rs2300743, rs914962, rs11806256, rs2248883, rs2676688, rs1810966	Buffer A	56

4.2.1. Denaturing Polyacrylamide Gels

Sequi-Gen GT (BioRad, USA) nucleic acid electrophoresis system assembled with 0.4 mm spacers was used for resolution of marker alleles in fine mapping studies. Denaturing instagel was used for this purpose, which was initially prerun for 15 min in

order to facilitate the gel temperature to rise to 40-45°C. The samples were mixed in equal ratio with 10 X Stop buffer, denatured at 95°C for four minutes, and chilled on ice before loading in individual slots of a sharks tooth comb. Table 4.4 shows the systems used with required amounts of instagels, APS and TEMED and the constant power to run the gels.

Table 4.4. Gel systems used for microsatellite genotyping

Gel Cast Size	Instagel	10 % APS	TEMED	Power
21 x 40 cm	35 ml	300 µl	30 µl	35 W
38 x 30 cm	45 ml	350 µl	35 µl	70 W

4.2.2. Silver Staining

Glass plates were separated gently by allowing the gel to remain intact on one of them. The gel was then transferred to staining buffer by first laying a piece of filter paper onto it and then detaching it from the glass plate together with the filter paper. It was soaked in staining buffer for 10 min. The gel was subsequently incubated in developing buffer until bands appeared (Kavaslar *et al.*, 2000). When staining reaction was inadequate, procedure was repeated after extensive washing inbetween.

4.3. Candidate Gene Approach

The mutation detection systems used in this study were Single Strand Conformational Polymorphism (SSCP) and High-Resolution Melting Curve Analysis in conjunction with DNA sequence analysis.

4.3.1. PCR Amplifications for the Analysis of the Candidate Genes

In order to detect any sequence variation in the candidate genes, intronic exon-flanking primers were designed by Primer 3 software to amplify exons and associated splice junctions of *WNT10b*, *TP63*, *BMP8b*, *HIBADH*, *CYCS*, *DRCTNNB1A* and *GUCY2D*. PCR uniqueness was checked with *in silico* PCR at UCSC database. Unless otherwise stated in the text, the PCR reactions were carried out in a total volume of 25 µl, consisting of 1 X PCR buffer, 0.2 mM of each dNTP, 400 nM of each primer pair, 20-100 ng of genomic DNA, 0.2 U of Taq DNA polymerase, and sufficient dH_2O to adjust the

volume. The cycling conditions for amplifications were as follows: an initial denaturation step at 95°C for 3 min, followed by 30 cycles of 30 sec denaturation at 94°C, 30 sec annealing at appropriate temperature and 1-2 min elongation at 72°C, and a final extension step for 10 min at 72°C. Fragments amplified for *WNT10b*, *DRCTNNB1A* and *GUCY2D* were screened for mutations by SSCP, and only fragments with aberrant migration patterns were sequenced. On the other hand, all fragments for genes *TP63*, *BMP8b*, *HIBADH*, and *CYCS* were sequenced, irrespective of observing a variant SSCP pattern or not. The primer sequences and PCR conditions optimized for the candidate genes are given in Table 4.5.

4.3.2. Analysis of PCR Products

To check the amount of amplification, a five µl aliquot of PCR product was mixed with one µl of 6 X loading buffer, loaded on a two per cent agarose gel containing 15 µg ethidium bromide, and subjected to electrophoresis in 0.5 X TBE at 150 volts for 10 minutes. Long PCR products amplified for HCC deletion mapping (Table 4.5) were run in 0.8 per cent pre-cooled agarose gels at 100 volts for four hours at 4°C. The bands were subsequently visualized over a UV light transilluminator.

4.3.3. SSCP Analysis

Each candidate gene for the particular disorder was initially screened by SSCP using the PCR products of three individuals: an affected individual, one of his/her parents, and an unrelated individual randomly chosen from the population. The analyses were carried out on nondenaturing gel matrices with crosslinking ratios of 2 per cent with and without five per cent glycerol. For fragments smaller than 200 bp ten per cent but otherwise eight per cent polyacrylamide gels were used. Whenever a variant SSCP pattern was observed in the affected individual, that region of the gene was analyzed by SSCP also in other members of the family as well as in at least 50 unrelated individuals, in order to assign this variance as a polymorphism or a mutation responsible for the particular disorder. Furthermore, the region was subjected to DNA sequence analysis to determine the nature of the variation. Lastly, if the base variation was found to create or abolish a restriction enzyme site, the samples were also subjected to restriction analysis.

4.3.4. Preparation of SSCP Gels

The gel plates were 20 cm x 20 cm in size and assembled using 0.75 mm spacers. Six ml of 40 per cent acrylamide stock was mixed with 1.8 ml of 10 X TBE, and the volume was adjusted to 30 ml by dH_2O. Three hundred µl of 10 per cent APS and 30 µl of TEMED were added, and the solution was poured between the glass plates. A 20-well comb was inserted, and the gel was left to polymerize for at least an hour. After polymerization the gel was cooled at 4°C for at least a half an hour before use.

Electrophoresis was carried out in 0.6 X TBE buffer at 4°C. Samples were mixed in equal ratio with 10 X Stop buffer, denatured at 95°C for 5 min, and immediately chilled on ice. Seven µl of each sample mix was loaded and subjected to electrophoresis at a constant power of 10 W for 10-15 hours in the BioRad DCode™ Universal Mutation detection System. Subsequently, the gel was silver stained to visualize the samples.

4.3.5. DNA Sequence Analysis

PCR-amplified fragments were purified from primers, nucleotides, polymerases and salts using QIAquick PCR cleanup columns (QIAGEN) and were sequenced on an ABI PRISM Genetic Analyzer (Applied Biosystems) at Boğaziçi University, Department of Molecular Biology or at Iontek (Istanbul, Turkey).

4.3.6. Restriction Analysis

The fifth exon of *WNT10b* was screened for the presence of a restriction enzyme *NlaIV* cutting site in the SHFM kindred and unaffected controls. Restriction enzyme digestion was carried out in a total volume of 10 µl, consisting of 5 µl of the amplified product, 1 X restriction buffer (NE Buffer 4), 10 µg BSA, 1 U *NlaIV* and sufficient dH_2O to adjust the volume. The digestions were incubated overnight at 37°C, run on a 2 per cent NuSieve gel and visualized under UV light.

4.3.7. High-Resolution Melting Curve Analysis

High-resolution melting curve analysis with LightCycler® 480 system was used for scanning control chromosomes for variant c.2846T→C in gene *GUCY2D*. Real-time PCR reactions were carried out in a total volume of 20 µl in 96-well plates, consisting of 10 µl of High Resolution Melting Master Mix, 200 nM of each primer pair (*GUCY2D*-ex15), final $MgCl_2$ concentration of 2 µM, 30 ng of total genomic DNA, and sufficient dH_2O to adjust the volume. PCR was carried out using a touchdown protocol with annealing temperatures ranging from 62°C to 54°C under the following conditions: 95°C for 10 minutes, and 45 cycles of 95°C 10 seconds, annealing at calculated temperature for 30 seconds and 72°C for 15 seconds. High-resolution melting curve data were obtained at a rate of 25 acquisitions per °C. Fluorescence data were visualized using normalization, temperature-shifting, and difference plotting and then analyzed using the LightCycler® 480 Gene Scanning Software.

Because high-resolution melting curve analysis is a heteroduplex method, i.e., it cannot discriminate between wild-type and mutant homozygotes, spikes of wild-type DNA were added to all samples individually, while screening the population. Spike amount used for each well was six ng, and results were compared to spiked and unspiked control reactions in order to address this issue. The gene scanning results were best when the amount of starting DNA was standardized as much as possible, since blood samples were derived from various origins, so the DNA quality varied.

4.3.8. Assessment of Relative WNT10b Transcript Levels

Blood samples from individuals 409, 415, 507 and 511 were available for RNA study. Total RNA was extracted from whole blood using PAXgene Blood RNA Kit (Qiagen). First strand cDNA synthesis from one µg total RNA was performed with use of M-MLV reverse transcriptase and random hexamer primers (Promega, USA). Real time quantitative RT-PCR was performed to investigate the relative transcript amounts of *WNT10b*, and *HPRT1* was used as the control gene (Table 4.6). Intron-spanning TaqMan assays were designed and purchased from Universal Probe Library (Roche Applied Science, Germany). Real-time PCR reactions were carried out in a total volume of 20 µl in

96-well plates, consisting of 10 µl of LightCycler® 480 ProbeMaster Mix, 200 nM of each primer pair, 100 nM of appropriate hydrolysis probe, 3 µl of cDNA, and sufficient dH_2O to adjust the volume. Primer-probe mix was preheated for one minute at 95°C prior to the reaction setup to avoid possible primer interactions. All reactions were performed using with three replicates per sample under the following conditions: 95°C for 10 minutes, and 40 cycles of 95°C 10 seconds, 55°C for 30 seconds and 72°C for one second. Relative transcript levels were calculated using LightCycler® 480 relative quantification software.

Table 4.5. Sequences, PCR product sizes and PCR conditions for primers designed for candidate gene search

Exon	Primer Sequence (5' → 3')	Size (bp)	Buffer + Additives	Annealing Temperature (°C)
SHFM				
WNT10b				
2	GTGTCTGATTGGGCAAGGTT	491	Buffer A + 6 % DMSO	57.5
	CTCATTGCTTAGAGCCCTGG			
3	GGAGAGTTGGAGGGGTCTG	405	Buffer A + 6 % DMSO	55.8
	GAAACCATCCCTTCCCGC			
4	TGCCTGTCAACCTTACCTCC	470	Buffer A + 6 % DMSO	53.5
	TAACCAGGCCTCAAAAGCTG			
5a	P1: TGTGCCTCTGTGTTCTGTCC	598	Buffer A + 6 % DMSO	56
	P2: GAAATCAGAGCAAAGGGCTG			
5b	P3: GCCTCTCAGGAGAGCTGGT	140	Buffer B	TouchDown 67→57
	P4: ACAGCACAGGCTGCCACA			
TP63				
1	TCCCGGCTTTATATCTATATATAC	220	Buffer A	54
	GACACATTCATAATACACAAGGCAC			
2	TCCACTTGGGTTTTCATGATAGAG	300	Buffer A	54
	GTAAGCAATATTTTGACCACCCAC			
3	GCTTGTTGTTAACAACAGCATG	281	Buffer A	TouchDown 64→54
	GAAAAGACAGGTTTAACAGAGC			
3'	GAGAGAGAGGGACTTGAGTTCTG	261	Buffer B	56
	GACCGAGAACCGCAAATACG			
4	GGCTAATATTGGGGTTTCTGG	321	Buffer A	56
	GGGGTCAGGTATGTGCGT			
5	CCTGTTGGTTCTCTCCTTCCT	306	Buffer A	56
	TCAAACAAAAATGCCCACAG			
6	CCACCAACATCCTGTTCATGC	257	Buffer B	56
	GTCTACTCAGTCCATAGAGGTGTTG			
7	GAAGGAACAACGTCAGTTTAAACCC	245	Buffer A	56
	AAAGCAGCCACGATTTCACTTTGCC			
8	GTGGTAGATCTTCAGGGGACTTTC	263	Buffer A	56
	CCAACATCTGGAGAAGATTC			

Table 4.5. Sequences, PCR product sizes and PCR conditions for primers designed for candidate gene search (continued)

Exon	Primer Sequence (5' → 3')	Size (bp)	Buffer + Additives	Annealing Temperature (°C)
9	GCTTTAGAAGTGTTCCCAGG	237	Buffer A	54
	ACACCTCCTTTCCCATTGTC			
10	TGAGGATTGACCACACTTCTAAC	287	Buffer A	54
	CATCAATCACCCTATTGCTGATC			
11	TGCTCACCATTATTTCCATGTTTGTC	257	Buffer B	54
	TCACAGAGTCTTGTCCTAAGC			
12	GGACTATAACAGTATCCGCCC	294	Buffer A	54
	CAAGATGGACCACTGGGATG			
13	CTTATCTCGCCAATGCAGTTGG	241	Buffer A	54
	AACTACAAGGCGGTTGTCATCAG			
14	GGGAATGATAGGATGCTGTGG	449	Buffer A + 6 % DMSO	TouchDown 64→54
	AAGATTAAGCAGGAGTGCTT			
15	GATGAAGTCCTAGGCCTTC	205	Buffer A + 6 % DMSO	Touchdown 62→52
	GGAAATACAACACACACACT			
BPM8b				
1	CAGGAGCCAGGACAGGTG	576	GC-rich PCR kit	Touchdown 65→55
	CCAGCTTACTCCGAGGGTC			
2	CAGCGCTGCTTTGTCTTCTA	277	Buffer A + 4 % DMSO	57
	GCTGCCTTGACCATGAGACT			
3	CGCCGGTTAATTGTTCTTTC	250	Buffer A + 4 % DMSO	57
	CACAGGAAGCCACTACCGCT			
4	TGAGTGACCCCTCTCTCCTT	282	Buffer A + 4 % DMSO	57
	CTGCCTCTCTCAGCCAGAAG			
5	CCCCATAGTAGCTGCACACA	214	Buffer B	58
	CCTCCCTGCAGATTCACTTC			
6	CTGGGTGGATTCAAGCCTCT	292	Buffer B	58
	ACCAGACCCCTCTCCACAG			
5+6	CCCCATAGTAGCTGCACACA	826	Buffer A + 4 % DMSO	54
	ACCAGACCCCTCTCCACAG			
7	GTGGGTCCTTGGAGGAGG	283	Buffer A + 4 % DMSO	55
	TTGAGGGTTTCCTGCTTCTG			
HCC				
HIBADH				
1	CACGCTCGCAGTCTGTGG	304	Buffer A + 5 % DMSO	55
	CAGGCCTTTAGTACCAGCCA			
2	TGCACCTGGTTCCTGAAAGT	398	Buffer A	TouchDown 59→55
	TTAGGTTTACAACTCCATTGGG			
3	TAGGCATGCATGAAAAGTGG	350	Buffer A	TouchDown 59→55
	CAATGAGAAAACCACCACACT			
4	ATGGCAGCTTTTCAGCAGAT	351	Buffer A	58
	TTGGCTTTATTTTTAATGAGAATCC			
5	CAGATTGGAGGCAGGATGTT	359	Buffer A	58
	TGAGCAAAGAATCCATAGGTTG			
6	CGCACTCGAGAAAATCAACA	392	Buffer A	58
	TGCTCTCCTGGGTCCTATTG			

Table 4.5. Sequences, PCR product sizes and PCR conditions for primers designed for candidate gene search (continued)

Exon	Primer Sequence (5' → 3')	Size (bp)	Buffer + Additives	Annealing Temperature (°C)
7	AGAGAAGATGGAGCATCCCC	355	Buffer A	58
	TTTTGCCTCTTACCTGAGACA			
8	CATTTTTCCTTCTTTCAAACCAA	381	Buffer A	58
	TGTGACCTAGACAATCAAAAGCA			
CYCS				
1	GGACTGGAGCCAATGAGGT	349	GC-rich PCR kit	58
	GTCTGACCACAGTCCAGGGT			
2+3	AAGTGGCTAGAGTGGTCATTCA	593	Buffer A + 8 % DMSO	57.2
	GGTGTATGAGATCTATTAAAGGATG			
DRCTNNB1A				
2	CAAAAATCACTGGAATTTAAACG	317	Buffer A	57
	GCTTGTTTGTGCACATTGG			
3	AGATGGCTTCTGGAATACGG	397	Buffer A	57
	TCTTCTCCCATCTGCAGTCC			
4	CGCTTGTATGTCTCCCAATCC	492	Buffer A	57.5
	GGAAGAAACTCCCTACAACTTAGC			
5	TTTGTGGGTGTTTATACTTTTGC	376	Buffer A	57
	CCGGTGTTGATGAATAATAATGG			
6	GCTGACACCTGAAGCAAAGC	394	Buffer A	57
	TGTTCGTGGTAGCTATTTTAG			
7	GGGAACTTTCCATGTGTTGG	344	Buffer A	57
	TATCTCTCCCCAAGGAGTGC			
8	TTTCACAAAAAGTATGCAAATCA	333	Buffer A	54
	GAAAGTGTACCTAGTACATTGTTGG			
9	ACATATTAATAAACTATGAATGGC	461	Buffer A	57.5
	TGCTTTGAAATTGCCTTAGC			
10	GTTAAGGGCAACTCCACAGC	382	Buffer A	57.5
	CCTGTTTAGCATCATGTTTTATCG			
12	GCAAAGTTGTATTTCCAGGTTCA	717	Buffer A	57.5
	TGTAAAGCATAACTGATTTGGTGT			
***DRCTNNB1A* (deletion mapping)**				
P1	P1_delF: CGATAAAACATGATGCTAAACAGG (reverse complement of 10R)			
P2	TTCTCTCCCATTGTCTAAGGGA	11,982 (P1_P2)	Long PCR + 3 % DMSO	56
P3	GCTGATCTCAAACTCCCGAC	375 (P1_P3)	Buffer B	58
P4	P1_delR: TTTTGAAATGGTCTGTGGCA	6,272 (P1_P4)	Long PCR + 3 % DMSO	56
P5	GCTGGTCTTGAAACCTGACC	8,311 (P1_P5)	Long PCR + 3 % DMSO	56
P6	CTTTCCGTGACCATCATTCC	10,116 (P1_P6)	Long PCR + 3 % DMSO	56

Table 4.5. Sequences, PCR product sizes and PCR conditions for primers designed for candidate gene search (continued)

Exon	Primer Sequence (5' → 3')	Size (bp)	Buffer + Additives	Annealing Temperature (°C)
CORD				
GUCY2D				
2	GGTCTCAGTCGCTCAGCCT ACCGAGTGCATCACCATGA	876	Buffer B + 6 % DMSO	54
3	CCAGGGTCACAGGTAGGCT GTTCTTTCTCCATTGGCTGC	492	Buffer A + 6 % DMSO	51.5
4	AATCTGGTCTGTCTGTGGGC CATCACTTTGTGGATGGTCC	472	Buffer A	Touchdown 64→54
5+6	CTGGCATCGCTCCTCAGTAT ACGGAAAGAAGACAACTGGC	555	Buffer A + 6 % DMSO	52
7	AAATCCCCAAAACTCAGCCT CTTCCCCCACTGTCTCTCTG	229	Buffer A	Touchdown 64→54
8	CAATGGAAATGAGGGGGAG GAAGGCAAGGAGGGAGAAAC	228	Buffer A	Touchdown 64→54
9+10	TGATTAACAGCCCCTTCCC GCCCTTGAAATAATGGGGAT	583	Buffer A + 6 % DMSO	52
11	GTGAGGGTGGGAGTCTTTCC TTTTCTAACTGCAGGGTGCC	259	Buffer A	Touchdown 64→54
12	TGTGTTCTGGGGGCACTC AGGTTGCTGACAAGCATCTG	260	Buffer A	Touchdown 64→54
13+14	CAGCAGCTTTACCAGCTTCC TGAATTGAAGGTCAGGAGGG	524	Buffer A	Touchdown 64→54
15	AGGCAATCGCTTCGTGTACT AGGCCCTAAAGAGGGAGATG	293	Buffer A	Touchdown 64→54
16+17	GGAGATAATGGGTGCGAAGA GTCAGAAGGGTGAGCTGAGG	469	Buffer B	Touchdown 64→54
18+19	CTCAGCTCACCCTTCTGACC CTGAGGGGGCAGTACCTGT	470	Buffer A + 6 % DMSO	52

Table 4.6. cDNA primers and probes used for quantitative RT-PCR

Gene	Primer Sequence (5' → 3')	Size (bp) on cDNA	Size (bp) on DNA	Universal ProbeLibrary Probe #
WNT10b	AATGCGAATCCACAACAACA TCCAGCATGTCTTGAACTGG	110	1388	27
HPRT1	TGACCTTGATTTATTTTGCATACC CGAGCAAGACGTTCAGTCCT	102	1712	73

5. RESULTS

5.1. SHFM

5.1.1. Recessive Inheritance and Analysis of Gene *WNT10b*

The data from the genome scan were subjected to two and multi point lod score analyses, assuming recessive inheritance with reduced penetrance (80 per cent), taking into account the general incomplete penetrance in SHFM. Due to lack of significant lod scores in multipoint analysis, fine mapping studies were conducted in loci with two criteria: relatively high two point lod scores and identical by descent (IBD) allele sharing.

Two point lod scores higher than 1.5 were obtained for single markers on chromosomes 1p34, 3q13, 4p15 and 7p22 and for two consecutive markers on chromosome 12q12-13 (Figure 5.1). Among those five loci, only for GATA91H06 at chromosome 12 the highest score was at theta=0, and at this locus all affected individuals were homozygous for an apparently IBD haplotype. To further analyze the haplotypes in the homozygosity region, thirteen additional known microsatellite markers (D12S1053, GATA167C12, D12S2194, D12S1296, D12S1687, D12S85, D12S1701, D12S1661, D12S1590, D12S1627, D12S1620, D12S1635 and D12S398) plus two identified in this study (D12SAAGG^{x18} and D12SAAAG^{x47}) were employed. An ancestral recombination event between D12S1661 and D12S1590 together with a recent one between D12SAAGG^{x18} and D12SAAAG^{x47} in individual 511 delineated the gene region to a 1.71-Mb interval (Figure 5.2). The cumulative genotyping data assuming again 80 per cent penetrance yielded maximum two-point and multipoint lod scores of 3.87 and 5.47, respectively (Table 5.1 and Figure 5.3). However, a reportedly unaffected individual (507) was also homozygous for the haplotype. Nevertheless, candidate gene analysis was carried out in this region, as SHFM is generally well-known for its incomplete penetrance. In the evaluation of the candidate genes, individual 407 who was homozygous only for part of the haplotype was disregarded, since he displayed atypical SHFM.

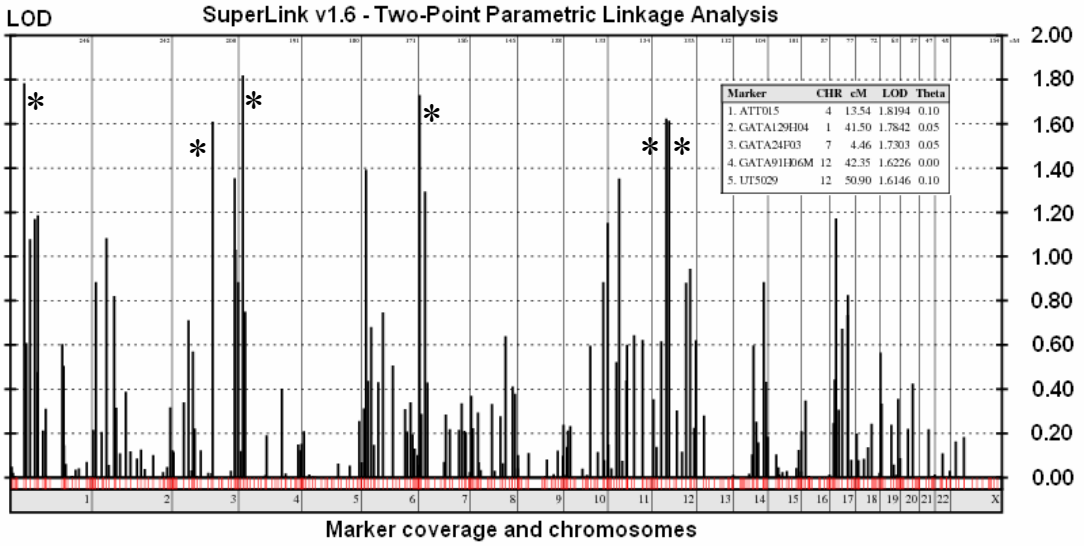

Figure 5.1. Two-point lod scores of the total data set generated by the genome scan in a recessive model with 80 per cent penetrance. Maximum scores for each marker are plotted in order of chromosomal position. Top five scores are given within the graph as a table. Loci with lod scores higher than 1.5 are depicted with asterisks (Ugur and Tolun, 2008a).

Table 5.1. Two-point lod scores at 12p11.23-q13.13 (Ugur and Tolun, 2008a)

	Position				Lod Score at θ =					
Marker	Mb	cM[1]	Z_{max}[2]	θ_{MLE}[3]	0.00	0.05	0.10	0.20	0.30	0.40
D12S1042	27.54	52.09	0.62	0.15	-8.03	-0.10	0.45	0.61	0.36	0.09
D12S1053	29.22	53.79	0.91	0.00	0.91	0.86	0.77	0.54	0.31	0.13
GATA167C12	37.48	58.19	0.22	0.15	-0.83	0.05	0.19	0.20	0.11	0.03
D12S2194	38.74	59.12	3.61	0.00	3.61	3.40	3.12	2.42	1.61	0.76
D12S1296	40.45	(59.7)	2.20	0.00	2.20	2.02	1.79	1.26	0.74	0.30
D12S1301	42.35	61.09	1.62	0.00	1.62	1.41	1.20	0.80	0.45	0.17
D12S1687	43.01	61.09	2.94	0.00	2.94	2.77	2.52	1.93	1.25	0.56
D12S85	45.62	63.46	2.94	0.00	2.94	2.69	2.41	1.80	1.14	0.49
D12S1701	46.21	64.12	3.50	0.00	3.50	3.30	3.04	2.37	1.58	0.74
D12S1661	46.89	65.12	1.32	0.00	1.32	1.17	1.01	0.67	0.36	0.13
D12S1590	47.82	65.54	1.65	0.00	1.65	1.44	1.24	0.84	0.48	0.19
D12S1627	48.07	65.71	3.57	0.00	3.57	3.26	2.90	2.10	1.24	0.47
$D12SAAGG^{x18}$	48.46	(66.0)	3.87	0.00	3.87	3.54	3.15	2.29	1.38	0.55
$D12SAAAG^{x47}$	48.60	(66.2)	1.20	0.10	-2.35	1.16	1.20	0.94	0.59	0.26
D12S1620	48.89	66.22	0.65	0.10	-2.31	0.55	0.65	0.54	0.33	0.14
D12S1635	49.32	66.22	2.58	0.05	-0.99	2.58	2.52	2.05	1.39	0.66
D12S297	50.90	68.44	1.61	0.10	-4.38	1.49	1.61	1.23	0.60	0.05

[1]Estimated cM distances are given in parenthesis.
[2]Maximum two-point lod score with Superlink (Autosomal recessive, 80 per cent penetrance)
[3]Maximum likelihood estimate of recombination fraction (θ).

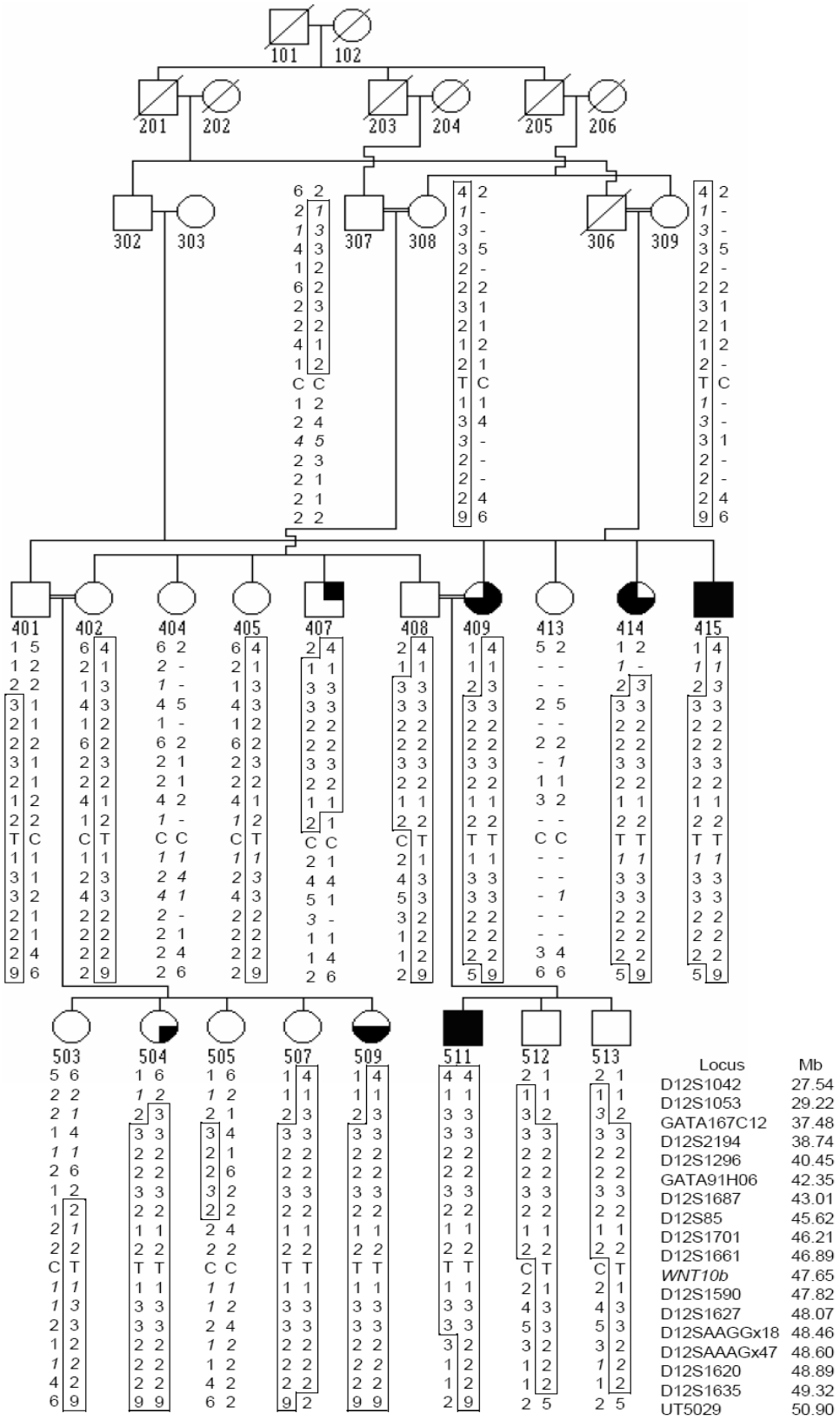

Figure 5.2. Partial pedigree diagram and haplotypes at 12p11.23-q13.13. Phenotypes in generations 1-3 are not known, except for 307, 308 and 309 (Ugur and Tolun, 2008a).

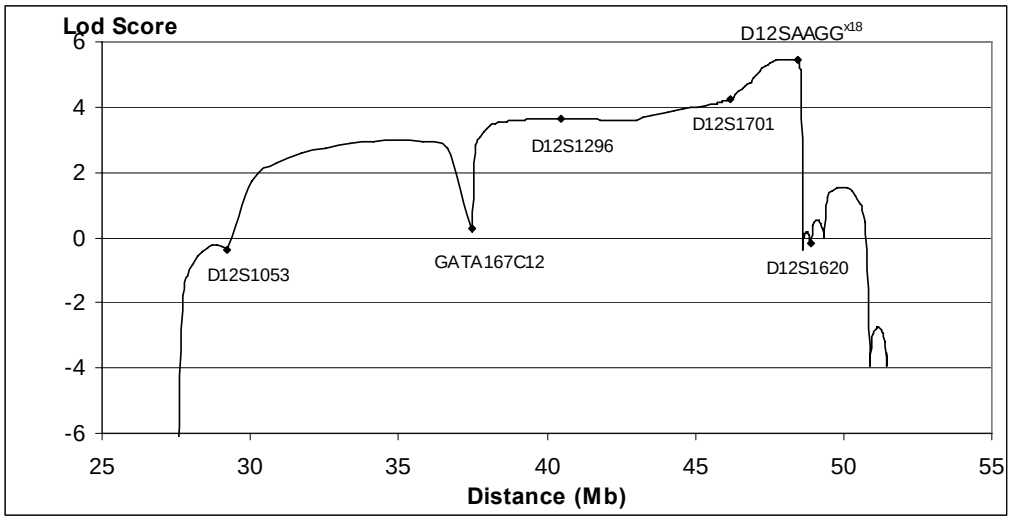

Figure 5.3. Multipoint lod score curve of 23.94 Mb region at 12p11.23-q13.13 (SimWalk). Autosomal recessive inheritance with 80 per cent penetrance was assumed (Ugur and Tolun, 2008a).

The databases reported 51 genes in the 1.71 Mb gene region identified. *WNT10b* stood out as the best candidate, being highly expressed in AER (Christiansen *et al.*, 1995) and limbs of developing mice (Wang and Schackleford, 1996). We identified a C→T transition in the homozygous state in exon 5 of the gene in all affected subjects except 407, as well as in individual 507. Several evidence indicated that this variant was a mutation and not a simple polymorphism. It was predicted to be damaging with high confidence by online tools predicting effect of amino acid substitutions on protein function, including MMB, PolyPhen, SIFT and SNPs3D (Table 5.2). 400 control chromosomes were screened for the mutation (Figure 5.4 and 5.5) to achieve at least 95 per cent power to detect a normal sequence variant with a frequency of 0.01 (Collins and Scwartz, 2002), and the mutation was not found in any. At the protein level, mutation c.994C→T leads to the substitution of an amino acid with a residue having completely different biochemical properties: positively charged arginine is replaced with a nonpolar tryptophan: p.R332W. The residue has been strictly conserved in all paralogs and across species (Figure 5.6).

Table 5.2. Effect of R332W substitution on protein function as predicted by tools online

Database	MMB	PolyPhen	SIFT	SNPs3D
Score	0.94	3.54	0	-1.59
Effect	Pathological with high reliability	Damaging with high confidence	Affects protein function	Intolerable amino acid change
Protein Accession	NP_003385	O00744	GI: 16936522	NP_003385

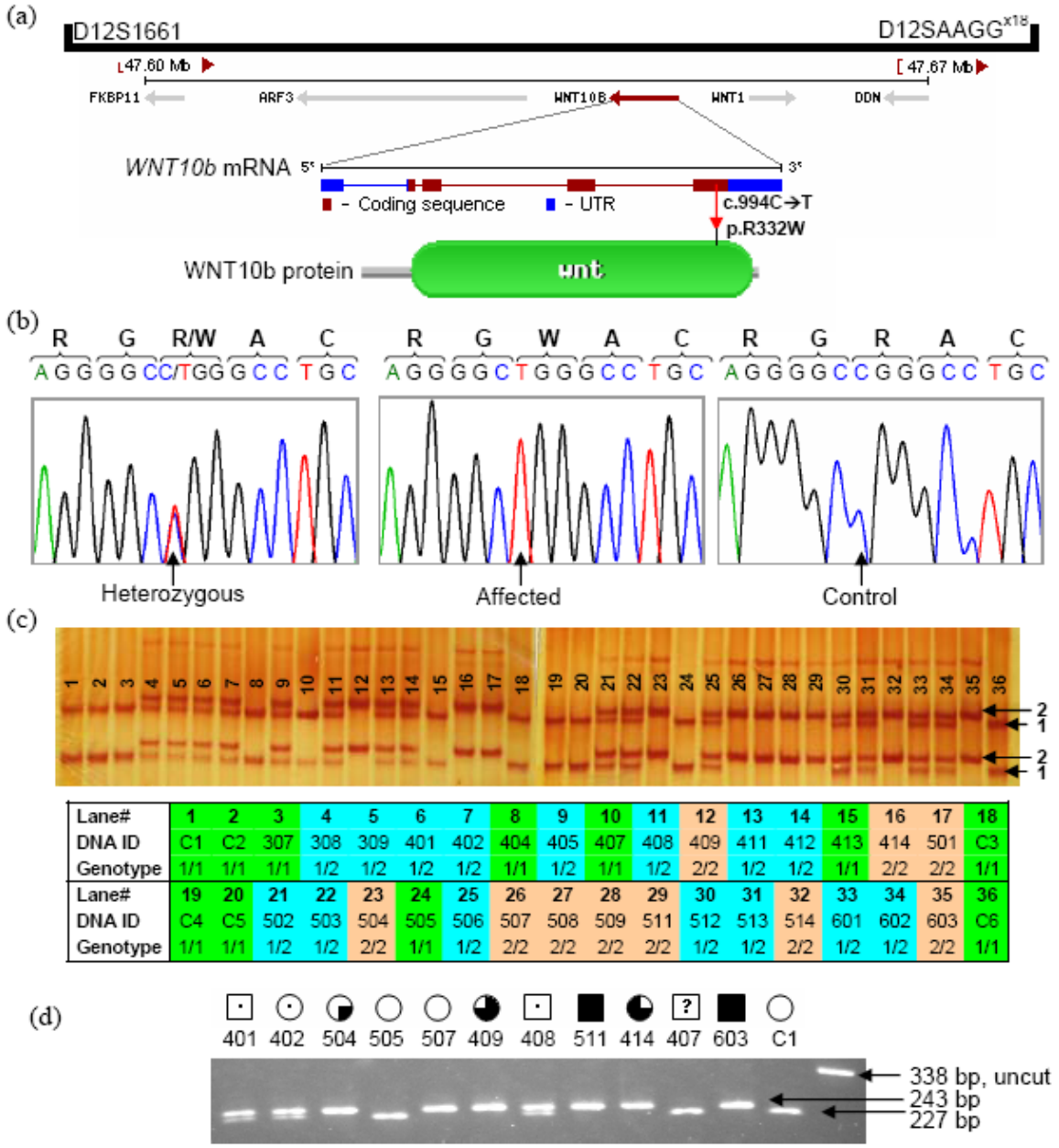

Lane#	1	2	3	4	5	6	7	8	9	10	11	12	13	14	15	16	17	18
DNA ID	C1	C2	307	308	309	401	402	404	405	407	408	409	411	412	413	414	501	C3
Genotype	1/1	1/1	1/1	1/2	1/2	1/2	1/2	1/1	1/2	1/1	1/2	2/2	1/2	1/2	1/1	2/2	2/2	1/1
Lane#	19	20	21	22	23	24	25	26	27	28	29	30	31	32	33	34	35	36
DNA ID	C4	C5	502	503	504	505	506	507	508	509	511	512	513	514	601	602	603	C6
Genotype	1/1	1/1	1/2	1/2	2/2	1/1	1/2	2/2	2/2	2/2	2/2	1/2	1/2	2/2	1/2	1/2	2/2	1/1

Figure 5.4. c.994C→T transition associated with SHFM phenotype (Ugur and Tolun, 2008a). (a) 1.71-Mb region between markers D12S1661 and D12SAAAG^{x47}. Genomic structure of *WNT10b* and schematic representation of WNT10b protein are also shown (modified from NCBI gene viewer). The sites of mutation c.994C→T and the corresponding p.R332W amino acid change are indicated. (b) Chromatograms showing the c.994C→T transition. (c) SSCP results for c.994C→T screening using primer pairs P2-P3 in the SHFM kindred and six controls (C1-C6) are shown and alleles are compiled in the table. The wild type allele bands are labeled 1 and mutant allele 2. (d) Confirmation of c.994C→T transition by PCR-RFLP assay (P2-P3 primers and *NlaIV* digestion).

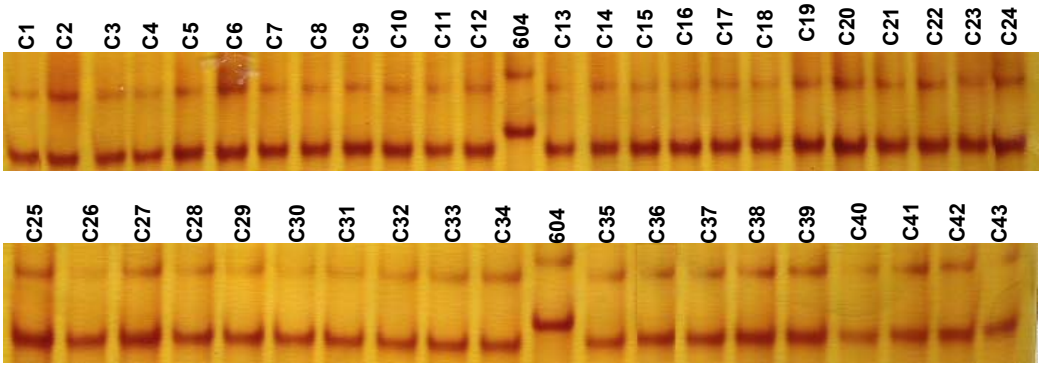

Figure 5.5. SSCP results for population screening of c.994C→T in 43 controls together with affected individual 604

		332R	
Homo sapiens	315	PDFCERDPTMGSPGTRGRACNKTSRLLDGCGSLCCGRGHNVLRQ	358
Pan troglodytes	315	PDFCERDPTMGSPGTRGRACNKTSRLLDGCGSLCCGRGHNVLRQ	358
Canis lupus familiaris	315	PDFCERDPTVGSPGTRGRACNKTSRLLDGCGSLCCGRGHNMLRQ	358
Bos taurus	359	PDFCERDPTVGSPGTQGRACNKTSHQLGSCGSLCCGRGHNVLRQ	402
Mus musculus	315	PDFCERDPTLGSPGTRGRACNKTSRLLDGCGSLCCGRGHNVLRQ	358
Rattus norvegicus	315	PDFCERDPALGSPGTRGRACNKTSRLLDGCGSLCCGRGHNVLRQ	358
Danio rerio	353	PDFCDREPAVDSLGTQGRICNKSSPGMDGCGSLCCGRGHNILKQ	396

Figure 5.6. Evolutionary conservation of WNT10b p.332R amino acid residue

To ascertain that the mutation was indeed non-penetrant in 507, repeated radiological investigations of the hands and feet were performed, and no evidence supportive of SHFM phenotype was found. Individual 407, having no foot involvement, no bone defect and no *WNT10b* mutation obviously had atypical SHFM, and so was left out in the subsequent linkage analyses for SHFM.

Linkage to chromosomes 3q13, 4p15 and 7p22 was not supported by the results of the additional genotyping with a total of 13 markers and the haplotype segregation analyses at those loci. But at 1p34.3-p32.3, an approximately 20-Mb haplotype justified with 17 additional markers and delineated by D1S496 and D1S200 was found in all affected subjects except for 510 in either heterozygous or homozygous state. This haplotype was not present in individual 507 either. *BMP8b* encoding bone morphogenetic protein 8b was chosen as a candidate gene in this region, and screened for mutations before linkage analysis for individuals later joined the study including 510 (Figure 3.1) was performed. However, no mutations could be identified.

5.1.2. Assessment of Relative WNT10b Transcript Levels

WNT10b transcript levels relative to an outsider in four mutation p.R332W homozygotes (three SHFM individuals and non-penetrant 507) were assayed by quantitative RT-PCR (qRT-PCR). The relative levels correlated well with the severity of the phenotype: highest in the severest case 415 and lowest in the non-penetrant 507 (Figure 5.7).

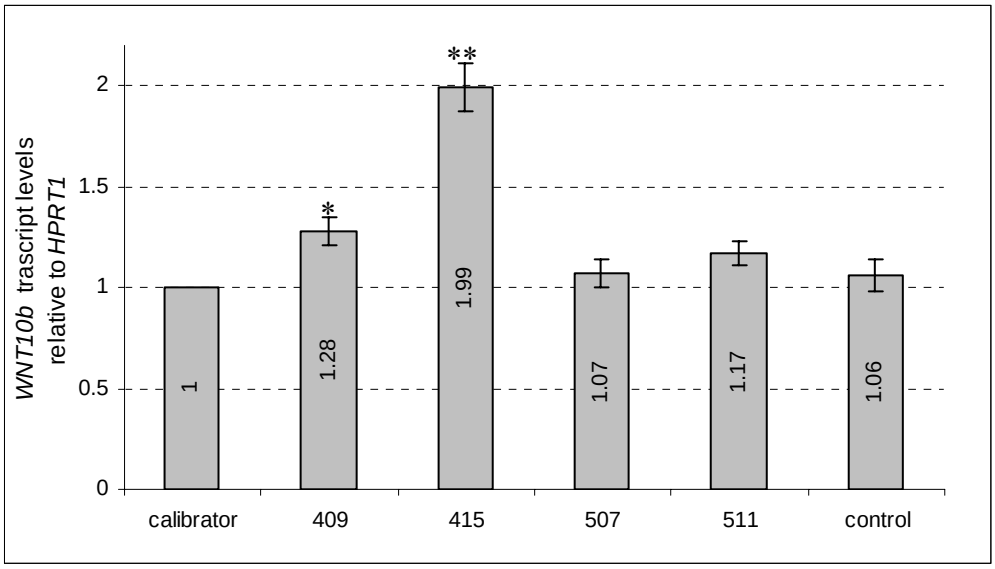

Figure 5.7. qRT-PCR of *WNT10b* transcript level to *HPRT1*. Data are mean ± standard deviation (error bars). Significant differences between 507 and other individuals are depicted with asterisks (Student's t test; *$p < 0.05$ and **$p < 0.0005$). These results are representative of three independent experiments.

5.1.3. Digenic Inheritance: Dominant Model

We investigated whether any dominant locus also was associated with SHFM in the family. Multipoint lod score analysis of the initial data set highlighted two loci, one at 7p22.3-p15.1 and the other at 14q21.3-q31.3, with lod scores higher than 2.3 (Figure 5.8). Further genotyping at those loci with 5 and 23 markers, respectively, rejected linkage to 7p, while complicating the picture at 14q.

At 14q24.2-q31.3, a haplotype of 13.1-Mb between markers D14S268 and D14S128 was shared by all affected individuals except 501, either in the heterozygous or homozygous state. Also, a centromeric but overlapping 5.3-Mb haplotype between markers D14S119 and D14S1025 was shared by all affected individuals plus 507, either in the heterozygous or homozygous state. Although that haplotype was not inherited in all cases from the same parent in a sibship, it was considered IBD since parents of all SHFM subjects were consanguineous.

In addition, amongst other loci with lower but positive lod scores, chromosomes 8p23.2-1, 11p14.3-q11 and 17p13.2-q22 were assessed significant in the light of haplotype segregation. Results of genotyping with additional 4, 18 and 9 markers, respectively, were suggestive of linkage only to chromosome 17. A 22.80-Mb haplotype delineated by D17S1791 and D17966 was found in all affected SHFM individuals either in heterozygous or homozygous state. The final genotype data yielded a multipoint lod score of 1.48. Remarkably, 8.95 Mb of this region (delineated by D17S691 and D17S966) was not carried at all by 507.

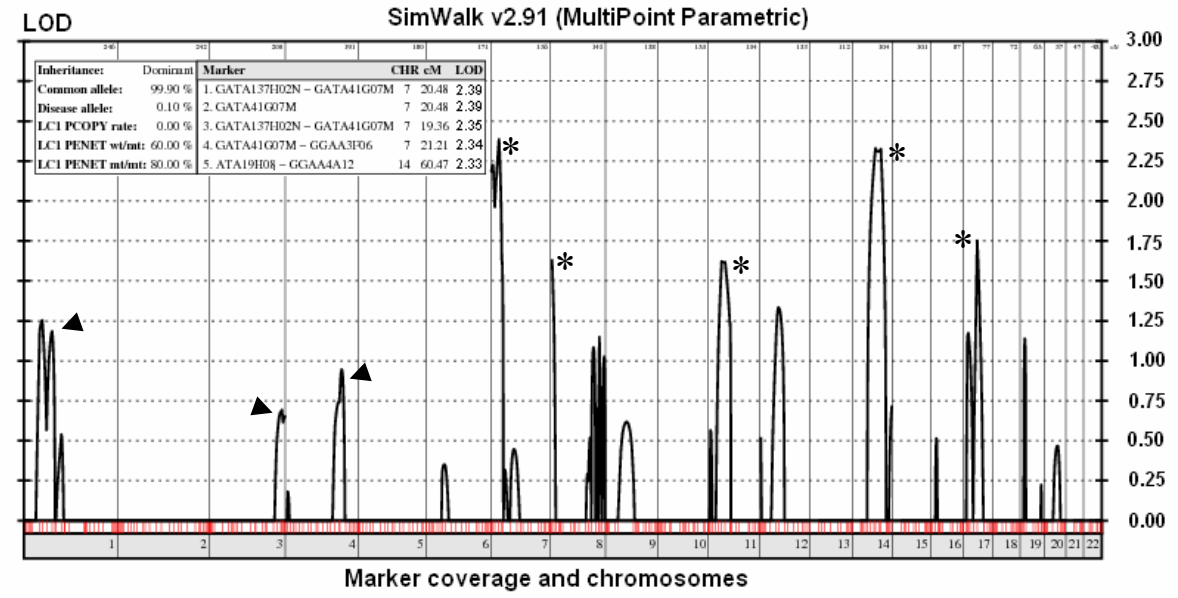

Figure 5.8. Multi-point lod scores of the total data set generated by the genome scan (SimWalk2) in a dominant model with reduced penetrance. Top five scores are given within the graph as a table and five loci fine-mapped in this study are depicted with asterisks. Arrow heads correspond to loci that had already been fine mapped in the analysis with recessive model.

5.1.4. Haplotype Analysis at Five Known SHFM Loci

We investigated by haplotype segregation analysis whether any of the five known SHFM loci could possibly be contributing to the etiology of SHFM in our family. Only two loci, SHFM4 at 3q28 and SHFM2 at Xq26.2-27.1 seemed candidates. Due to a common haplotype observed in many of our SHFM subjects at 3q28 and to similar phenotypic similarity between members of our family and SHFM4 cases reported (Ianakiev *et al.*, 2000), we screened all of the exons of *TP63* for mutations in individual 409, who was homozygous at the locus. No obvious disease causing mutation was found, but a rare insertion polymorphism (rs34201045) was detected at the alternate promoter used for transcription of the N-terminal-truncated p63 isotype (ΔNp63) (Figure 5.9). The frequency of the rare insertion variant (c.-71insAG from GenBank accession no. AF091627) in 100 control chromosomes was 0.073 and that of the frequent allele 0.69. We detected also a novel allele (c.-71insAGAG) at a frequency of 0.24 in the control samples. We did not detect any homozygotes for the rarest allele. Such homozygotes would be expected at a frequency of about 0.005 per cent, indicating that homozygosity for this allele is highly significant. All SHFM subjects but 508 were either homozygous or heterozygous for the rarest allele.

Genotyping at Xq26.2-27.1 with 4 markers excluded linkage to SHFM2. However, we identified a common haplotype at Xq22.3-25 (between markers DXS6797 and ATCT003) in all affected males but 604.

Results of genotyping studies at nine loci with significance, namely 12q13.12, 3q28 (SHFM4), 1p34.3-31.1, 14q23.2-31.3, 14q24.1-24.3, 17p13.1-q11.1, 17q11.1-q12, Xq22.3-q25 and Xq26.2-q27.1 (SHFM2), are summarized in Table 5.3, and relevant haplotypes for chromosomes 1, 14, 17 and X are given in Figures 5.10 to 5.13.

5.2. HCC

A genome scan for the family at NHLBI Mammalian Genotyping Service, followed by statistical analysis (Figure 5.14) and fine-mapping with eleven additional markers including all family members available identified a 9.02-Mb gene locus between markers

D7S493 and D7S632 (Figure 5.15). Maximum two and multipoint lod scores in this interval were 3.70 and 4.41, respectively (Table 5.4 and Figure 5.16). Two genes *HIBADH* (GeneID: 11112) and *CYCS* (GeneID: 54205) were assigned as candidate genes by position and function. *HIBADH*, or 3-hydroxyisobutyrate dehydrogenase or 3-hydroxy-2-methylpropanoate: NAD(+) oxidoreductase (EC 1.1.1.31), is a dimeric mitochondrial enzyme that catalyzes the NAD(+)-dependent, reversible oxidation of 3-hydroxyisobutyrate (3HIBA), an intermediate of valine catabolism, to methylmalonate semialdehyde. The other candidate gene was the nuclear gene encoding mitochondrial cytochrome c, *CYCS*. Cytochrome c is a component of electron transport chain in mitochondria. It accepts electrons from the b-c1 complex and transfers them to the cytochrome oxidase complex. It also acts as an apoptotic initiator; its secretion to the cytoplasm activates apoptotic initiator procaspase 9. However, no causative mutations but only polymorphisms were identified for these two genes. Polymorphisms detected are summarized in Table 5.5, and an example for SSCP and sequence analysis is given in Figure 5.17.

This locus also included gene *DRCTNNB1A* reported later as responsible for HCC by Zara *et al.*, 2006. We analyzed exons 1-7, 10 and 12 by SSCP but did not observe any aberrant pattern in the three patients available for molecular study. However, exons 8 and 9 were refractory to PCR amplification, suggesting the presence of a homozygous deletion mutation. Exon 11 was not analyzed, since it is part of a low expressed isoform.

Amplification using intronic primers P1_delF and P1_delR with a PCR kit suitable for long templates yielded an approximately 2-kb fragment rather than the 6.3-kb fragment observed from the normal individuals, supporting the presence of a deletion (Figure 5.18). Sequence analysis of the small fragment identified a deletion of 4001-bp encompassing exons 8 and 9 (Figure 5.19). The region of the deletion is flanked by an 82 – 83-bp direct repeat (Figure 5.20). In the mutant allele, a 4001-bp region together with the adjacent halves of the flanking repeat copies had been lost. This mutation c.531-439_743+348del is predicted to lead to the shift of the translational reading frame at the beginning of exon 10 and thus the truncation of the protein, 5 codons into the exon.

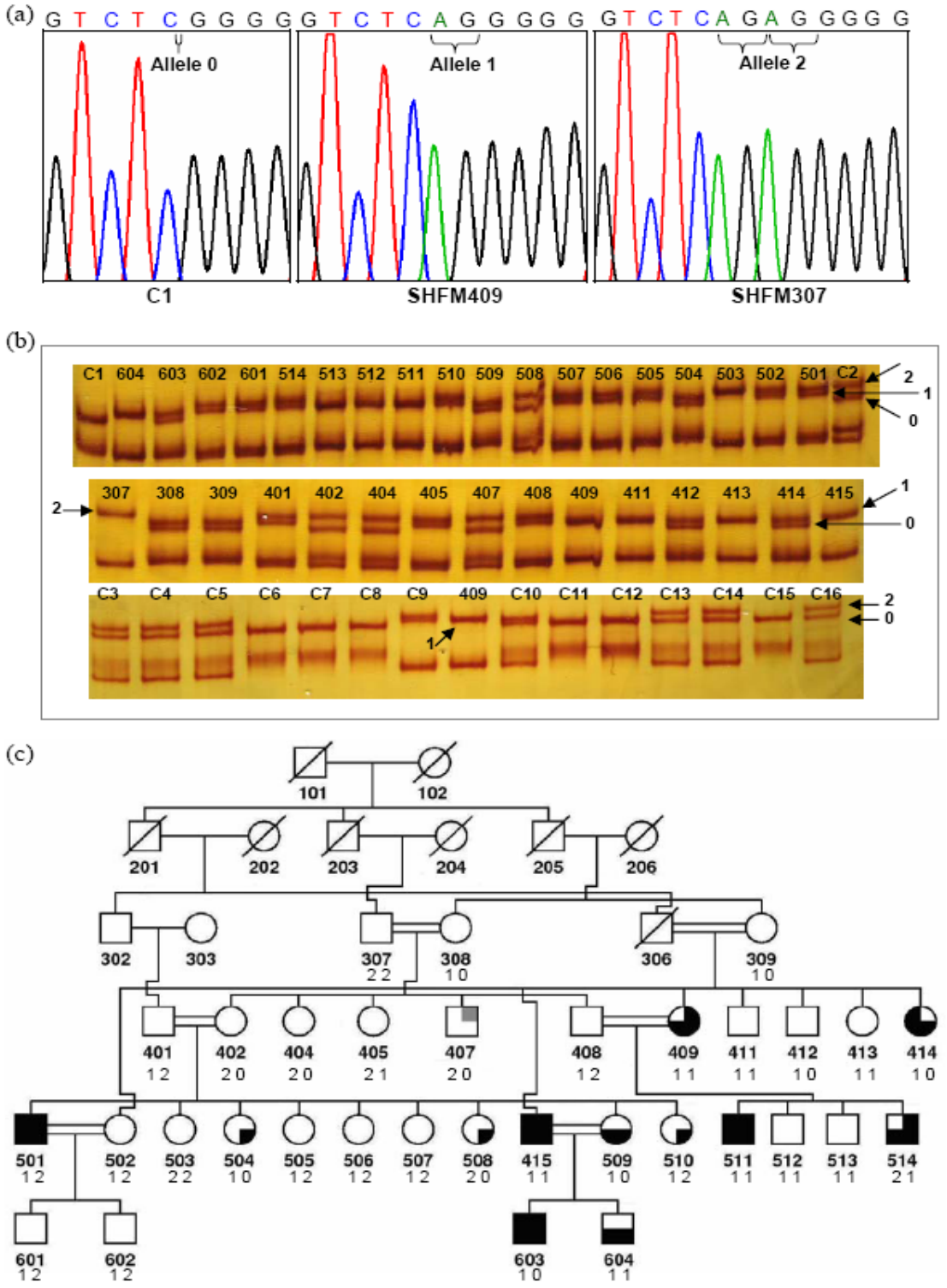

Figure 5.9. Screening of polymorphism rs34201045 in SHFM kindred and control individuals. Alleles are scored according to the number of AG dinucleotide insertions in the promoter region of *TP63* encoding the ΔNp63 isotype (0: no insAG, 1: insAG, 2: insAGAG). (a) Chromatograms showing different alleles. (b) SSCP results for rs34201045 screening. (c) rs34201045 genotypes shown on the SHFM kindred.

Table 5.3. Summary of haplotypes for all affected individuals plus individual 507 at nine loci. A plus sign indicates that the relevant mutation, haplotype or polymorphism is present.

Locus	Gene/Marker	Model	407	409	414	415	501	504	507	508	509	510	511	514	603	604
12q13.2	*WNT10b*	AR[2]	- -	+ +	+ +	+ +	+ +	+ +	+ +	+ +	+ +	+ +	+ +	+ +	+ +	+ +
3q28[1]	*TP63* (SHFM4)	AD	0 2	1 1	0 1	1 1	1 2	0 1	1 2	0 2	0 1	1 2	1 1	1 2	0 1	1 1
1p34.3-31.1	D1S496-D1S3736	AD	- -	+ +	+ +	+ +	+ -	+ -	- -	+ -	+ -	- -	+ -	+ -	+ -	+ +
14q23.2-q31.3	D14S997-D14S128	AD	- -	+ -	+ -	+ -	- -	+ -	- -	+ -	+ -	+ -	+ -	+ -	+ +	+ -
14q24.1-q24.3	D14S119-D14S1025	AD	+ -	+ -	+ -	+ -	+ -	+ +	+ -	+ +	+ -	+ +	+ +	+ -	+ +	+ -
17p13.1-q11.1	D17S1791-D17S691	AD[3]	+ -	+ -	+ -	+ +	+ +	+ -	+ -	+ +	+ +	+ +	+ -	+ -	+ +	+ +
17q11.1-q12	D17S691-D17S966	AD	+ -	+ -	+ -	+ +	+ -	+ -	+ -	+ -	+ -	+ -	+ -	+ -	+ -	+ -
Xq22.3-q25	DXS6797-ATCT003	X-R[4]	+	+ -	- -	+	+	- -	+ -	+ -	+ -	+ -	+	+	+	-
Xq26.2-q27.1	DXS8033-GATA31E08 (SHFM2)	X-R	+	+ -	- -	+	-	+ -	+ -	+ -	+ -	+ -	+	+	+	-

[1]Alleles represent the number of AG dinucleotide insertion in the promoter region of *TP63* encoding the ΔNp63 isotype (0: no insAG, 1: insAG, 2: insAGAG).
[2]Autosomal Recessive. [3]Autosomal Dominant. [4]X-linked Recessive.

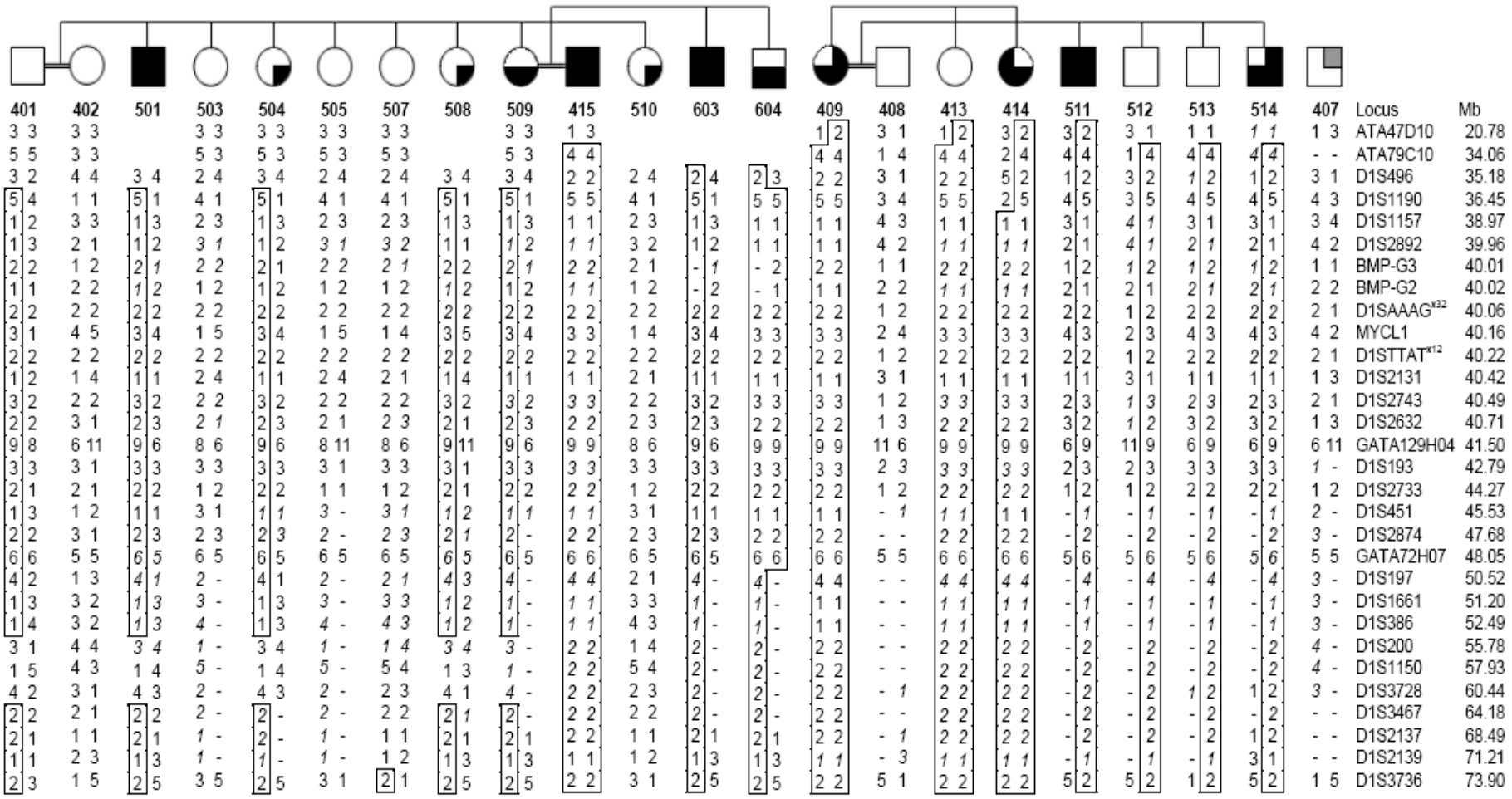

Figure 5.10. Haplotypes of SHFM kindred at 1p36.12-p31.1. Shared haplotype is boxed.

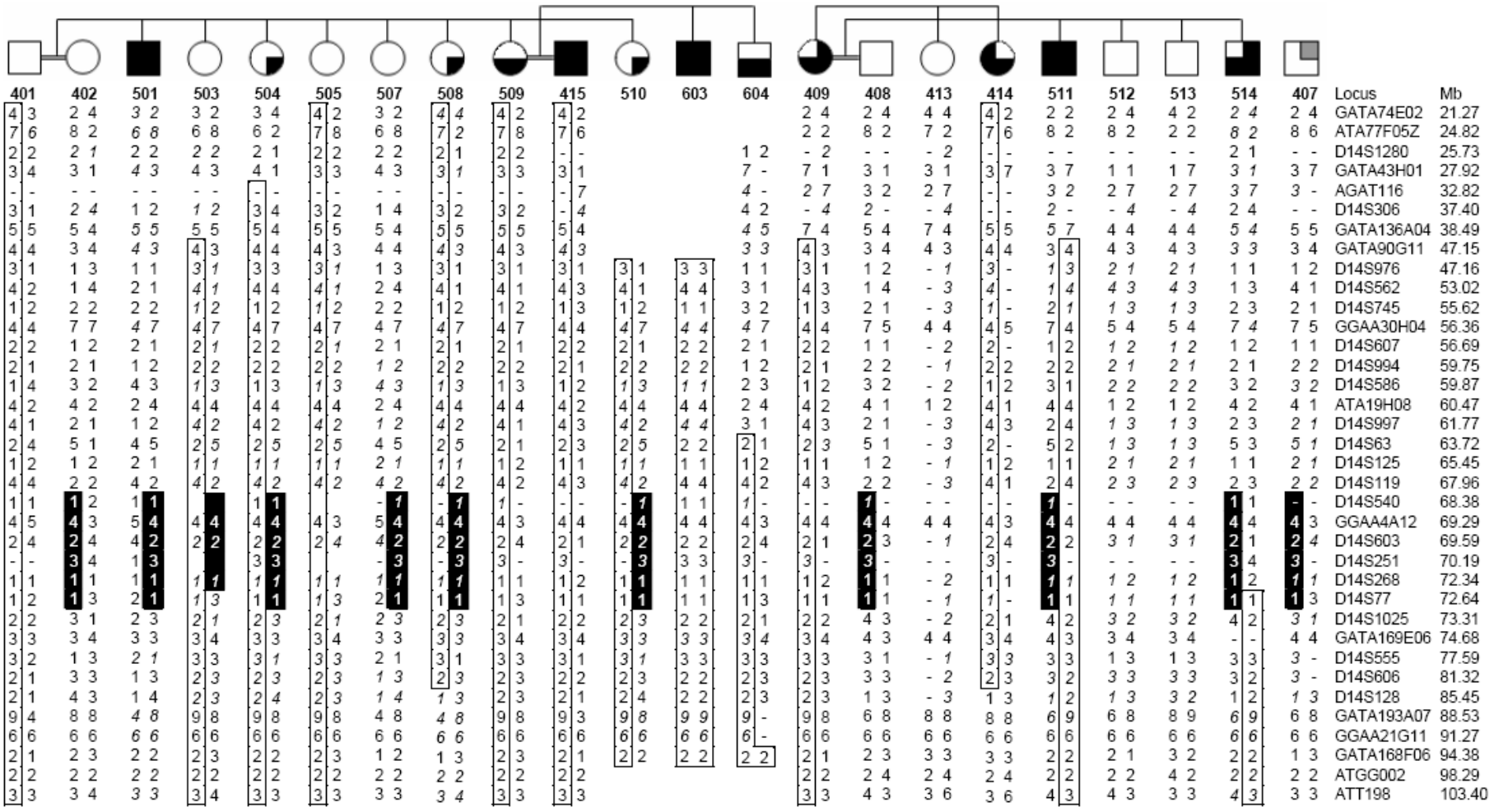

Figure 5.11. Haplotypes of SHFM kindred at 14q11.2-q32.33. Shared haplotype is boxed. An alternative haplotype at 14q24.1-q24.3 is shown in black.

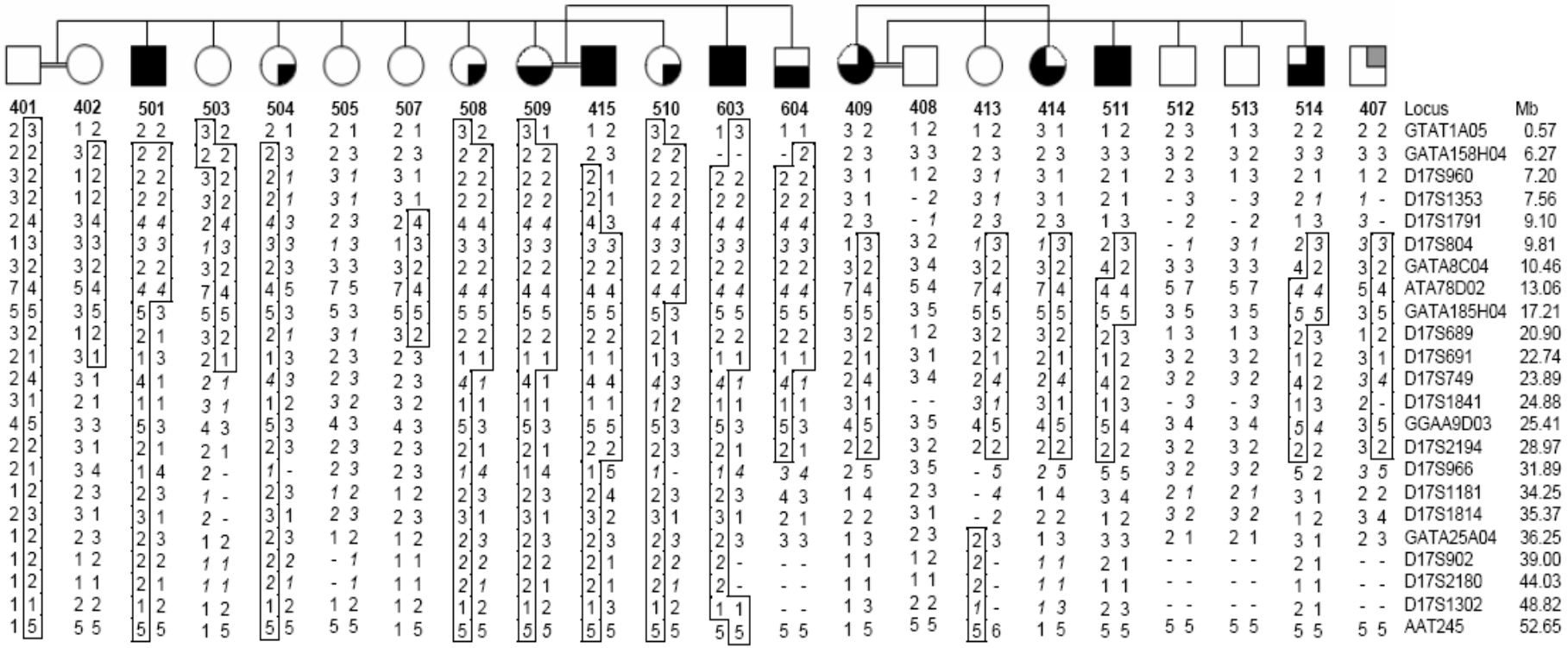

Figure 5.12. Haplotypes of SHFM kindred at 17p13.3-q22. Shared haplotype is boxed.

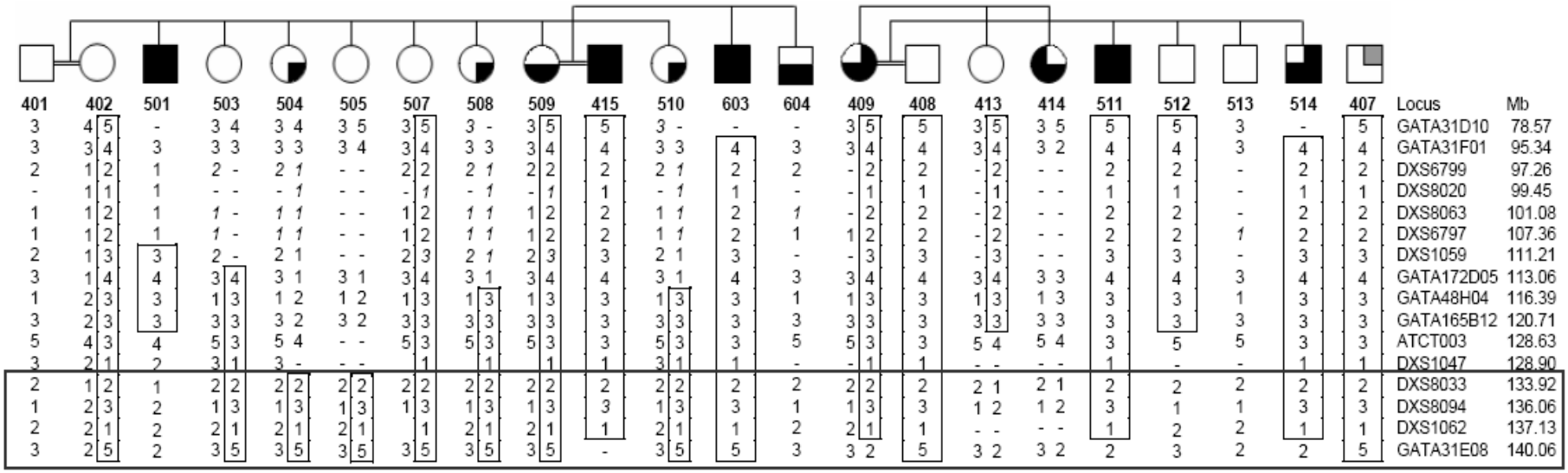

Figure 5.13. Haplotypes of SHFM kindred at Xq21.1-q27.1. Shared haplotype is boxed. At Xq26.2-q27.1, the haplotypes extending to SHFM2 locus are framed.

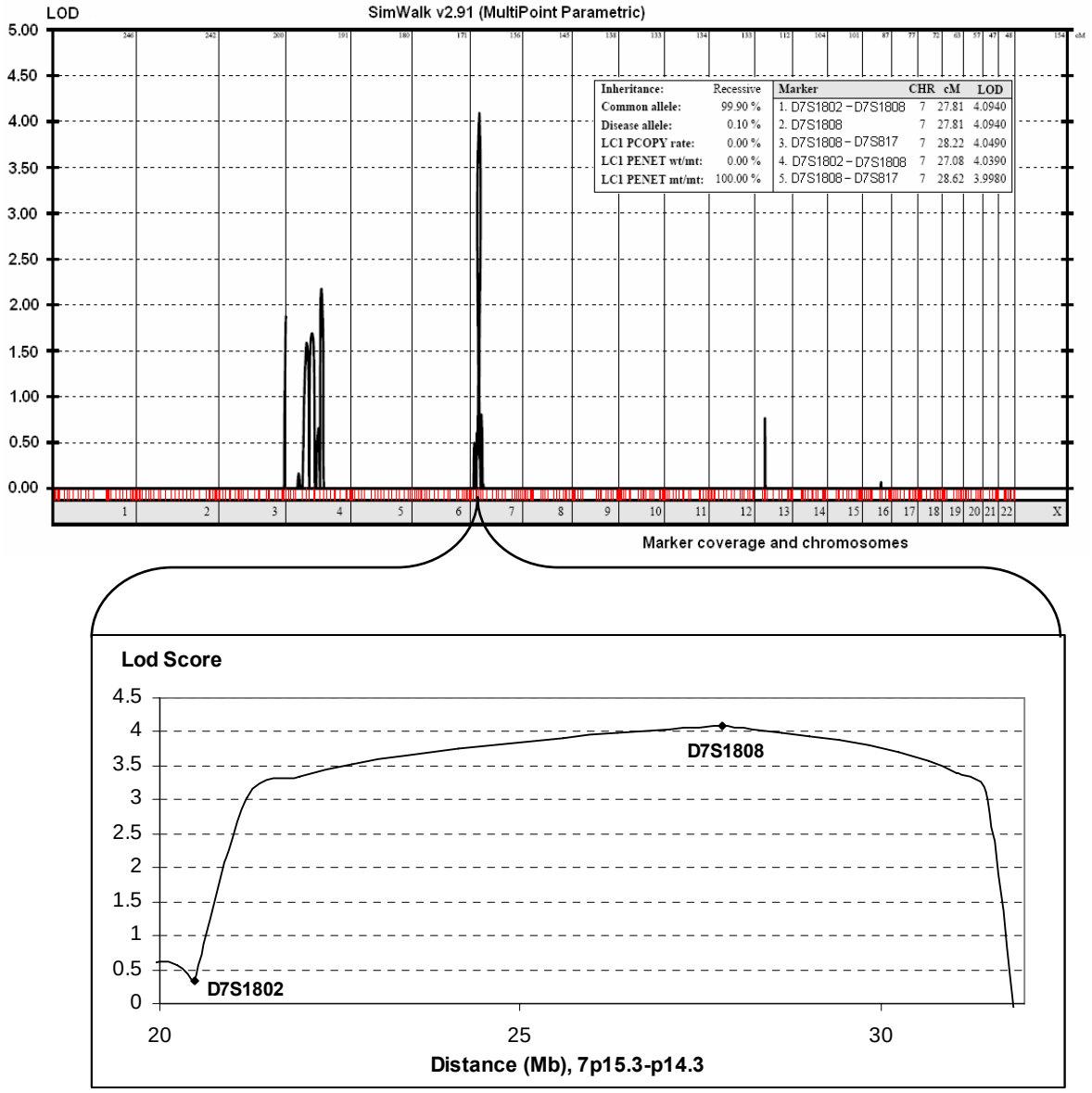

Figure 5.14. Multi-point lod scores (SimWalk2) of the total data set generated by the genome scan in a recessive model with full penetrance. Lod scores are plotted in the order of chromosomal position. Top five scores are given within the graph together with their loci and chromosomal positions. The lod score graph of chromosome 7p15.3-p14.3 is enlarged.

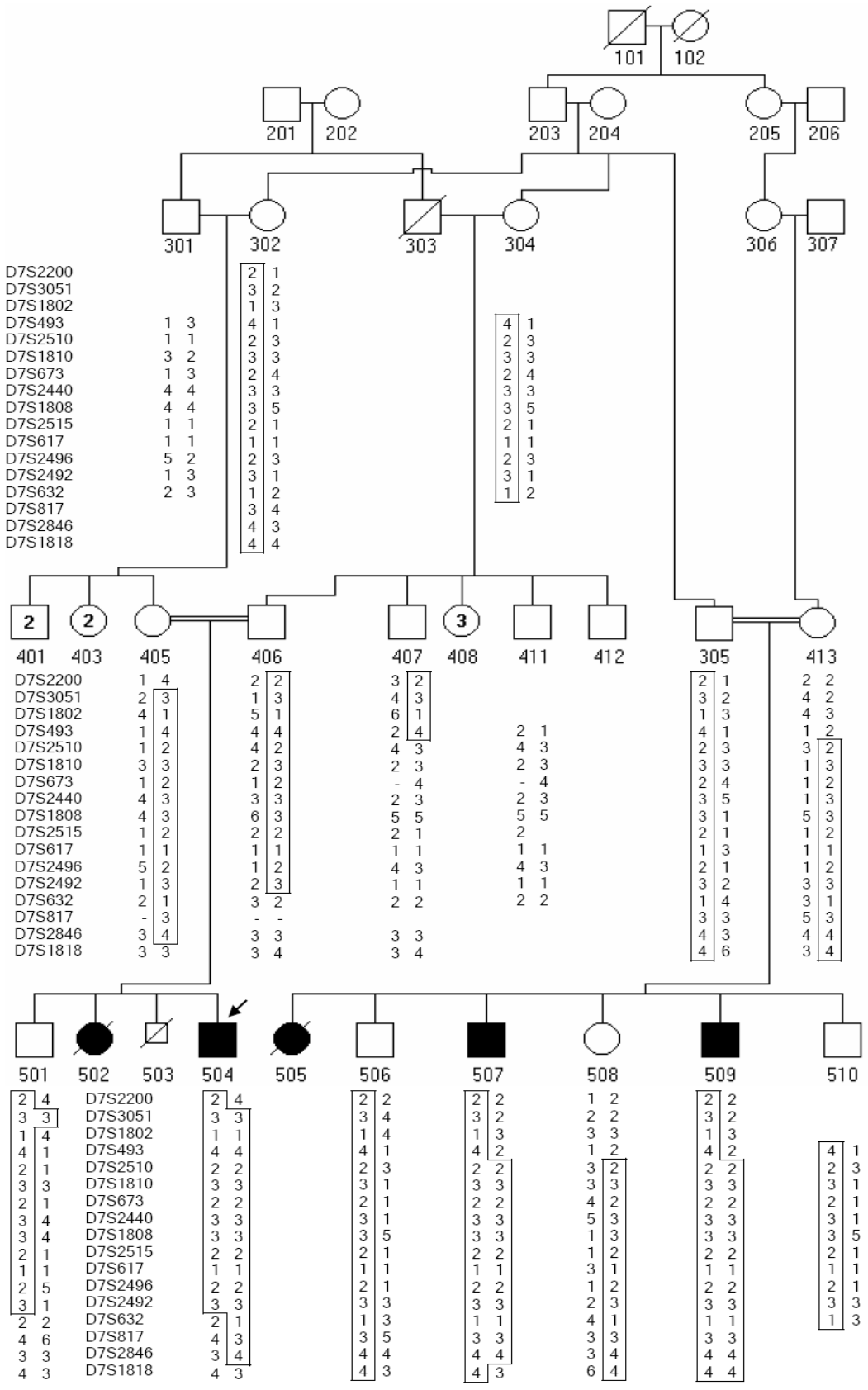

Figure 5.15. Partial pedigree diagram and haplotypes at 7p21.3-p12.3. Disease haplotype is boxed (Ugur and Tolun, 2008b).

Table 5.4. Two-point lod scores for 17 markers at the 39.92-Mb region on chromosome 7p21.3-p12.31

	Position				Lod Score at θ =					
Marker	Mb	cM[1]	Z_{max}[2]	θ_{MLE}[3]	0.00	0.05	0.1	0.2	0.3	0.4
D7S2200	9.44	18.81	0.33	0.18	-2.69	0.02	0.25	0.32	0.23	0.10
D7S3051	18.25	31.04	0.49	0.15	-∞	0.13	0.43	0.46	0.29	0.11
D7S1802	20.67	34.63	1.46	0.06	-1.14	1.45	1.41	1.02	0.55	0.19
D7S493	21.77	36.08	1.38	0.06	-1.05	1.37	1.33	0.96	0.48	0.11
D7S2510	22.14	37.35	3.58	0.00	3.58	3.18	2.77	1.95	1.14	0.42
D7S1810	22.67	(38.1)	1.78	0.00	1.78	1.60	1.40	1.01	0.61	0.25
D7S673	23.81	39.38	3.57	0.00	3.57	3.19	2.80	2.02	1.23	0.51
D7S2440	26.53	42.92	1.96	0.00	1.96	1.75	1.54	1.10	0.67	0.28
D7S1808	28.00	42.92	3.58	0.00	3.58	3.18	2.77	1.95	1.14	0.42
D7S2515	28.68	44.38	3.28	0.00	3.28	2.91	2.53	1.77	1.02	0.37
D7S617	29.29	46.59	1.11	0.00	1.11	0.97	0.83	0.56	0.30	0.10
D7S2496	29.53	47.04	3.70	0.00	3.70	3.29	2.89	2.07	1.25	0.51
D7S2492	30.08	47.44	2.37	0.00	2.37	2.11	1.84	1.29	0.75	0.29
D7S632	30.79	48.65	2.03	0.06	-3.42	2.02	1.94	1.47	0.9	0.38
D7S817	32.10	50.85	1.73	0.06	-2.31	1.72	1.67	1.27	0.77	0.32
D7S2846	38.10	58.35	0.44	0.16	-2.91	0.17	0.38	0.42	0.31	0.16
D7S1818	49.36	71.09	0.10	0.25	-∞	-0.85	-0.25	0.08	0.09	0.05

[1]Estimated cM distances are given in parenthesis.
[2]Maximum two-point lod score with Superlink (Autosomal recessive, full penetrance)
[3]Maximum likelihood estimate of recombination fraction (θ).

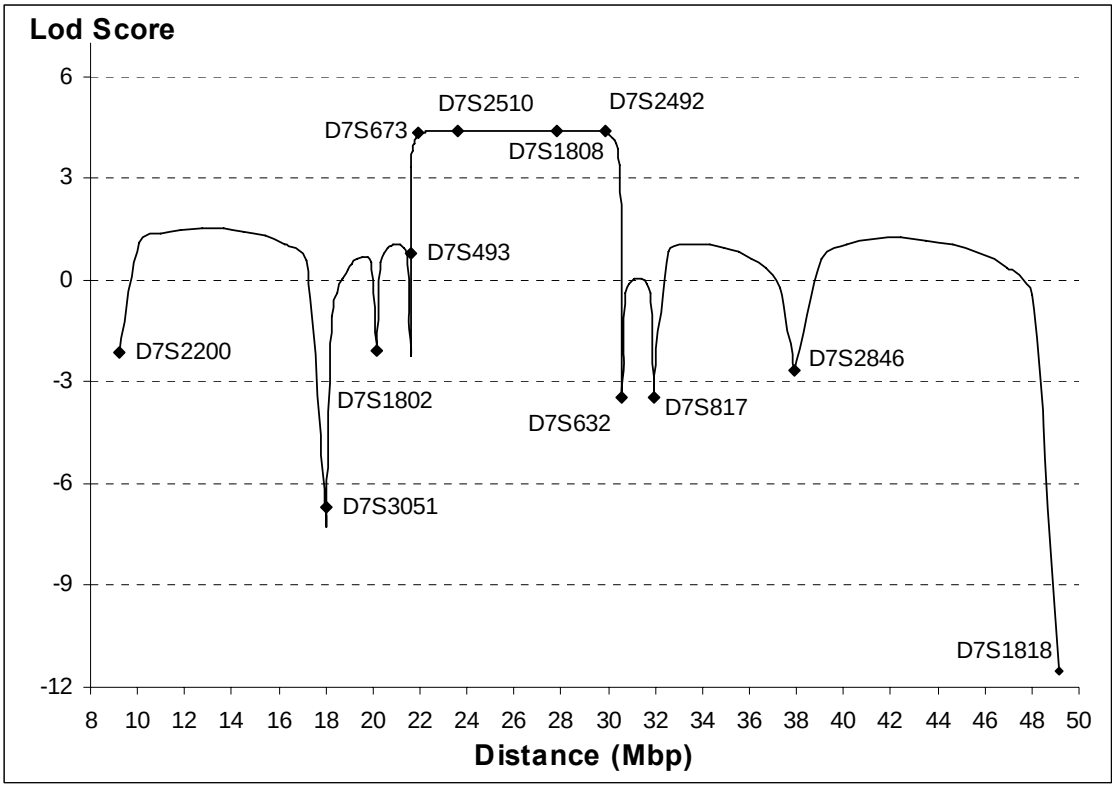

Figure 5.16. Multipoint linkage analysis at 7p21.3-p12.3 (SimWalk2). Microsatellite markers used in this study are plotted on the graph (Ugur and Tolun, 2008b).

Tablo 5.5. SNPs detected for *HIBADH*

Exon	Variation	Codon Position	Function	Consequence	Allele Frequency		dbSNP
					Estimated	Reported	
1	c.18G→T	3	Synonymous	p.R6R	0.50	0.16	rs11550134
3	g.30,704A→G	-	Intron	-	-	0.89	rs7779990
5	c.525T→A	3	Synonymous	p.G175G	0.80	-	-
8	g.136,550C→G	-	Intron	-	0.70	0.43	rs12700813

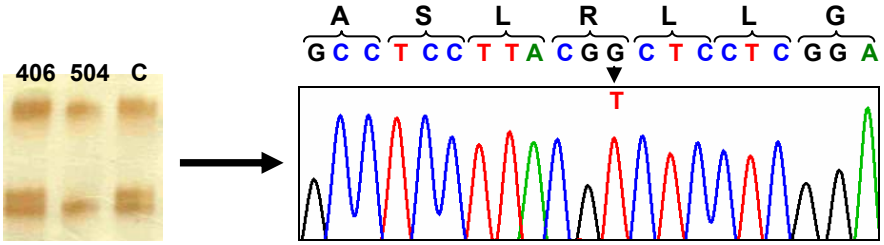

Figure 5.17. Screening of exon 1 of *HIBADH* in individuals 406, 504 and in a control individual by SSCP and identification of c.18G→T polymorphism in patient 504 by sequence analysis

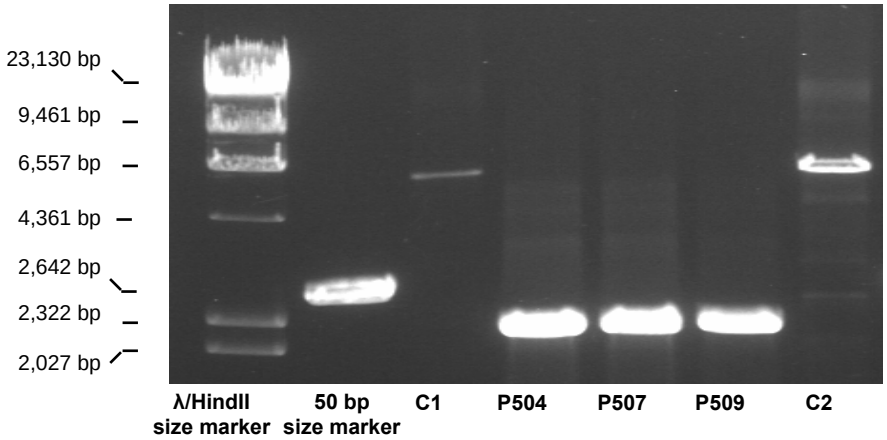

Figure 5.18. Agarose gel showing the products amplified by using primers P1_delF and P1_delR in two control individuals (C1 and C2) and three patients (P504, P507 and P509). Size markers are in first and second lanes (λDNA/HindIII and 50 bp, respectively) (Ugur and Tolun, 2008b).

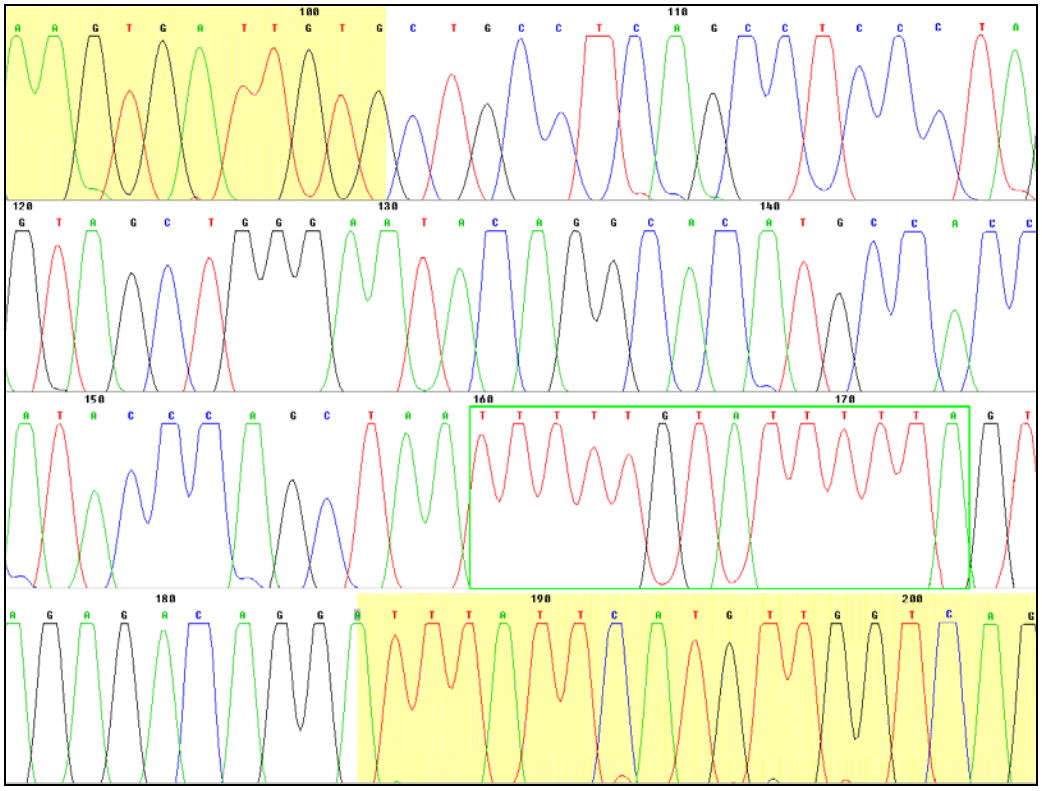

Figure 5.19. Sequence analysis of the deletion region using primer P1_delF in an affected individual. The sequence including the break-point is boxed. The upstream and downstream sequences flanking the fused repeats are shown in yellow (Ugur and Tolun, 2008b).

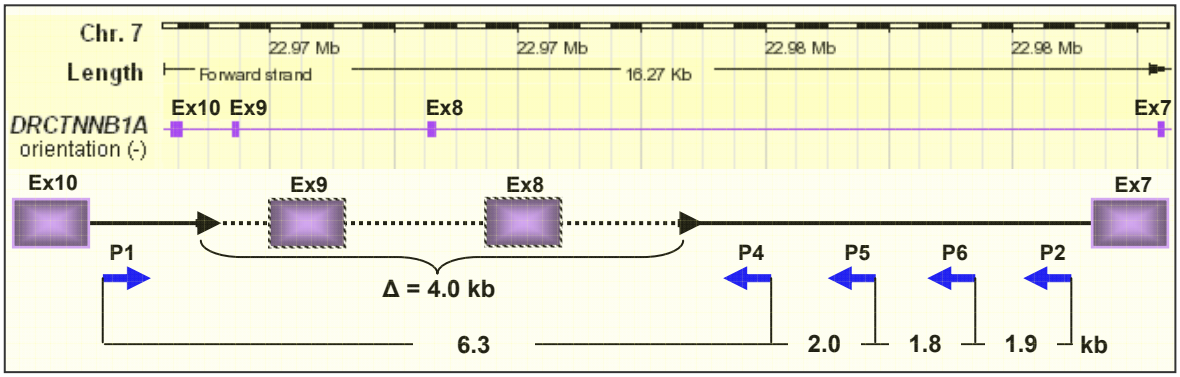

Figure 5.20. 16.27-Mb region in gene *DRCTNNB1A* encompassing exons 7 to 10 (modified from Ensembl contig view). In the lower schema, the deletion region (in dashed lines) is shown together with flanking direct repeats (arrow heads) and primers used for deletion mapping.

5.3. CORD

Genome-wide multipoint lod score analysis of the initial genotyping data with autosomal recessive inheritance and full penetrance yielded a single locus at chromosome 17p13.3 with a highly significant lod score of 4.23 (Figure 5.21). Additional genotyping with ten markers and all family members refined the gene locus to a 4.14 Mb interval between markers D17S559 and D17S1791 (Figure 5.22), with maximum two and multipoint lod scores of 4.57 and 5.48 (Table 5.6 and Figure 5.23). Two cross-over events, a recent one between D17S559 and GATA158H04 in unaffected individual 511 and an ancestral one between D17S1844 and D17S1791 defined the borders of this gene region.

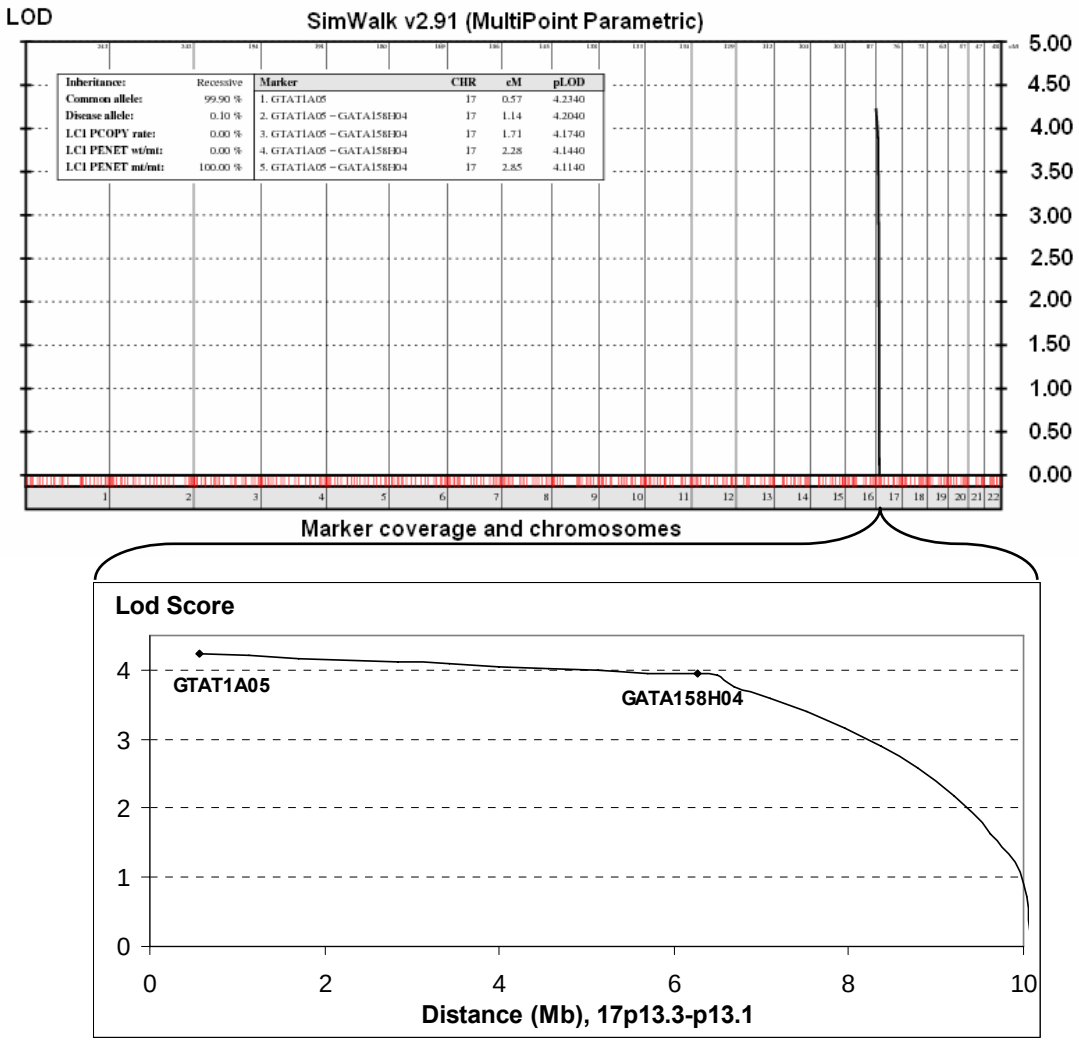

Figure 5. 21. Multi-point lod scores of the total data set generated by the genome scan in a recessive model with full penetrance. Lod scores are plotted in the order of chromosomal position. Top five scores are given within the graph together with their loci and chromosomal positions. Lod score graph of chromosome 17p13.3-p13.1 is enlarged.

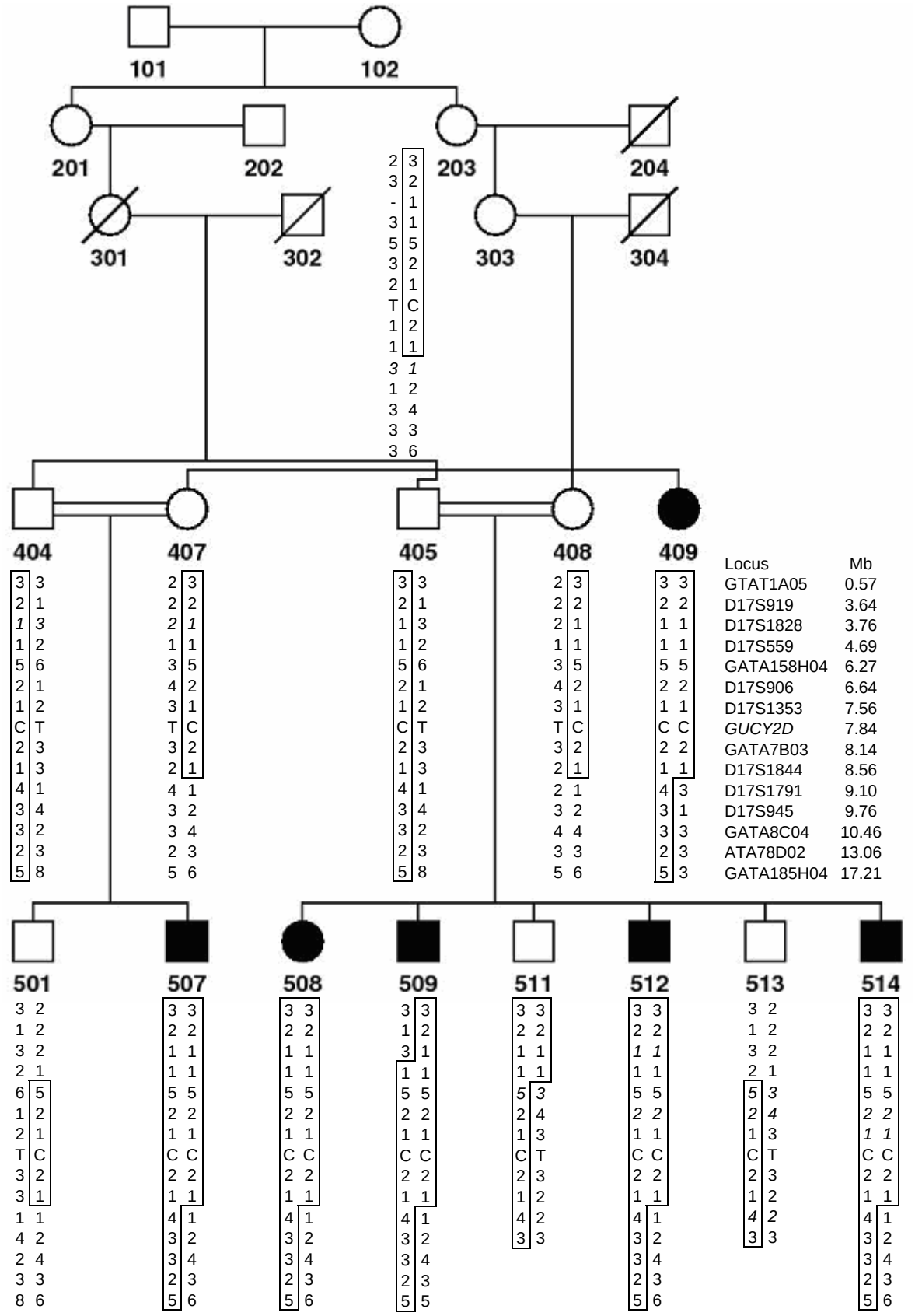

Figure 5.22. Partial pedigree diagram and haplotypes at 17p13.3-p11.2. Disease haplotype is boxed. Deduced alleles are in italics.

Table 5.6. Two-point lod scores for 14 markers on chromosome 17p13.3-p11.2

	Position				Lod Score at θ =					
Marker	Mb	cM[1]	Z_{max}[2]	θ_{MLE}[3]	0.00	0.05	0.10	0.20	0.30	0.40
GTAT1A05	0.57	4.52	2.87	0.00	2.87	2.53	2.18	1.46	0.77	0.23
D17S919	3.64	13.24	0.59	0.15	-∞	0.43	0.58	0.54	0.35	0.14
D17S1828	3.76	13.74	1.28	0.10	-∞	1.08	1.28	1.04	0.58	0.18
D17S559	4.69	(15.5)	1.86	0.00	1.86	1.71	1.53	1.14	0.71	0.28
GATA158H04	6.27	19.97	3.65	0.00	3.65	3.23	2.81	1.97	1.14	0.42
D17S906	6.64	20.99	3.24	0.00	3.24	2.83	2.41	1.56	0.76	0.20
D17S1353	7.56	23.31	3.90	0.00	3.90	3.42	2.93	1.94	0.99	0.26
GATA7B03	8.14	(23.4)	4.57	0.00	4.57	4.05	3.51	2.42	1.34	0.42
D17S1844	8.56	24.61	3.90	0.00	3.90	3.44	2.98	2.06	1.18	0.42
D17S1791	9.10	26.87	1.52	0.10	-∞	1.32	1.52	1.28	0.77	0.25
D17S945	9.76	30.55	1.12	0.15	-∞	0.82	1.10	1.03	0.66	0.22
GATA8C04	10.46	33.56	1.01	0.15	-∞	0.69	0.98	0.94	0.65	0.27
ATA78D02	13.06	(40.4)	0.33	0.15	-2.34	-0.06	0.24	0.32	0.18	0.02
GATA185H04	17.21	50.99	0.40	0.25	-∞	-0.66	0.00	0.38	0.34	0.13

[1]Estimated cM distances are given in parenthesis.
[2]Maximum two-point lod score with Superlink (Autosomal recessive, full penetrance)
[3]Maximum likelihood estimate of recombination fraction (θ).

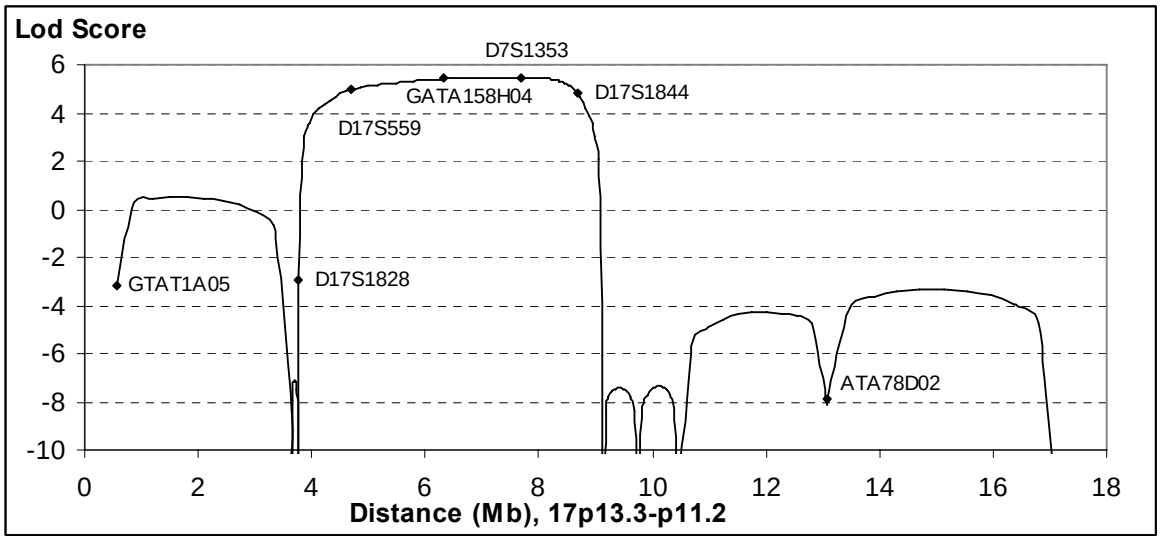

Figure 5.23. Multipoint linkage analysis of the 17.21-Mb region at 17p13.3-p11.2 (SimWalk). Autosomal recessive inheritance with full penetrance was assumed.

The 4.14 Mb region reportedly contains a very high number of genes; 171 genes in total (NCBI Build 36.3). Nevertheless, one of those genes, *GUCY2D*, stood out as likely the disease gene, since it was implicated at least in two retinal disorders, autosomal recessive Leber congenital amaurosis type 1 (LCA1) and autosomal dominant cone-rod dystrophy 6 (CORD6). Eighteen coding exons of *GUCY2D* were analyzed in thirteen fragments for mutations by SSCP. Exon 15 with an aberrant mobility shift in the patients

were sequenced, and homozygous mutation c.2846T→C was detected (Figure 5.24). This amino acid change is predicted to be a mutation rather than a polymorphism, since it was not found in 186 control chromosomes screened (44 by SSCP and 142 by HRM analyses, Figures 5.25 and 5.26) which corresponds to a power of 80 per cent to detect a normal sequence variant with a frequency of 0.01 (Collins and Scwartz, 2002) and was predicted to be damaging by various tools online (Table 5.7).

At the protein level, this transition caused Isoleucine to Threonine change (p.I949T) in the catalytic domain of the protein. Isoleucine is the most hydrophobic amino acid, while threonine is a polar uncharged one. The residue is evolutionary highly conserved and rarely replaced with the two of the eight highly hydrophobic amino acids methionine and valine (Figure 5.25, a). I949 is positioned within an alpha-helical region on the outer surface of the catalytic domain formed by a ret-GC homodimer (Figure 5.25, b).

Table 5.7. Effect of I949T substitution on protein function as predicted by four online tools

Database	MMB	PolyPhen	SIFT	SNPs3D
Score	0.11	1.41	0.02	-2.61
Effect	Neutral	Predicted to be benign	Affects protein function	Intolerable amino acid change
Protein Accession	NP_000171	Q02846	GI: 4504217	NP_000171

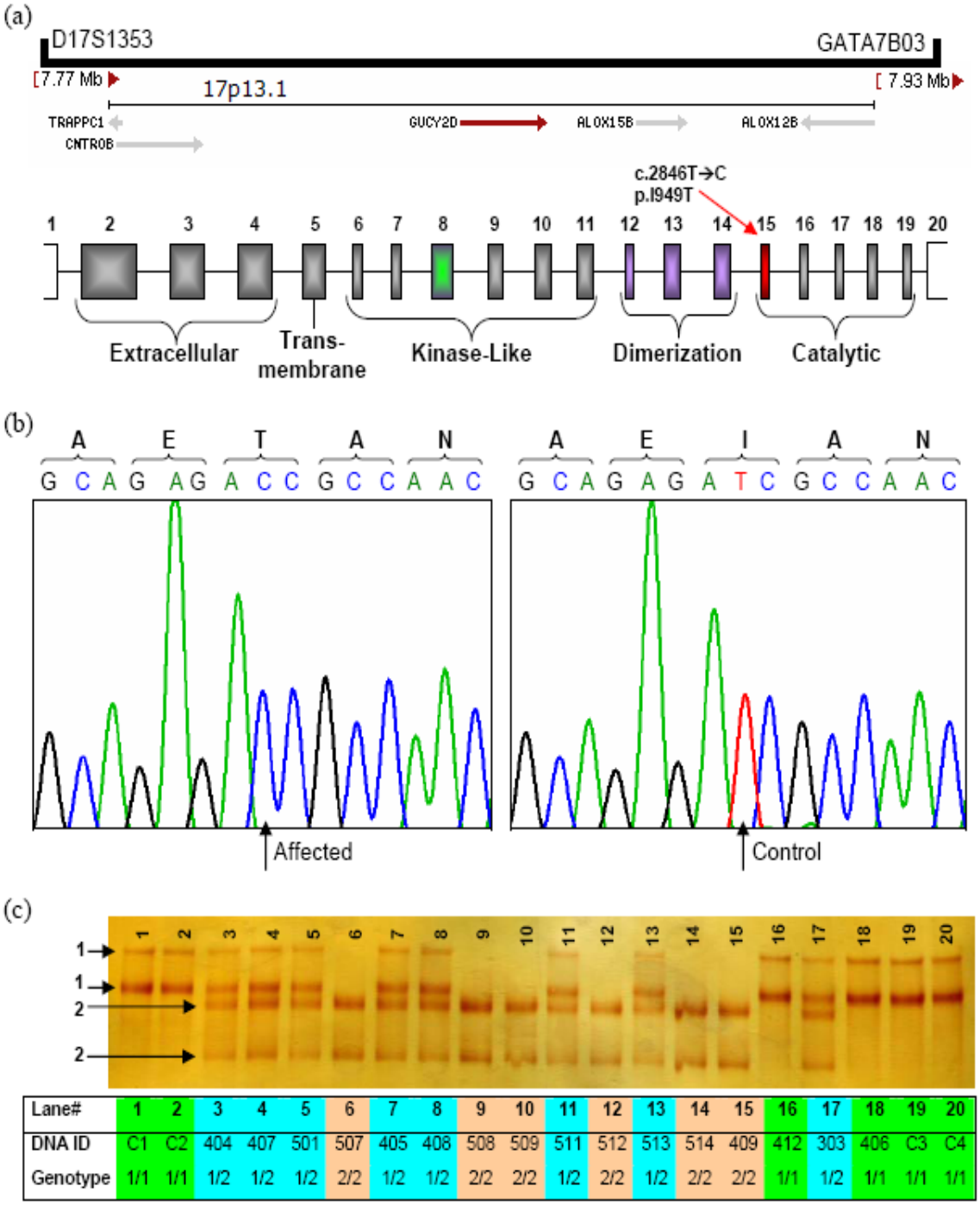

Lane#	1	2	3	4	5	6	7	8	9	10	11	12	13	14	15	16	17	18	19	20
DNA ID	C1	C2	404	407	501	507	405	408	508	509	511	512	513	514	409	412	303	406	C3	C4
Genotype	1/1	1/1	1/2	1/2	1/2	2/2	1/2	1/2	2/2	2/2	1/2	2/2	1/2	2/2	2/2	1/1	1/2	1/1	1/1	1/1

Figure 5.24. c.2846T→C transition associated with CORD phenotype. (a) 1.2-Mb region at 17p13.1 including gene *GUCY2D*. Schematic representation of *GUCY2D* exon structure and encoded domains are also shown. Mutation c.2846T→C in exon 15 corresponds to an amino acid change (p.I949T) in the catalytic domain. (b) Chromatograms showing the c.2846T→C transition. (c) SSCP results for c2846T→C screening in the CORD kindred and four controls (C1-C4) are shown, and alleles are compiled in the table. The wild type allele bands are labeled 1 and mutant allele 2.

(a)

949I

Homo sapiens	921	VYKVETIGDAYMVASGLPQRNGQRHAAEIANMSLDILSAVGTFR	964
Canis lupus familiaris	925	VYKVETIGDAYMVASGLPQRNGQRHAVEIANMALDILSAVGSFR	968
Mus musculus	924	VYKVETIGDAYMVASGLPQRNGQRHAAEIANMSLDILSAVGSFR	967
Rattus norvegicus	924	VYKVETIGDAYMVASGLPQRNGQRHAAEIANMSLDILSAVGSFR	967
Danio rerio	955	VYKVETIGDAYMVASGVPNRNGTRHAAEMANMSLDILHCIGTFK	998

(b)

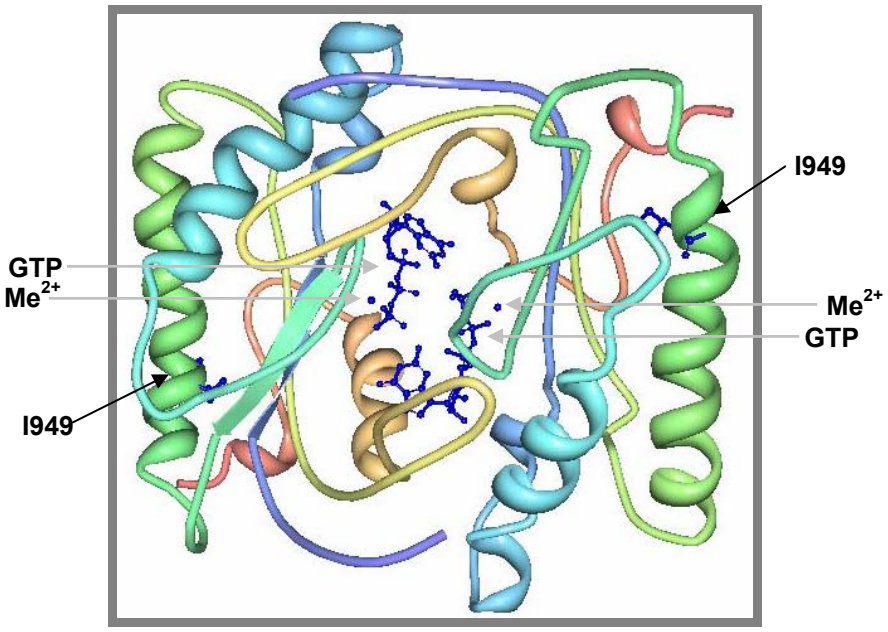

Figure 5.25. Sequence conservation and structural context of p.I949T substitution. (a) Evolutionary conservation of GUCY2D 949I amino acid across species. (b) Theoretical homodimer structure of retGC catalytic domain. The positions of mutated I949 residues in α-helixes together with bound Me^{2+}-GTPs are indicated with arrows, and their atomic structures are shown in blue. The structure was modeled using the Protein Workshop tool (Protein Data Bank, accession ID: 1AWL).

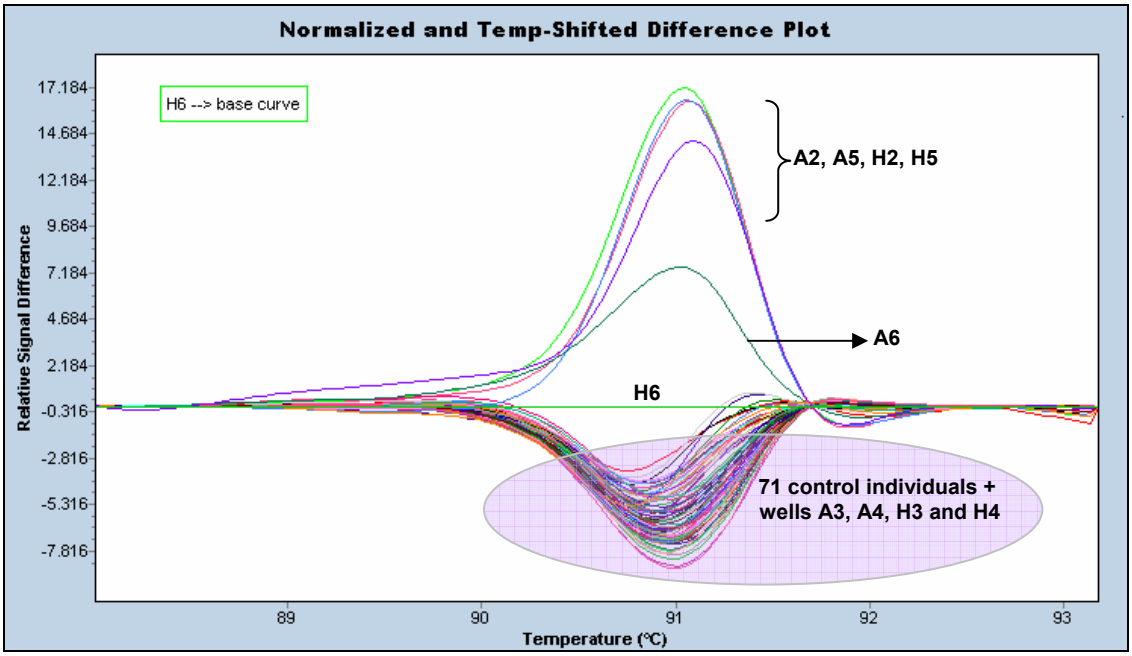

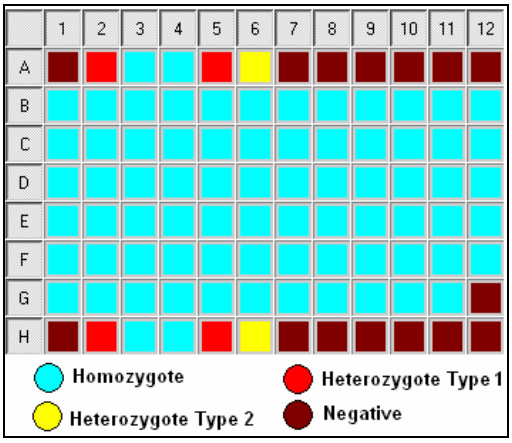

Well#	Genotyped Individual	Spike (12%)
A1 and H1	No DNA	-
A2 and H2	Heterozygote	-
A3 and H3	Mutant Homozygote	-
A4 and H4	WT Homozygote	-
A5 and H5	Heterozygote	WT DNA
A6 and H6	Mutant Homozygote	WT DNA
B1 to G11	Population DNAs	WT DNA

Figure 5.26. High Resolution Melting Curve analysis with LC480 system used for scanning 142 control chromosomes for variant c.2846T→C. As this is a heteroduplex method, i.e., it cannot discriminate between wild type (WT) and mutant homozygotes (wells A3, A4, H3 and H4), a spike DNA was added in screening the population. Spike DNA has been sequenced and so known to be WT homozygous for c.2846T. Its addition creates artificial heterozygotes (A6 and H6) in both mutant and WT homozygotes, which lead to their discrimination. In wells A5 and H5, it is shown that adding a spike DNA does not affect the melting analysis of real heterozygotes. Wells A7-A12, H7-H12 and G12 were not used.

5.4. MR-HT

A genome scan for MR-HT family had been performed previously in our laboratory with microsatellite markers of 25 cM spacing and only using DNA of four affected individuals. However, no significant linkage to a locus was found. Therefore, this time the family was genotyped with more densely spaced markers at the NHLBI Mammalian Genotyping Service. The highest and sole significant multipoint lod score was 1.88 at 7q (Figure 5.27), but even this score was far lower than 3 to accept linkage. Nevertheless, fine mapping study at this region was launched which delineated the region between markers D7S1820 and D7S1817 only in the three affected sibs (Figure 5.28). The affected cousin (502) carried only part of the haplotype in the heterozygous state. Recent clinical information suggested that diagnosis of 502 might be somewhat erroneous. This information prompted us to analyze the genome scan data once more by excluding 502 from the analysis. Chromosome 7q was again the only significant region, with lod score approaching to 2.7 this time (Figure 5.29). So, the gene for MR-HT was localized to a 15.83 Mb region at 7q21.3-q31.1 with a multipoint lod score of 2.65 (Figure 5.30). This interval contains 243 genes.

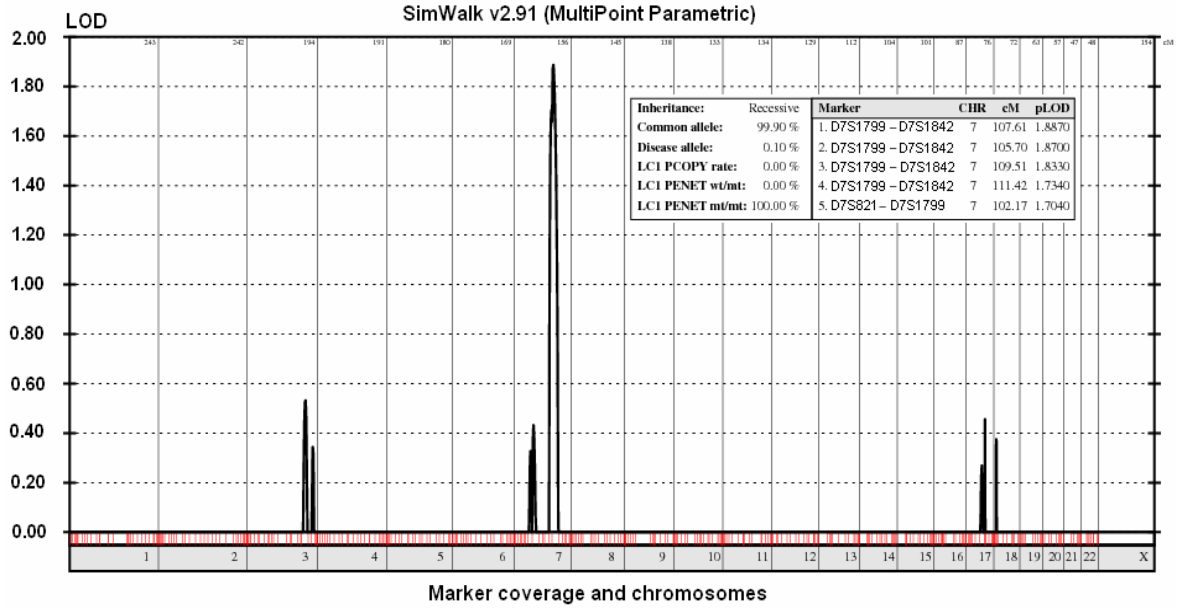

Figure 5.27. Multi-point lod scores of the genome scan data in a recessive model with full penetrance (SimWalk2). All four patients are included.

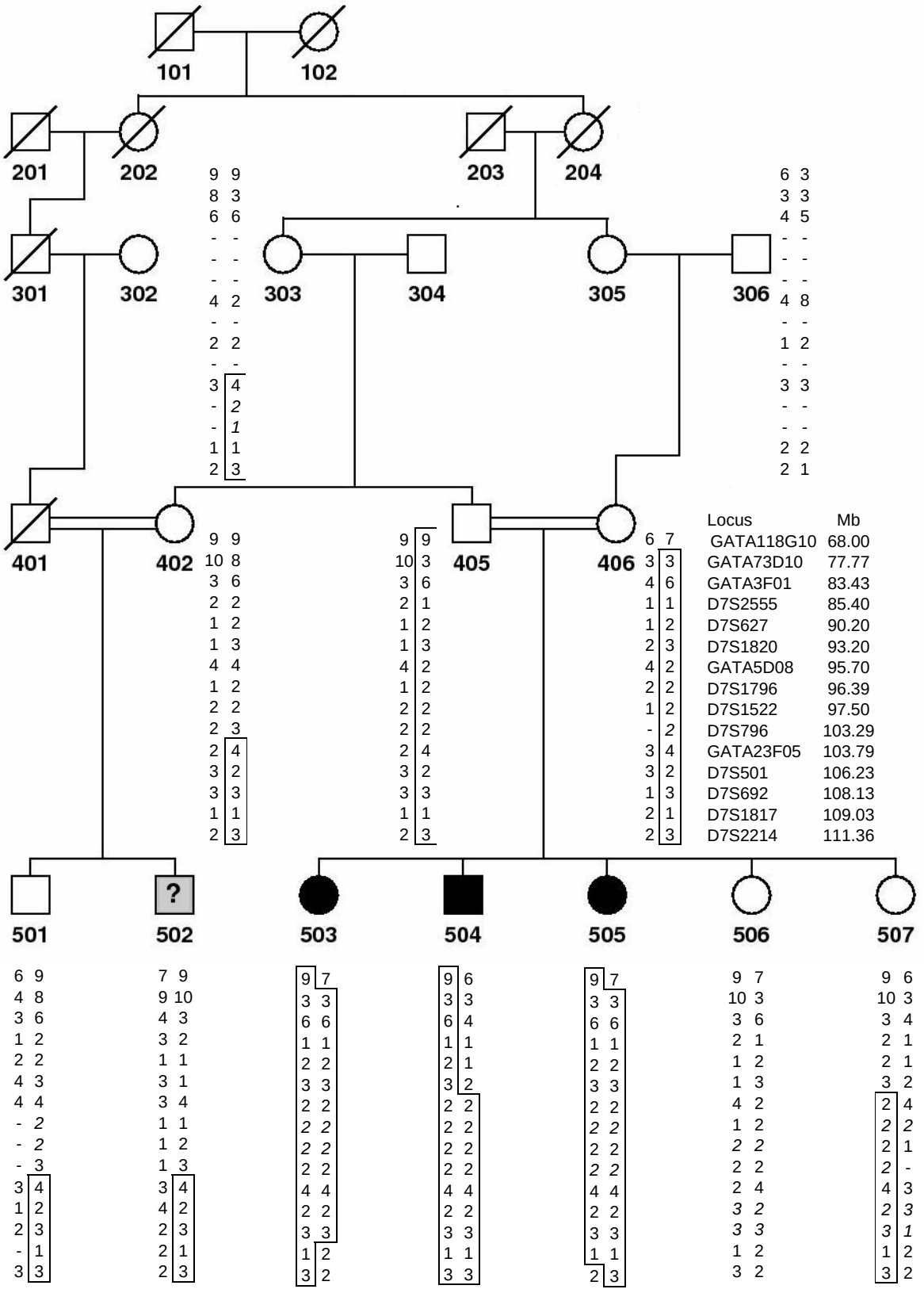

Figure 5.28. Partial pedigree diagram and haplotypes at 7q11.22-q31.1. Shared haplotype is boxed. Deduced alleles are in italics.

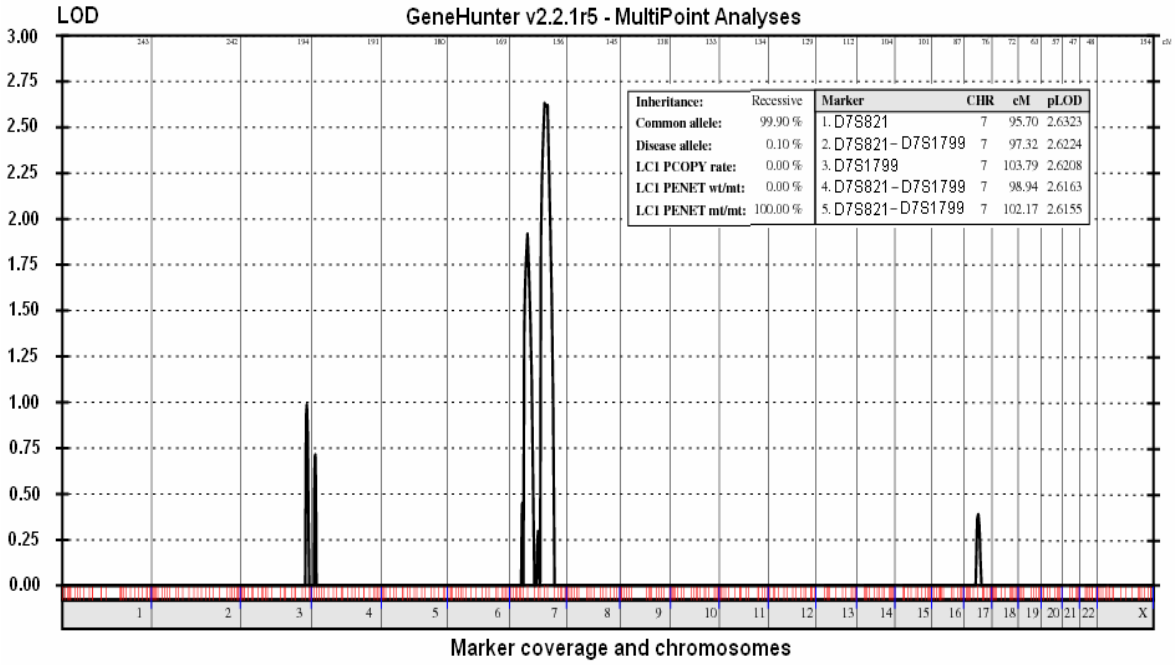

Figure 5.29. Multi-point lod scores of the genome scan data in a recessive model with full penetrance (GeneHunter). Patient 502 was excluded from the analysis.

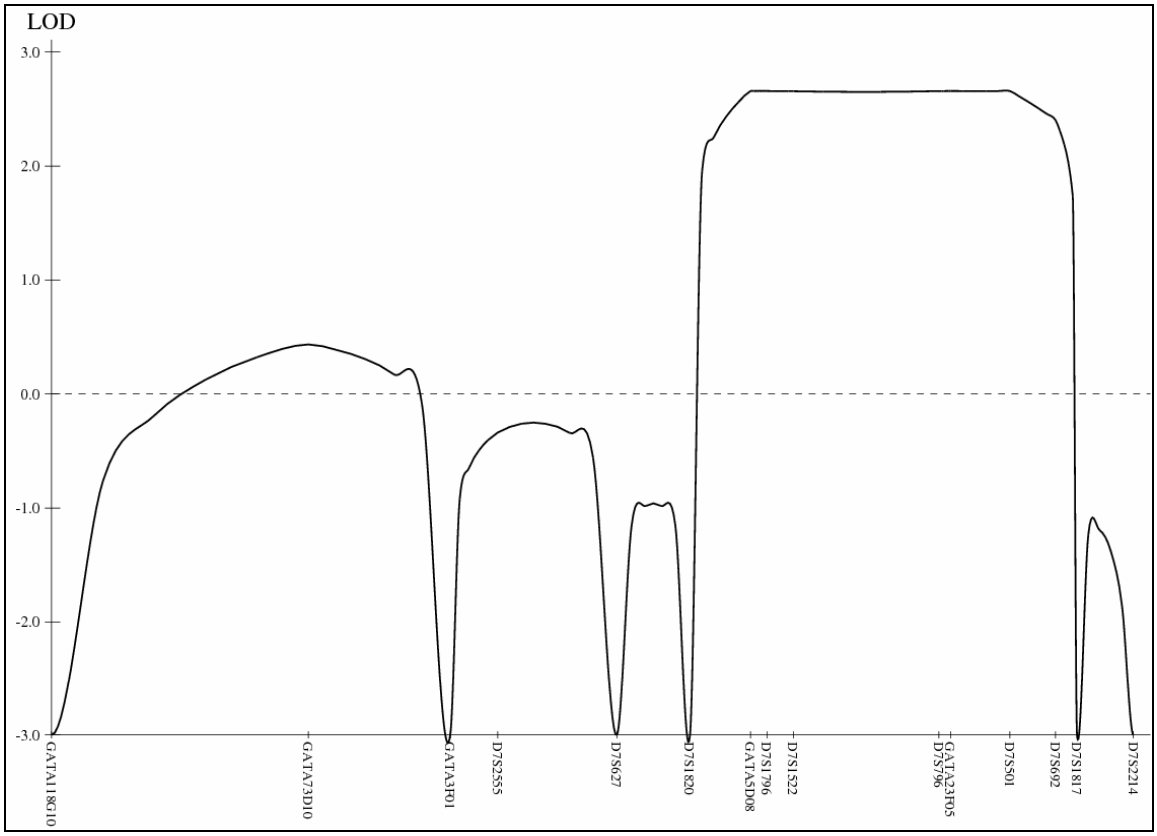

Figure 5.30. Multipoint linkage analysis of the 15.83 Mb region at 7q21.3-q31.1 (GeneHunter). Autosomal recessive inheritance with full penetrance was assumed.

A twopoint lod score of 1.35 (theta = 0) for the whole family was obtained at GATA2A12 located in the major pseudoatosomal region (PAR1). PAR1 covers a 2.7 Mb region at the extreme tips of the short arms of X and Y and is known to contain 40 genes, many of which are hypothetical. It is the site for an obligate crossover during male meiosis. This high recombination frequency at this region increases the genetic distance to approximately ten times the physical distance (Table 5.8). Further genotyping at PAR1 with 12 additional markers did not detect a shared homozygosity in all of the affected and showed that the positive lod score at this marker is due to a noninformative homozygosity of 405 for GATA2A12 (Figure 5.31). Expected crossover events in all male meioses could not be detected clearly, since DNA of 401 was not available, and not all meioses were informative. Also, many of the markers for fine mapping studies were designed for this study, so genetic distances are not available.

Table 5.8. Physical and genetic positions of markers used to fine map PAR1 region

		Map Position (cM)		
Marker	Bp	Sex-averaged	Female	Male
DXYS8	307,322	(0)[1]	(0)	(0)
DXYS9	385,607	(0)	(0)	(0)
DXYS4	501,544	(0)	(0)	(0)
DXYS5	685,651	(0)	(0)	(0)
DXYS233	818,388	(0)	(0)	(0)
GATA2A12	860,138	0	0	0
DXYS2	978,341	(0.8)	(0)	(1.6)
DXYS3	1,282,729	(2.9)	(0)	(5.8)
GGAT3F08	1,306,724	3.18	0	6.1
DXYS228	2,631,455	13.04	2.82	25.98

[1]Estimated cM distances are given in parenthesis

Chromosome 17 was analyzed before the genome scan at NHLBI Mammalian Genotyping Service, due to the high incidence of homozygosity in the patients. However, a shared region of homozygosity in all affected patients could not be identified, as shown in Figure 5.32, where the genotyping results before and after the genome scan were pooled.

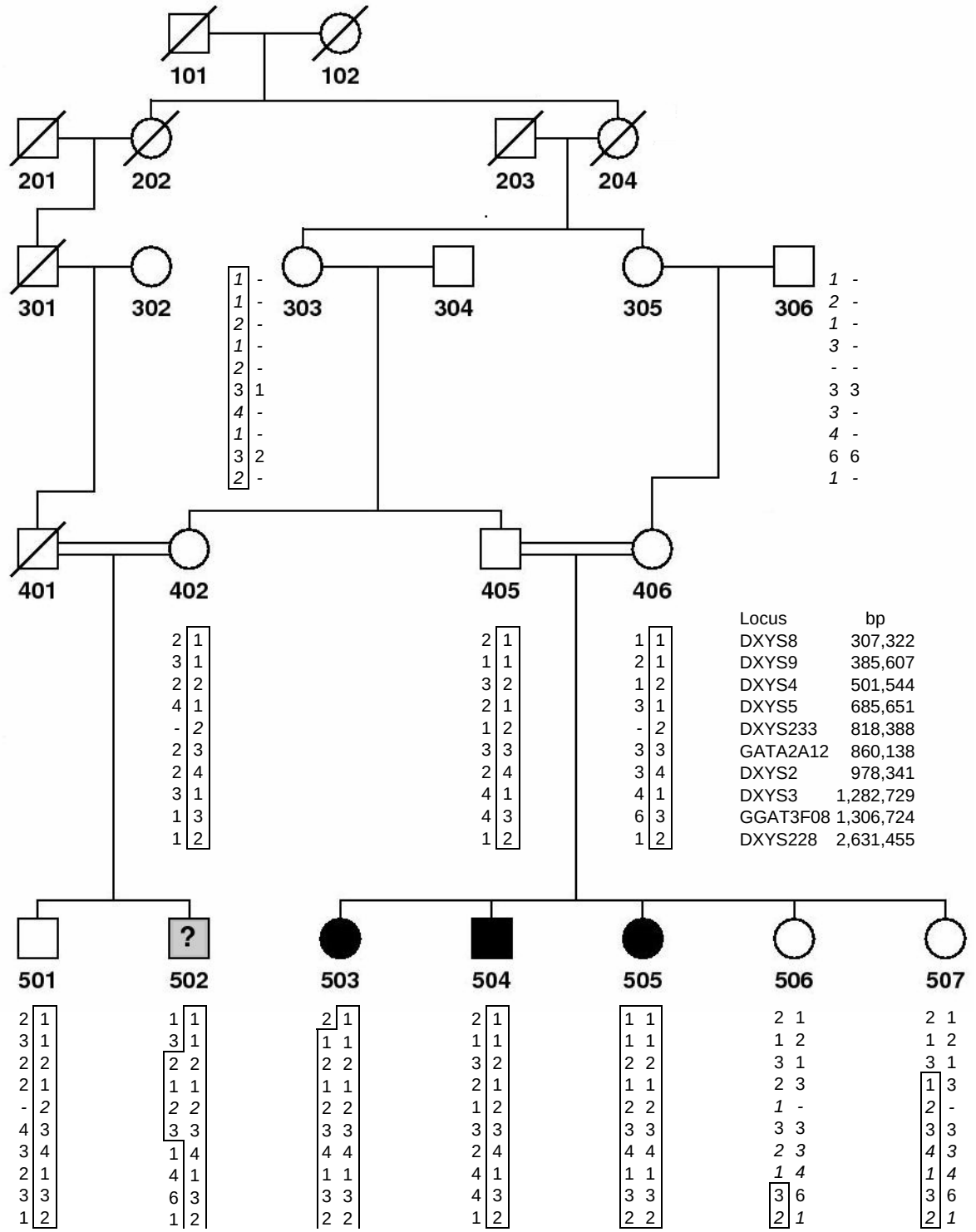

Figure 5.31. Partial pedigree diagram and haplotypes at PAR1. Shared haplotype is boxed. Deduced alleles are in italics.

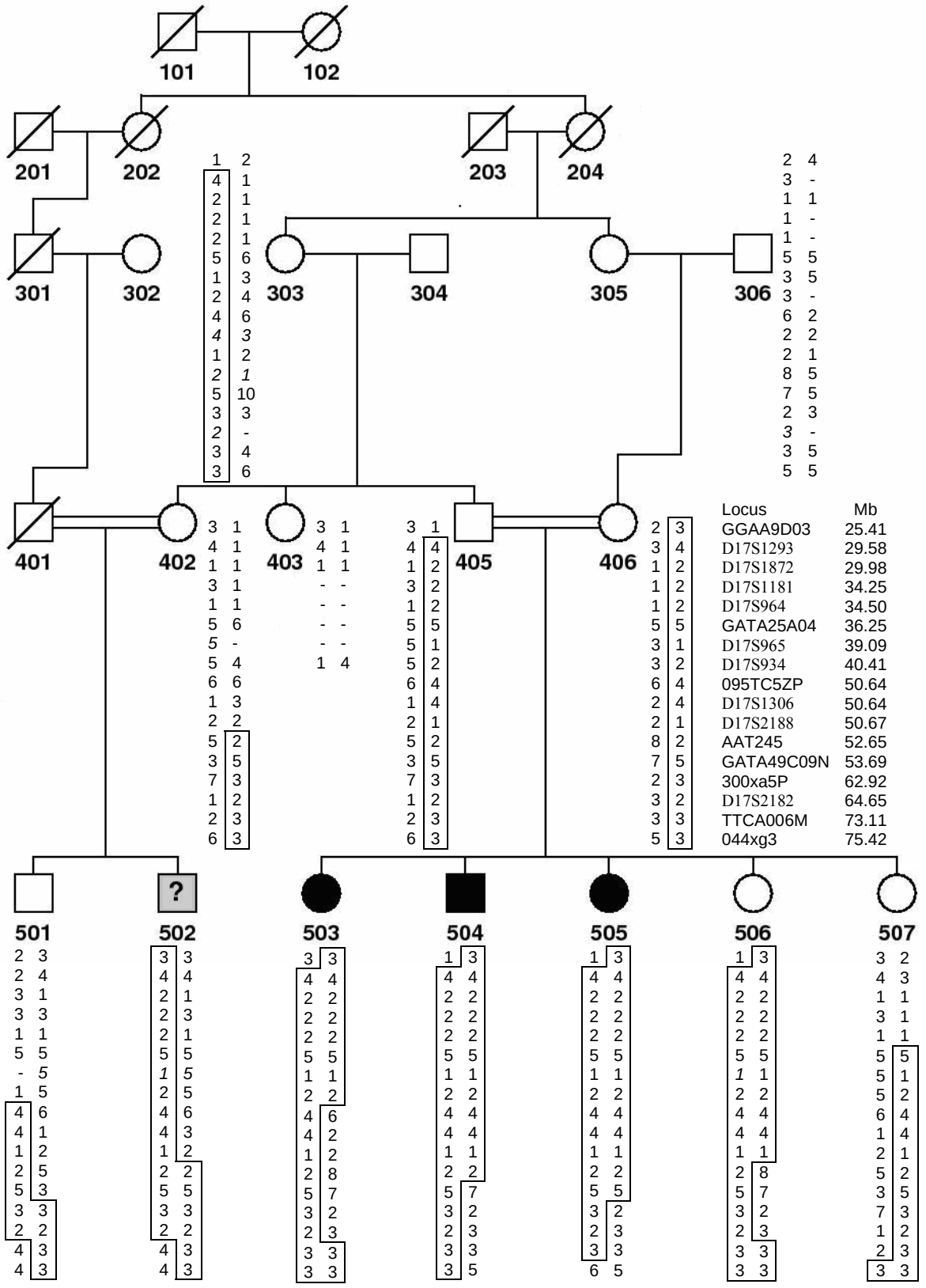

Figure 5.32. Partial pedigree diagram and haplotypes at 17q11.2-q25.3. Shared haplotype is boxed. Deduced alleles are in italics.

5.5. PAG-L

Multipoint lod score analysis of the genome scan data of PAG-L kindred resulted in a single significant peak of 3.2 between markers D13S784 and D13S317 (Figure 5.33). However, further genotyping studies with twenty additional markers and including DNA of other family members available yielded negative multipoint lod scores along chromosome 13. As chromosome 13 was the sole significant locus, we decided to fine-map the region as much as possible with affected individuals that apparently carried a common IBD haplotype. This approach mapped the gene region to a 3.04-Mb interval between markers D13S91-7 and D13S631 with a multipoint lod score of 4.25 (Table 5.9, Figure 5.34, 5.35 and 5.36). However, neither affected individual 312 nor his affected sons 414, 415 and 416 carried this haplotype, and the sons inherited the same haplotype from the father (Figure 5.37).

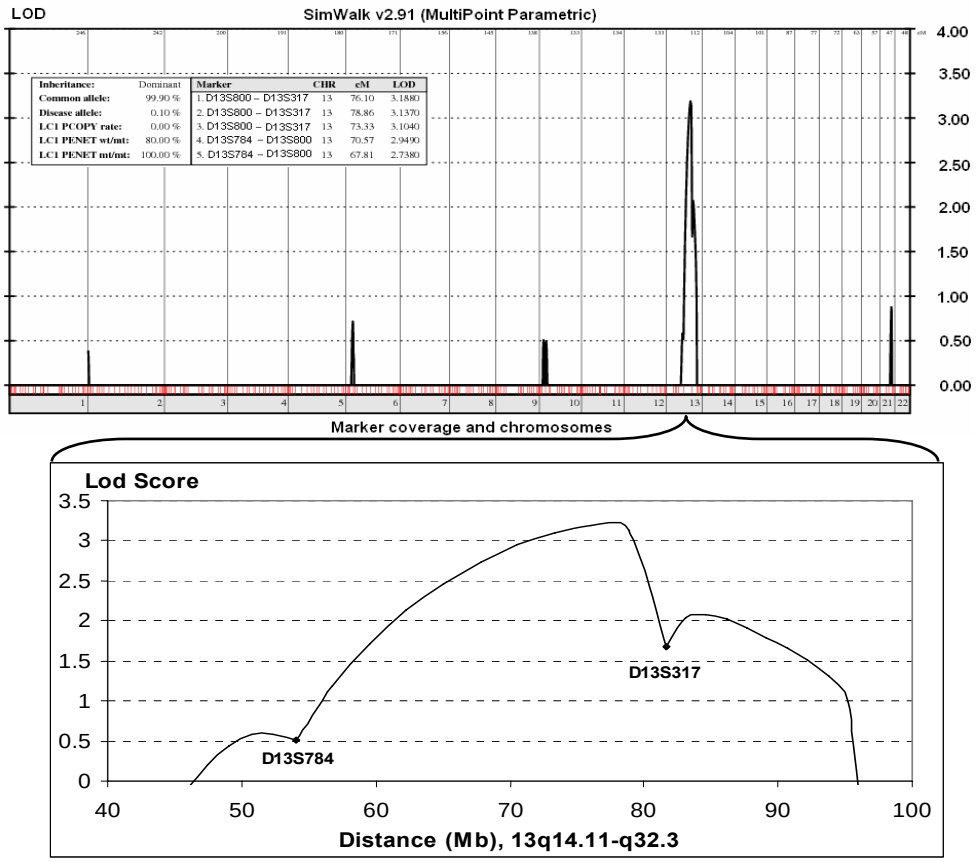

Figure 5.33. Multi-point lod scores of the total data set generated by the genome scan in a dominant model with 80 per cent penetrance. Lod scores are plotted in the order of chromosomal position. Top five scores are given within the graph together with their loci and chromosomal positions. Lod score graph of chromosome 13q14.11-q32.3 is enlarged.

Table 5.9. Two-point lod scores for 32 markers used in fine mapping approach on chromosome 13pter-qter

	Position				Lod Score at θ =					
Marker	Mb	cM[1]	Z_{max}[2]	θ_{MLE}[3]	0.00	0.05	0.1	0.2	0.3	0.4
D13S787	23.28	8.75	0.10	0.25	-1.99	-0.49	-0.10	0.09	0.08	0.03
ATA5A09	26.00	16.05	0.00	0.50	-2.35	-1.77	-1.14	-0.51	-0.21	-0.05
D13S893	30.96	28.35	0.84	0.10	-0.81	0.79	0.84	0.65	0.37	0.13
D13S1493	32.91	31.13	0.00	0.50	-6.36	-2.07	-1.55	-0.81	-0.36	-0.11
D13S894	37.64	37.87	0.04	0.35	-1.36	-0.75	-0.40	-0.09	0.03	0.03
D13S765	39.36	(40.6)	0.00	0.50	-3.65	-1.61	-0.98	-0.38	-0.13	-0.03
D13S325	42.07	43.84	0.05	0.30	-3.56	-1.46	-0.67	-0.06	0.05	0.00
D13S788	50.79	54.17	0.51	0.20	-0.62	0.04	0.38	0.51	0.37	0.13
D13S784	54.00	(55.5)	0.12	0.20	-1.70	-0.11	0.07	0.12	0.08	0.03
D13S801	61.46	58.51	1.23	0.15	0.49	1.01	1.23	1.13	0.81	0.41
D13S318	69.47	62.00	0.00	0.40	-1.29	-0.57	-0.30	-0.08	-0.01	0.00
D13S800	72.77	67.39	0.59	0.10	-0.89	0.50	0.59	0.48	0.26	0.07
D13S1804	76.03	72.48	0.97	0.15	-3.00	0.63	0.93	0.91	0.63	0.27
D13S170	80.01	76.26	1.02	0.10	-0.30	0.98	1.02	0.81	0.48	0.16
D13S317	81.62	77.30	3.96	0.00	3.96	3.55	3.13	2.26	1.39	0.56
D13S628	84.58	79.02	0.43	0.10	-0.85	0.34	0.43	0.34	0.18	0.06
D13S767	88.92	81.54	2.14	0.05	0.79	2.14	2.08	1.67	1.10	0.46
D13S795	91.49	83.90	1.34	0.00	1.34	1.17	0.99	0.65	0.35	0.12
D13S91-7	91.70	(83.9)	1.77	0.05	0.47	1.77	1.73	1.35	0.86	0.37
D13S1811	92.31	(84.7)	1.34	0.00	1.34	1.17	0.99	0.65	0.35	0.12
D13S762	93.23	(85.8)	0.51	0.00	0.51	0.43	0.35	0.22	0.10	0.03
D13S631	94.74	89.14	0.88	0.15	-0.11	0.65	0.88	0.80	0.52	0.21
D13S793	96.75	(91.0)	0.62	0.10	-1.25	0.48	0.62	0.54	0.31	0.10
D13S770	98.43	94.29	0.07	0.25	-1.93	-0.26	-0.04	0.07	0.06	0.02
D13S1284	98.69	94.77	0.00	0.50	0.00	0.00	0.00	0.00	0.00	0.00
D13S1267	99.70	95.67	0.00	0.45	-1.70	-1.03	-0.60	-0.21	-0.06	-0.01
D13S779	100.30	97.08	1.30	0.10	-0.10	1.29	1.30	1.00	0.59	0.19
D13S796	106.69	111.13	0.13	0.30	-2.45	-0.84	-0.42	0.05	0.13	0.06
L18097	106.89	112.74	1.83	0.00	1.83	1.57	1.32	0.84	0.43	0.14

[1]Estimated cM distances are given in parenthesis.
[2]Maximum two-point lod score with Superlink (Autosomal recessive, 80 per cent penetrance)
[3]Maximum likelihood estimate of recombination fraction (θ).

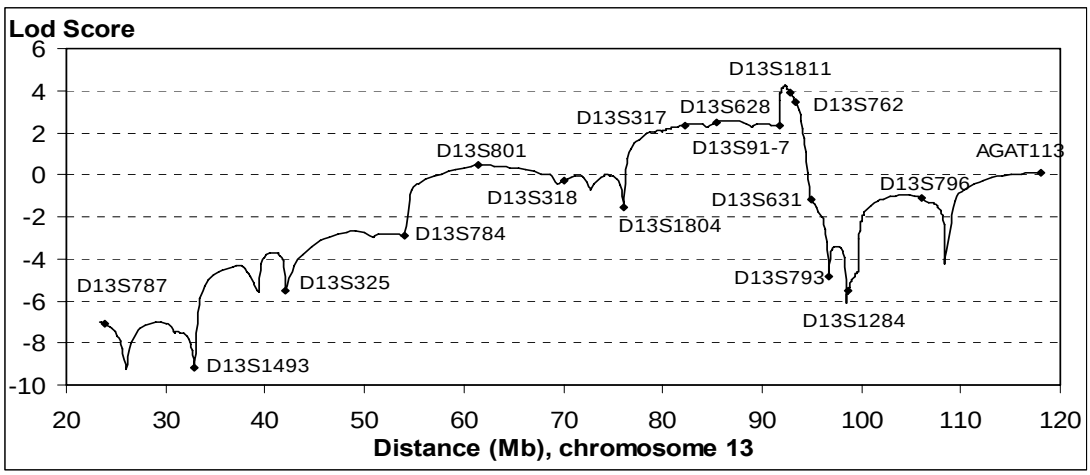

Figure 5.34. Multipoint lod score curve obtained for markers on Table 5.9 (SimWalk)

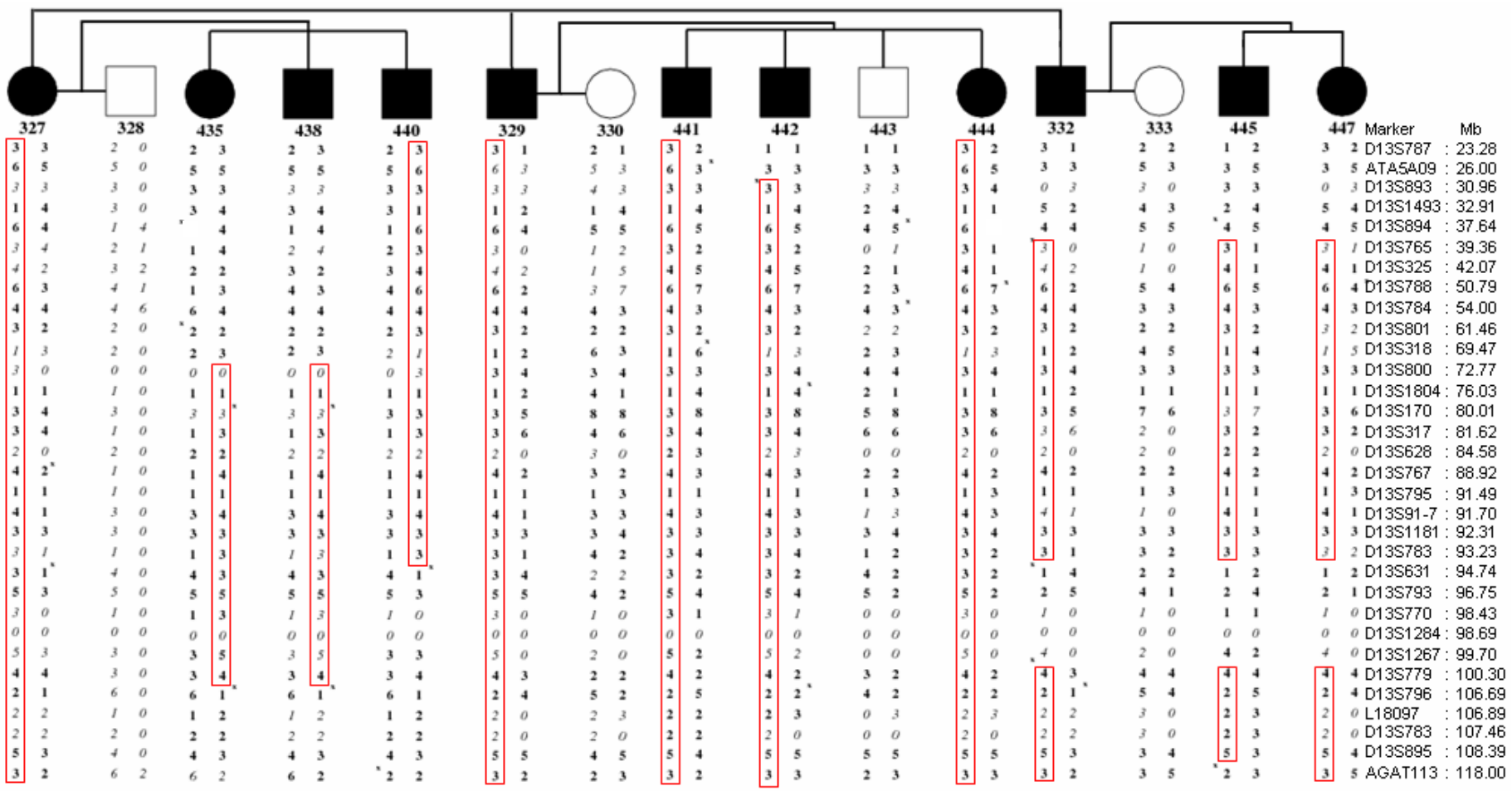

Figure 5.35. Haplotypes of PAG-L kindred (branch 1) on chromosome 13. Shared haplotype is boxed.

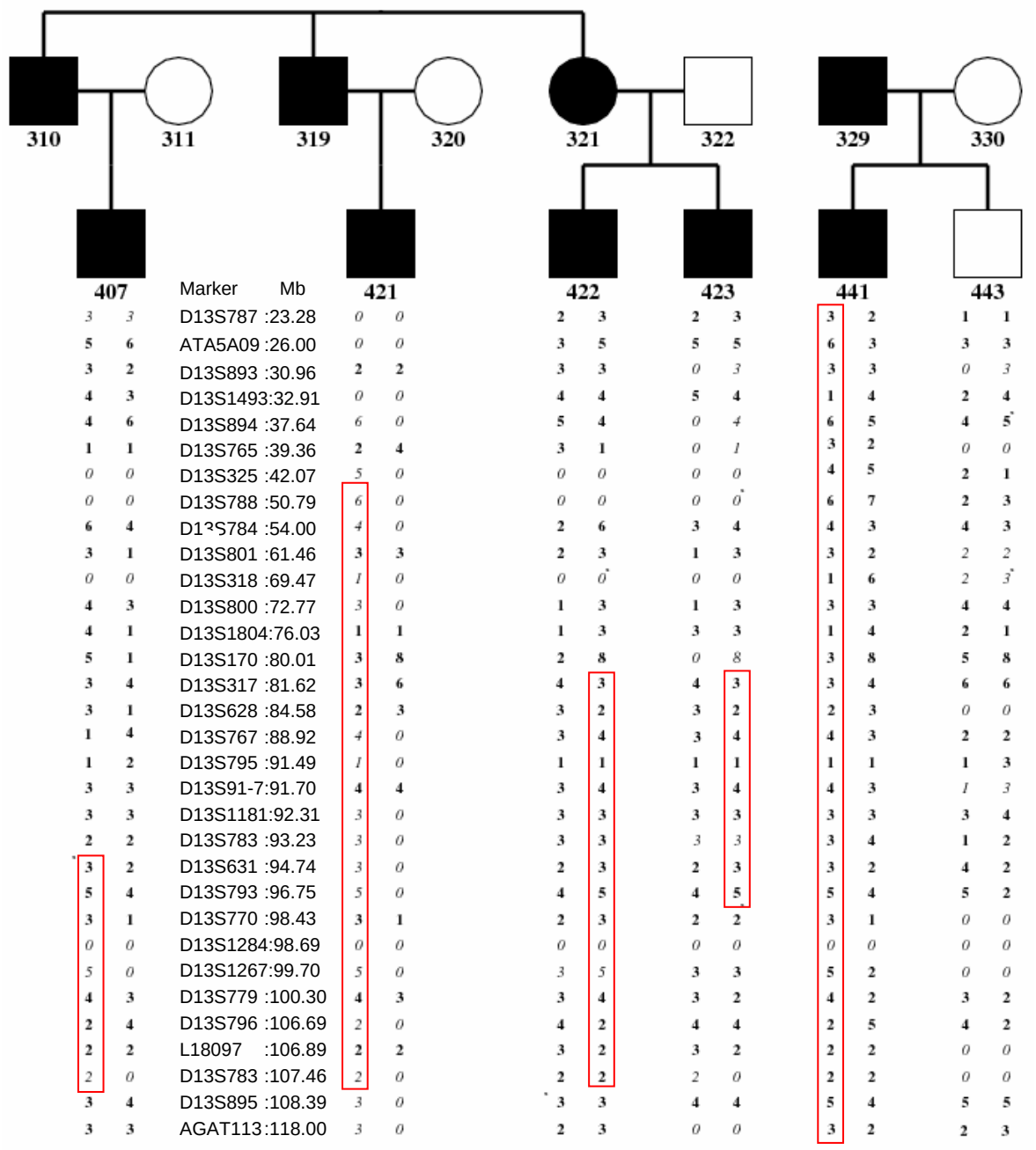

Figure 5.36. Haplotypes of PAG-L kindred (branch 2) on chromosome 13. Shared haplotypes are boxed. Haplotypes of individuals 441 and 443 are given as references to Figure 5.37.

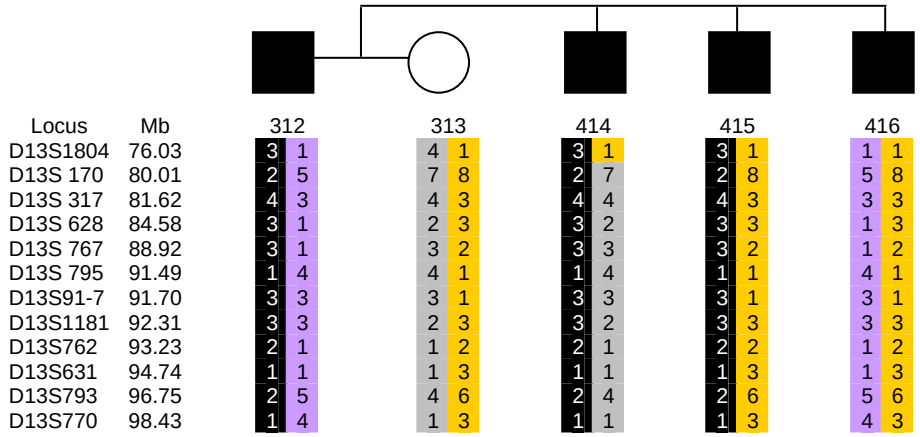

Locus	Mb	312	313	414	415	416
D13S1804	76.03	3 1	4 1	3 1	3 1	1 1
D13S 170	80.01	2 5	7 8	2 7	2 8	5 8
D13S 317	81.62	4 3	4 3	4 4	4 3	3 3
D13S 628	84.58	3 1	2 3	3 2	3 3	1 3
D13S 767	88.92	3 1	3 2	3 3	3 2	1 2
D13S 795	91.49	1 4	4 1	1 4	1 1	4 1
D13S91-7	91.70	3 3	3 1	3 3	3 1	3 1
D13S1181	92.31	3 3	2 3	3 2	3 3	3 3
D13S762	93.23	2 1	1 2	2 1	2 2	1 2
D13S631	94.74	1 1	1 3	1 1	1 3	1 3
D13S793	96.75	2 5	4 6	2 4	2 6	5 6
D13S770	98.43	1 4	1 3	1 1	1 3	4 3

Figure 5.37. Haplotypes of individuals 312, 313, 414, 415 and 416 on chromosome 13q22.2-q32.3. Haplotypes are colored to track their inheritance.

6. DISCUSSION

Large-scale genotyping centers together with the availability of high-density marker maps have facilitated cost effective genotyping. Mammalian Genotyping service funded by the National Heart, Lung, and Blood Institute (NHLBI) had been performing genome scans with multiallelic microsatellite markers to support world-wide studies of mapping genes which cause or influence human diseases for 12 years until December, 2006. The service accepted three genotyping projects from our laboratory and produced a total of 121,210 genotypes from 293 samples. This study describes locus and gene analysis in five of the inherited disorders submitted to the service, starting from the initial genotyping data.

Extended families with several affected members as a result of the high rate of consanguineous marriages in certain parts of Turkey have provided the starting point for this study. In all but one (PAG-L) of the disorders analyzed, it could be assumed that disease alleles were homozygous by descent, and in turn homozygosity mapping could be applied. Then in the identified loci, candidate genes were evaluated on the basis of their genetic location, expression pattern, tissue specificity, reported function and similarity to known genes.

6.1. Split-Hand/Foot Malformation (SHFM)

The kindred we analyzed was the only one reported so far exhibiting autosomal recessive inheritance for SHFM (Gul and Oktenti, 2002). Incomplete penetrance reported for all SHFM with known locus except for the X-linked one (a single family) strongly implies the contribution of more than one locus to each autosomal SHFM. In addition, general variability of the trait among the autopods of a single individual further complicates the picture, indicating that the contributions of genes to the trait are not absolutely additive. Therefore, our results that revealed the complex inheritance for SHFM in the kindred studied were not unexpected. A homozygous mutation in *WNT10b* having a penetrance of 92.3 per cent underlies the trait in subjects with foot involvement, while the atypical SHFM individual did not carry the mutation at all. Additionally, a dominant locus at 17p13.1-q12 was identified, making an oligogenic inheritance model possible. The lod

score at this locus did not reach significance, because both the number of subjects and the penetrance were low. It is noteworthy that the severest cases (415, 501 and 603) shared homozygosity for part of the haplotype. Alternatively, a digenic model is also possible, in which the part of the haplotype (17q11.1-q12 between markers D17S691-D17S966, Table 5.3 and Figure 5.11) inherited by all SHFM subjects but not by 507 would be essential for the penetrance of *WNT10b* mutation. Thus, the finding that SHFM phenotype did not manifest in 507 who was homozygous for the mutation could be explained by two alternative models: Either the coinheritance of additional locus/loci was essential for SHFM manifestation, or a protective modifier locus suppressed or rescued the trait manifestation. The first model proposes oligogenic inheritance as explained above, and the 13.35-Mb region between markers D17S689-D17S1181 is a good candidate. As for the second model, the sample size was too small for a meaningful investigation, 507 being the only individual homozygous for p.R332W and not manifesting SHFM. Suppressor genes/loci for other human traits have been reported and are reviewed by Nadeau, 2001. Since sisters of 507 are only very mildly affected, it is possible that only minor genetic differences have led to a shift from the equilibrium for the normal phenotype in favor of the SHFM phenotype.

Spinal muscular atrophy (SMA) is a very recent example how a protective modifier locus rescues an otherwise lethal condition. SMA is an autosomal recessive neuromuscular disorder caused by mutations in the survival motor neuron 1 gene (*SMN1*). In some families, despite having homozygous *SMN1* gene deletions, the penetrance is low and there are asymptomatic individuals. This condition is partly explained by the number of *SMN2* gene copies located centromeric to *SMN1*. The copy number of *SMN2* affects the amount of SMN protein produced and thus the severity of the SMA phenotype (Lorson *et al.*, 1999). However, in rare conditions, two sibs having no SMN1 gene product and identical number of *SMN2* gene copies can be either affected or asymptomatic. It was shown recently that a significantly high expression of yet another gene, plastin 3 (*PLS3*), rescued the trait in unaffected SMN1 deleted females (Oprea *et al.*, 2008).

As for the variability of the SHFM phenotype, the simplest model would suggest that combinations of various loci shared by various combinations of SHFM subjects act in concert with the two loci we identified (*WNT10b* mutation and 17p13.1-q12). Several

haplotypes shared by most SHFM members of the family could be interpreted in favor of this model (summarized on Table 5.3). An interesting candidate locus example was 1p34.3-31.1, where a haplotype was found in all SHFM subjects except the atypical case 407 and 510, in either heterozygous or homozygous state. It is remarkable that the phenotype of 510 was unique in the family in the sense that she had postaxial involvement in the affected foot. Postaxial syndactyly in foot was not observed alone in any other member of the family but in association with a preaxial defect (Table 3.1). Another locus of interest was 3q27 harboring *TP63*, the gene for SHFM4. We analyzed all sixteen exons of *TP63* encoding the six p63 isotypes (Yang *et al.*, 1998). Only a rare insertion polymorphism at the promoter for isotype ΔNp63 was identified. The homozygosity for the allele was highly significant (p=0.005) and was observed in four SHFM subjects. Two SHFM subjects (407 and 508) did not carry the allele (Table 5.3 and Figure 5.9). No functional study has been reported for the alleles. ΔNp63 lacks the transactivation domain for transcriptional activity and was suggested to have dominant-negative effects on p53 and p63 activities (Yang *et al.*, 1998). Whether any of the loci found to be shared by most of the SHFM cases indeed contributes to phenotype severity cannot be assessed for sure before the responsible genes are identified. One factor that hinders such an evaluation is that a quantitative phenotypic classification was not possible in our SHFM subjects. Moreover, complex inheritance is generally complicated also by environmental factors, and nothing is known yet about possible effects of environment on SHFM phenotype.

A general feature of SHFM is that males are more affected than females. No locus on the X-chromosome was shared by all male SHFM subjects in the family. Locus Xq22.3-q25 was shared by all but 604. Although it is possible that the locus may have a modifier effect on the severity in males, acting as an X-linked recessive locus, it is more likely that in this family the trait severity is sex influenced rather than modified by an X-linked gene.

Homozygous *WNT10b* mutation was definitely non-penetrant in 507, since radiological investigations excluded SHFM. No malformation could be observed in hands or feet. However, two clinical findings in her feet are remarkable: unusually large navicular bones fused to accessory bones and reduced bone density as evidenced by the hollow appearance in calcaneus bones. Available radiograms allowed the investigation of those phenotypes in two SHFM cases as well: The navicular bones were bilaterally large

but not fused in individual 409, who also had a weak calcaneus appearance. In individual 407, who did not carry mutation p.R332W at all, the bone density was normal and the navicular bones were neither large nor fused. The somewhat lower bone density in mutation homozygotes is in agreement with the positive role of *Wnt10b* in osteoblastogenesis and regulation of bone density (Bennett *et al.*, 2005; Kang *et al.*, 2007).

In order to investigate whether there is a correlation between *WNT10b* transcript levels, which in turn may be an indicative of protein level, with phenotype severity, we assayed *WNT10b* transcript levels in four individuals, all homozygous for mutation p.R332W. Indeed, there was about a two-fold difference between the non-penetrant individual 507 and individual 415, with severest SHFM phenotype.

The other perplexing phenotype was that of individual 407, who did not carry the mutation. He exhibited the atypical SHFM phenotype: just a mild hand involvement. This together with the observation that seven of the remaining twelve SHFM cases had hand involvement (in addition to foot) suggests that a particular set of genes could underlie hand involvement. SHFM individuals 407, 409, 414 and 514 were afflicted with postaxial cutaneous hand syndactyly type I, while three males (501, 415 and 603) had severe hand malformations. We propose that yet unidentified locus/loci other than gene *WNT10b* could be responsible for the mild syndactyly phenotype without bone involvement as in 407, 409, 414 and 514. As for 501, 415 and 603, phenotype is perhaps too complex to distinguish a probable syndactyly component alone. Further evidence in support of the presence of a hand-involvement locus is the phenotype of brothers 603 and 604: both have severely affected feet as their father, but only 603 had hand involvement, and it was as severe as the father's.

Oligogenic inheritance might be not very rare in bone morphogenesis. Recently SHFM with long bone deficiency was shown to link simultaneously to two dominant loci in an extended kindred (Naveed *et al.*, 2007), but still parental consanguinity raised the question whether a recessive gene could also be involved. The clinical variability was extremely high as in our family and it was mentioned in the report that mild cases were not included in the study.

This is the first report on the pathogenesis of a *WNT10b* mutation in limb development (Ugur and Tolun, 2008a). WNT10b acts as a key signaling molecule promoting osteoblastogenesis and inhibiting adipogenesis. WNT genes were shown to be mutated in at least four other autosomal recessive developmental human disorders: *WNT3* in tetra-amelia (Niemann *et al.*, 2004), *WNT7a* in Fuhmann Syndrome and Al-Awardi/Raas-Rothschild Syndrome (AARRS) (Woods *et al.*, 2006), and *WNT10a* in Odonto-onychodermal Dysplasia (Adaimy *et al.*, 2007). It is remarkable that mutation p.R292C in *WNT7a* reported for AARRS is at the homologous position for mutation p.R332W identified in this study. This position is perhaps important for regulation or receptor recognition by the WNT protein.

It was a challenge to work with such a large family with a large number of affected members having such a variable phenotype. Several frequent haplotypes were observed. It is difficult to speculate which of those haplotypes harbor additional genes contributing to the trait, not only because of the high consanguinity but also because several inheritance models could be proposed for the highly variable phenotype. The hands were either not affected at all or much less affected than the feet, indicating that separate but overlapping molecular mechanisms may exist for morphogenesis of hand and foot. Individual 407 lacked both *WNT10b* mutation and foot malformation. It is therefore justified to propose that mutations in that gene underlie typical recessive SHFM phenotype and work in concert with defects in several other genes to fully manifest the phenotype. In spite of the high parental consanguinity, the genetic background in the family cannot be expected to be as uniform as in inbred mice with dactylaplasia, the mouse model for SHFM. This may explain why a clear cut phenotypic classification could not be drawn in humans and effects of locus combinations on the phenotype could not be established. Nevertheless, recessive genetic components have never been considered previously in SHFM families, and this report emphasizes the importance of studying such components and evaluates possible complex inheritance models which are extensions of an underlying recessive gene defect (Ugur and Tolun, 2008a).

6.2. Hypomyelination and Congenital Cataract (HCC)

In this study, we investigated a family with an autosomal recessive neurological condition initially diagnosed as sensory motor demyelinating neuropathy followed by a diagnosis of a new form of leukodystrophy. We launched a linkage study in the family in order to map and subsequently identify the causative gene for this novel condition. The manuscript was submitted for publication after the mapping studies were completed and two candidate genes, namely *HIBADH* and *CYCS* were excluded from the disease phenotype by mutation analysis. The manuscript got rejected because of insufficient clinical description. Later Zara *et al.*, 2006 described HCC as a new disorder in five unrelated families and identified the causative gene as *DRTCCNB1*. Linkage to 7p in the family we studied together with close clinical resemblance to the disorder reported by Zara *et al.*, 2006 led us to assign the condition in our patients as HCC.

We subsequently showed that our patients carried in the disease gene a homozygous large deletion that apparently resulted from an unequal crossover at the direct copies of an imperfect repeat (Ugur and Tolun, 2008b). The mutation would cause skipping of exons 8 and 9 and, due to the one-nucleotide shift in the translational reading frame, is predicted to lead to a premature stop codon at position 214. The truncation deletes 308 amino acid residues from the carboxy-terminal of the native 521-amino acid protein. This mutation c.531-439_743+348del is predicted to result in absence of the protein since the deleted region spans more than half the coding region, including amino acids 230 to 248, which comprise one of the two putative transmembrane segments. The mutations reported in the mentioned study were either splice site (c.51+1G→A and c.414+1G→T) or missense (c.158T→C). It is difficult to speculate on the relative severities of the splicing and truncating mutations. All 10 patients in the previous report could walk with support until at least age eight years, while none of our four patients that survived beyond age two years could walk with support past six years. However, while all patients in the former study had bilateral congenital cataracts, two of our patients did not: patient 509 developed cataracts at age nine years and her sister (patient 505) had cataract seemingly only unilaterally until she died at age 12 years. Our findings add to the clinical variability already reported, in that congenital or bilateral cataract should not be considered a prerequisite for the diagnosis of

HCC. Especially in isolated cases, bilateral or congenital cataract as a criterion for HCC would lead to misdiagnosis.

6.3. Cone Rod Dystrophy (CORD)

The third disorder analyzed was a nonsyndromic autosomal recessive cone-rod dystrophy observed in six individuals of a consanguineous family. A genome-wide search followed by further genotyping at the single suggestive locus localized the gene to a 4.14 Mb interval at 17p13.2-p13.1 with two and multipoint lod scores of 4.57 and 5.48, respectively. A database search revealed 171 genes in this critical gene region (NCBI Build 36.3). Although this number was very high to initiate a candidate gene analysis, one of those genes *GUCY2D* encoding retina specific guanylyl cyclase (retGC) stood out to be a highly promising candidate. Mutations in *GUCY2D* have been associated with autosomal recessive LCA1 and autosomal dominant CORD5/6. Eighteen coding exons of *GUCY2D* were screened for mutations in the family, and indeed a novel variation c.2846T→C was identified in the fifteenth exon of the gene. This variation was assessed as a mutation, since it was not observed in about 200 chromosomes tested and it caused substitution of the most hydrophobic amino acid (Isoleucine, I) for a polar uncharged one (Threonine, T) at the catalytic domain of the protein. In a theoretical model for the catalytic domain of retGC (Liu *et al.*, 1997) based on the crystal structure of the catalytic domain of type II adenylyl cyclase (Zhang *et al.*, 1997), I949 is positioned within an alpha-helical region on the outer surface. The insertion of a polar residue instead of a strongly hydrophobic one into this region would likely to affect the folding of the helical segment. Additionally, two online tools used for predicting the effect of amino acid variations (SIFT and SNP3D) suggested that this change is intolerable for the protein (Table 5.7). The other two tools (MMB and PolyPhen) predict the change as neutral, possibly due to an error in the scope of their alignment files. These programs include natriuretic peptide receptor type C (NPR-C) in the alignment, which disturbs the conservation of I949 residue. However, NPR-C is the only member of the natriuretic peptide receptors without a guanylyl cyclase domain (Rose and Giles, 2008).

The mutation segregating with the condition in the family created p.I949T amino acid change in the catalytic domain of the retGC, and homozygous mutations in this

domain is shown to be associated with LCA in several instances. Nevertheless, LCA which is a common cause of childhood blindness was ruled out from differential diagnosis in the family upon fundus examination and electrophysiological findings. Although the patients exhibited a great degree of variability in their ophthalmologic manifestations, the condition was diagnosed as a novel form of cone rod dystrophy (CORD). CORDs are inherited retinal dystrophies from the group of pigmentary retinopathies. CORDs are characterized by retinal pigment deposits, principally in the macular area in the ophthalmologic examination of the fundus. Cone loss precedes the rod loss in CORD, which explains the generally sequential symptoms of CORDs: reduced visual sharpness, defects in color vision, photophobia and decreased sensitivity in the central visual field, later followed by progressive night blindness and peripheral visual field loss.

Functional consequences of missense mutations found in the catalytic domain of ret-GC have been studied extensively (Rozet *et al.*, 2002; Tucker *et al.*, 2004). In general, mutant GUCY2D constructs are expressed *in vitro* and subsequently assayed for their ability to hydrolyze GTP to cGMP. All mutations within the catalytic domain were shown to abolish cyclase activity completely. In addition, Tucker *et al.*, 2004 have shown that the catalytic domain mutant alleles act in a dominant negative fashion to reduce the activity of wild-type construct when co-expressed. Such a dominant negative activity reflects formation of inactive mutant/wild-type dimer (Thompson and Garbes, 1995). This finding was consistent with abnormalities in cone electroretinograms (ERG) detected in obligate *GUCY2D* heterozygotes for the p.L954P mutation (Konekoop *et al.*, 2002). In this sense, the p.I949T variation identified in this study most probably does not abolish but only decreases the activity of the protein, since an abolishing mutation would create a very severe phenotype leading to childhood blindness as in LCA. Alternatively, modifier locus/loci may have had a role in this less severe phenotype. It will be interesting also to test the p.I949T carriers in the family for cone ERG.

Intrafamilial differences in the severity of the phenotype are well known for retinal dystrophies. Application of microarray technology for screening disease-associated variants for LCA not only proved to be a strong diagnostic tool but also explained the variable expressivity in LCA by modifier alleles. Zernant *et al.*, 2005 have performed a comprehensive study in 300 patients using an LCA genotyping microarray platform

containing 307 variants from eight genes. Interestingly, eight per cent of the patients were found to have a homozygous defect in one gene together with a heterozygous defect in a second gene. The clinical findings were also supportive: the phenotypes were more severe in the affected individuals with three defective alleles compared to their age-matched affected siblings with only homozygous mutations in one gene. The CORD family in this study was reconsidered clinically in order to address the phenotypical differences. The clinical findings for patients 509 and 512 were compatible with tapetoretinal degeneration, which is a disorder of the retina mainly affecting photoreceptors and retinal pigment epithelium, while a diagnosis of CORD was more suitable for patients 409, 507 and 514. In this regard, the former patients may be considered as having a more severe phenotype.

The genome scan data were reanalyzed by grouping the patients according to the severity in their phenotypes in order to detect modifier locus/loci with various penetrance models. A 14-Mb recessive locus on chromosome 14q23.1-q24.3 between markers D14S592 and D14S1433 was a good candidate that could account for the observed severity in individuals 509 and 512. Among affected individuals, only 509 and 512 were homozygous for the locus and multipoint lod score approached 1.6 when penetrance was reduced (66 per cent). Interestingly, this region contained gene *RDH12* implicated in LCA3.

6.4. Mental Retardation Associated with Hypertension (MR-HT)

In this study, we identified the genetic loci for an autosomal recessive mental retardation on chromosome 7q21.3-q31.1. The linkage studies in this family were rather challenging. Initially, the genome scan data performed previously in our laboratory were utilized, which consisted of genotyping results of only three affected sibs with microsatellite markers having 25 cM spacing. Fine mapping studies in candidate loci did not result in linkage. Therefore, the pedigree was genotyped once more at NLHBI Genotyping Service with more densely spaced markers and including this time all four affected individuals, their available parents and siblings. However, the results were disappointing again, as shared homozygosity in the patients was not found in any locus.

We were recently informed that patient 501 had never been clinically evaluated but was assigned as having the same clinical manifestations as his cousins upon the claim of the family. We have requested a clinical examination for this patient which resulted in a diagnosis as a different form of mental retardation. We therefore reanalyzed the genome scan data with excluding this individual. The gene locus was then mapped to a 15.83 Mb interval on chromosome 7q21.3-q31.1 between markers D7S1820 and D7S1817 with a maximum multipoint lod score of 2.65. As both the structure of the pedigree and the number of affected individuals were different after individual 502 was excluded from the analysis, simulation programs were run under the hypothesis of linkage in order to estimate the power of this reduced pedigree to yield a significant lod score. Simulation studies of 1000 replicates resulted in maximum estimated lod scores of 2.48 (two-point, FastSlink) and 2.86 (multipoint, Allegro). These results imply that this pedigree structure is not sufficient to detect significant linkage and our actual analysis has gathered nearly the maximum linkage information that can be extracted from this pedigree. Therefore, it is justified that the gene locus was indeed at 7q21.3-q31.1. It was risky to initiate candidate gene analysis in this region considering the uncertainties in the clinical diagnosis of the individuals and the very large number of genes in this region (243 genes, NCBI Build 36.3).

The roles of autosomal genes in mental retardation are not very well known. It is partly because severe autosomal dominant forms are almost exclusively sporadic, since affected individuals rarely have children. For recessive cases, it is not always possible to find large pedigrees with multiple affected individuals. To date, only four genes mutated in autosomal recessive mental retardation were reported, and seven additional loci were mapped in an extensive study with consanguineous Iranian families by large-scale homozygosity mapping (Najmabadi *et al.*, 2006). None of those genes or loci seems to be the common cause of MR, which is not surprising, since about half of the human genes are expressed in brain. Our findings describe a new locus for AR-MR and support the evidence for genetic heterogeneity in this disorder. Identification of underlying gene defects in all identified loci will accelerate our understanding of the basic mechanisms underlying mental development.

6.5. Pseudoarthrogryposis-like Syndrome (PAG-L)

The last disorder analyzed in this study was PAG-L. The PAG-L phenotype was observed in an extended kindred, inherited in an autosomal dominant fashion. A genome-wide linkage scan in this kindred highlighted a sole locus with significance: 13q14.11-q32.3 with a multipoint lod score of 3.2. Surprisingly, fine mapping studies on chromosome 13 did not support linkage for all of the affected individuals. Still, we mapped the gene region to a 3.04-Mb interval between markers D13S91-7 and D13S631 using only the affected individuals with shared IBD haplotypes. The purpose for such an approach was to initially map a critical region as small as possible and then check the genotypes of unlinked individuals at this locus to make sure that a likely haplotype was not hidden by ancestral cross-over events. However, affected individual 312 and his affected sons 414, 415 and 416 neither carried this haplotype, and the sons had not inherited the same paternal haplotype.

Having chromosome 13 as the only significant locus and eliminating other chromosomes also by haplotype inspection prompted us to conduct detailed linkage studies on this chromosome. However, there is always a risk to overlook a haploype with a limited size. A better approach for the family would be to repeat the genotyping with high density SNP arrays that would cover the genome with less spacing and with more homogeneityin a more uniform fashion. Several reports have demonstrated the ability of SNP linkage scans to identify loci not detectable by in multiple microsatellite-based scans (Yang *et al.*, 2005). A relevant example is identification of the gene *PLA2G6* responsible for the infantile neuroaxonal dystrophy in an extended pedigree. A 400 microsatellite based scan missed the 1.5 Mb shared haplotype in the patients which later was identified by a 10K SNP array (Khateeb *et al.*, 2006). Nonmendelian genotyping errors that are not detected by the computer programs may also be the cause of missing the likely gene locus. Yet a new scan would help reevaluation of such loci with correctly genotyped markers. Alternatively, the challenge in this study may also reflect that the apparently monogenicly inherited phenotype in the family has in fact a heterogeneous etiology. Phenotypic classification within the pedigree together with likely effects of other loci should be reconsidered.

7. CONCLUSION

In the framework of this study, causative genes have been identified for three autosomal recessive disorders; *WNT10b* for Split-Hand/Foot Malformation, *DRCTNNB1A* for Hypomyelination and Congenital Cataract, and *GUCY2D* for Cone Rod Dystrophy. Additionally, a novel gene locus for an autosomal recessive mental retardation associated with hypertension has been mapped and a candidate locus for autosomal dominant Pseudoarthrogryposis-like Syndrome has been identified.

REFERENCES

Adaimy, L., E. Chouery, H. Megarbane, S. Mroueh, V. Delague, E. Nicolas, H. Belguith, P. de Mazancourt and A. Megarbane, 2007, "Mutation in *WNT10A* is Associated with an Autosomal Recessive Ectodermal Dysplasia: The Odonto-Onycho-Dermal Dysplasia", *American Journal of Human Genetics*, Vol. 81, No. 4, pp. 821-828, October.

Ahmad, M., H. Abbas, S. Haque and G. Flatz, 1987, "X-chromosomally Inherited Split-Hand/Split-Foot Anomaly in a Pakistani Kindred", *Human Genetics*, Vol. 75, No. 2, pp. 169-173, February.

Ahmed, E. and J. Loewenstein, 2008, "Leber Congenital Amaurosis: Disease, Genetics and Therapy", *Seminars in Ophthalmology*, Vol. 23, No. 1, pp. 39-43, January.

Allikmets, R., 2004, "Leber Congenital Amaurosis: A Genetic Paradigm", *Ophthalmic Genetics*, Vol. 25, No. 2, pp. 67-79, June.

Bamshad, M., L. B. Jorde and J. C. Carey, 1996, "A Revised and Extended Classification of the Distal Arthrogryposes", *American Journal of Medical Genetics*, Vol. 65, No. 4, pp. 277-281, November.

Bardoni, B., J. L. Mandel and G. S. Fisch, 2000, "*FRM1* Gene and Fragile X Syndrome", *American Journal of Human Genetics*, Vol. 97, No. 2, pp. 153-163, June.

Basel, D., M. W. Kilpatrick and P. Tsipouras, 2006, "The Expanding Panorama Of Split Hand Foot Malformation", *American Journal of Medical Genetics Part A*, Vol. 140, No.13, pp. 1359-65, July.

Basel-Vanagaite, L., R. Attia, M. Yahav, R. J. Ferland, L. Anteki, C. A. Walsh, T. Olender, R. Straussberg, N. Magal, E. Taub, V. Drasinover, A. Alkelai, D. Bercovich, G. Rechavi, A. J. Simon and M. Shohat, 2006, "The *CC2D1A*, a Member of a New

Gene Family with C2 Domains, is Involved in Autosomal Recessive Non-Syndromic Mental Retardation", *Journal of Medical Genetics*, Vol. 43, No. 3, pp. 203-210, March.

Bennett, C. N., K. A. Longo, W. S. Wright, L. J. Suva, T. F. Lane, K. D. Hankenson and O. A. MacDougald, 2005, "Regulation of Osteoblastogenesis and Bone Mass by Wnt10b", *Proceedings of the National Academy of Sciences of the United States of America*, Vol. 102, No. 9, pp. 3324-3329, March.

Bui, T. D., J. Rankin, K. Smith, E. L. Huguet, S. Ruben, T. Strachan, A. L. Harris and S. Lindsay, 1997, "A Novel Human Wnt Gene, *WNT10b*, Maps to 12q13 and is Expressed in Human Breast Carcinomas", *Oncogene*, Vol. 14, No. 10, pp. 1249-1253, March.

Calzolari, E., D. Manservigi, G. P. Garani, G. Cocchi, C. Magnani and M. Milan, 1990, "Limb Reduction Defects in Emilia Romagna, Italy: Epidemiological and Genetic Study in 173,109 Consecutive Births", *Journal of Medical Genetics*, Vol. 27, No. 6, pp. 353-357, June.

Casanova, J. C. and J. J. Sanz-Ezquerro, 2007, "Digit Morphogenesis: Is The Tip Different?", *Development, Growth and Differentiation*, Vol. 49, No. 6, pp. 479-491, August.

Castellvi-Bel, S. and M. Mila, 2001, "Genes Responsible for Nonspecific Mental Retardation", *Molecular Genetics and Metabolism*, Vol. 72, No. 2, pp. 104-108, February.

Celli, J., P. H. G. Duijf, B. C. Hamel, M. Bamshad, B. Kramer, A. P. Smiths and H. van Bokhoven 1999, "Heterozygous Germline Mutations in the p53 Homolog p63 are the Cause of EEC Syndome", *Cell*, Vol. 99, No. 2, pp 143-153, October.

Chai, C. K., 1981, "Dactylaplasia in Mice, a Two-Locus Model for Developmental Anomalies", *The Journal of Heredity*, Vol.72, No. 4, pp. 234-237, July.

Chelly, J. and J. L. Mandel, 2001, "Monogenic Causes of X-Linked Mental Retardation", *Nature Reviews Genetics*, Vol. 2, No. 9, pp. 669-680, September.

Chiurazzi P., C. E. Schwartz, J. Gecz and G. Neri, 2007, " XLMR Genes: Update 2007", *European Journal of Human Genetics*, Vol. 16, No. 4, pp. 422-434, January.

Christiansen, J. H., C. L. Dennis, C. A. Wicking, S. J. Monkley, D. G. Wilkinson and B. J. Wainwright, 1995, "Murine Wnt-11 and Wnt-12 Have Temporally and Spatially Restricted Expression Patterns During Embryonic Development", *Mechanisms of Development*, Vol. 51, No. 2, pp. 341-350, June.

Collins, J. S. and C. E. Schwartz, 2002, "Detecting Polymorphisms and Mutations in Candidate Genes", *American Journal of Human Genetics,* Vol. 71, No. 5, pp. 1251-1252, November.

Crackower, M. A., J. Motoyama and L. Tsui, 1998, "Defect in the Maintenance of the Apical Ectodermal Ridge in the *Dactylaplasia* Mouse", *Developmental Biology*, Vol. 201, pp. 78-89, September.

Dawn Teare, M. and J. H. Barrett, 2005, "Genetic Linkage Studies", *Lancet*, Vol. 366, No. 9490, pp. 1036-44, September.

Dizhoor, A. M., D. G. Lowe, E. V. Olshevskaya, R. P. Laura and J. B. Hurley, 2002, "The Human Photoreceptor Membrane Guanylyl Cyclase, retGC, is Present in Outer Segments and is Regulated by Calcium and a Soluble Activator", *Neuron*, Vol. 12, No. 6, pp. 1345-1352, June.

Duda, T. and K. W. Koch, 2002, "Retinal Diseases Linked with Photoreceptor Guanylate Cyclase", *Molecular and Cellular Biochemistry*, Vol. 230, No. 1, pp. 129-138, January.

Dudbridge, F., 2003, "A Survey of Current Software for Linkage Analysis", *Human Genomics*, Vol. 1, No. 1, pp. 63-65, Noverber.

Dudley, A. T., M. A. Ros and C. J. Tabin, 2002, "A Re-Examination of Proximodistal Patterning during Vertebrate Limb Development", *Nature*, Vol. 418, No. 6897, pp. 539-44, August.

Duijf, P. H. G., H. Bokhoven and H. G. Brunner, 2003, "Pathogenesis of Split-Hand/Split-Foot Malformation", *Human Molecular Genetics*, Vol. 12, No. 1, pp. 51-60, April.

Elliott, A. M., J. A. Evans and A. E. Chudley, 2005, "Split Hand Foot Malformation (SHFM)", *Clinical Genetics*, Vol. 68, No. 6, pp. 501-505, December.

Faiyaz-Ul-Haque, M., S. H. Zaidi, L. M. King, S. Haque, M. Patel, M. Ahmad, T. Siddique, W. Ahmad, L. C. Tsui and D. H. Cohn, 2005, "Fine Mapping of the X-Linked Split-Hand/Split-Foot Malformation (SHFM2) Locus to a 5.1-Mb Region on Xq26.3 and Analysis of Candidate Genes", *Clinical Genetics*, Vol. 67, No. 1, pp. 93-97, January.

Goodman, F. R., F. Majewski, A. L. Collins and P. J. Scambler, 2002, "A 117-kb Microdeletion Removing HOXD9-HOXD13 and EVX2 Causes Synpolydactyly", *American Journal of Human Genetics*, Vol. 70, No. 2, pp. 547-555, January.

Graw, J., 2003, "The genetic and molecular basis of congenital eye defects", *Nature Reviews Genetics*, Vol. 4, No. 11, pp. 876-888, November.

Gül, D. and C. Öktenli, 2002, "Evidence for Autosomal Recessive Inheritance of Split Hand/Split Foot Malformation: A Report of Nine Cases", *Clinical Dysmorphology*, Vol. 11, No. 3, pp. 183-186, July.

Hamel, C. P., 2007, "Cone Rod Dystrophies", *Orphanet Journal of Rare Diseases*, Vol. 2, No. 2, pp. 1-7, February.

Hardiman, G., R. A. Kastelein and J. F. Bazan, J. F, 1997, "Isolation, Characterization and Chromosomal Localization of Human *WNT10B*", *Cytogenetics and Cell Genetics*, Vol. 77, No. 3, pp. 278-282, January.

Higgins, J. J., D. R. Rosen, J. M. Loveless, J. C. Clyman and M. J. Grau, 2000, "A Gene for Non-Syndromic Mental Retardation Maps to Chromosome 3p25-pter", *Neurology*, Vol. 55, No. 3, pp. 335-340, August.

Hoffmann, K. and T. H. Lindner, 2005, "easyLINKAGE-Plus--Automated Linkage Analyses Using Large-Scale SNP Data", *Bioinformatics*, Vol. 21, No. 17, pp. 3565-3567, September.

Ianakiev, P., M. W. Kilpatrick, I. Toudjarska, D. Basel, P. Beighton and P. Tsipouras, 2000, "Split-Hand/Split-Foot Malformation is Caused by Mutations in the p63 Gene on 3q27", *American Journal of Human Genetics*, Vol. 67, No. 1, pp. 59-66, July.

Ingham, P. W. and M. Placzek, 2006, "Orchestrating Ontogenesis: Variations on a Theme by Sonic Hedgehog", *Nature Reviews Genetics*, Vol. 7, No. 11, pp. 841-850, November.

International HapMap Consortium, 2007, "A Second Generation Human Haplotype Map of over 3.1 Million SNPs", *Nature*, Vol. 449, No. 7164, pp. 851-861, October.

Itoh, K., K. Shiga, K. Shimizu, M. Muranishi, M. Nakagawa and S. Fushiki, 2006, "Autosomal Dominant Leukodystrophy with Axonal Spheroids and Pigmented Glia: Clinical and Neuropathological Characteristics", *Acta Neuropathologica*, Vol. 111, No. 1, pp. 39-45, January.

Johnson, K. R., P. W. Lane, P. Ward-Bailey and M. Davisson, 1995, "Mapping the Mouse Dactylaplasia mutation, Dac, and a Gene that Controls Its Expression, Mdac", *Genomics*, Vol. 29, No. 2, pp. 457-464, September.

Kang, S., C. N. Bennett, I. Gerin, L. A. Rapp, K. D. Hankenson and O. A. Macdougald, 2007, "Wnt Signaling Stimulates Osteoblastogenesis of Mesenchymal Precursors by Suppressing CCAAT/Enhancer-Binding Protein Alpha and Peroxisome Proliferator-Activated Receptor Gamma", *The Journal of Biological Chemistry*, Vol. 282, No. 19, pp. 14515-14524, May.

Kavaslar, G. N., S. Önengüt, O. Derman, A. Kaya and A. Tolun, 2000, "The Novel Genetic Disorder Microhydranencephaly Maps to Chromosome 16p13.3-12.1", *American Journal of Human Genetics*, Vol. 66, No. 5, pp. 1705-1709.

Kawasoe, T., Y. Furukawa, Y. Daigo, T. Nishiwaki, H. Ishiguro, M. Fujita, S. Satoh, N. Miwa, Y. Nagasawa, Y. Miyoshi, M. Ogawa and Y. Nakamura, 2000, "Isolation and Characterization of a Novel Human Gene, *DRCTNNB1A*, the Expression of which is Down-Regulated by Beta-Catenin", *Cancer Research*, Vol. 60, No. 13, pp. 3354-3358, July.

Kaye, E. M., 2001, "Update on Genetic Disorders Affecting White Matter", *Pediatric Neurology*, Vol. 24, No. 1, pp. 11-24, January.

Khateeb, S., H. Flusser, R. Ofir, I. Shelef, G. Narkis, G. Vardi, Z. Shorer, R. Levy, A. Galil, K. Elbedour and O. S. Birk, "*PLA2G6* Mutation Underlies Infantile Neuroaxonal Dystrophy", *American Journal of Human Genetics*, Vol. 79, No. 5, pp. 942-948, November.

Kikuchi A, H. Yamamoto and S. Kishida, 2007, "Multiplicity of the interactions of Wnt proteins and their receptors", Cell Signal., Vol. 19, No. 4, pp. 659-671, April.

Knight, S. J. L., R. Regan, A. Nicod, S. W. Horsley, L. Kearney, T. Homfray, R. M. Winter, P. Bolton and J. Flint, 1999, "Subtle Chromosomal Rearrangements in Children with Unexplained Mental Retardation", *Lancet*, Vol. 354, No. 9191, pp. 1676-1681, November.

Koenekoop, R. K., G. A. Fishman, A. Iannaccone, H. Ezzeldin, M. L. Ciccarelli, A. Baldi, J. S. Sunness, A. J. Lotery, M. M. Jablonski, S. J. Pittler and I. Maumenee, 2002, "Electroretinographic Abnormalities in Parents of Patients with Leber Congenital Amaurosis who Have Heterozygous *GUCY2D* Mutations", *Archives of Ophthalmology*, Vol. 120, No. 10, pp. 1325-1330, October.

Koenekoop, R. K., 2004, "An Overview of Leber Congenital Amaurosis: A Model to Understand Human Retinal Development", *Survey of Ophthalmology*, Vol. 49, No. 4, pp. 379-398, July.

Lander, E. S. and D. Botstein, 1987, "Homozygosity Mapping: A Way to Map Human Recessive Traits with the DNA of Inbred Children", *Science*, Vol. 236, No. 4808, pp. 1567-1570, June.

Li, M., C. Li and W. Guan, 2008, "Evaluation of Coverage Variation of SNP Chips for Genome-Wide Association", *European Journal of Human Genetics*, Vol. 16, No. 5, pp. 635-643, May.

Liu, Y., A. E. Ruoho, V. D. Rao and J. H. Hurley, "Catalytic Mechanism of the Adenylyl and Guanylyl Cyclases: Modeling and Mutational Analysis", *Proceedings of the National Academy of Sciences of the United States of America*, Vol. 94, No. 25, pp. 13414-13419, December.

Lorson, C. L., E. Hahnen, E. J. Androphy and B. Wirth, 1999, "A Single Nucleotide in the *SMN* Gene Regulates Splicing and is Responsible for Spinal Muscular Atrophy", *Proceedings of the National Academy of Sciences of the United States of America*, Vol. 96, No. 11, pp. 6307-6311, May.

Manouvrier-Hanu, S., M. Holder-Espinasse and S. Lyonnet, 1999, "Genetics of Limb Anomalies in Humans", *Trends in Genetics*, Vol. 15, No. 10, pp. 409-417, October.

Mikels, A. J. and R. Nusse, 2006, "Purified Wnt5a Protein Activates or Inhibits Beta-Catenin-TCF Signaling Depending on Receptor Context", *The Public Library of Science Biology*, Vol. 4, No. 4, pp. 115, April.

Miller, J. R., A. M. Hocking, J. D. Brown and R. T. Moon, 1999, "Mechanism and Function of Signal Transduction by the Wnt/Beta-Catenin and Wnt/Ca^{2+} Pathways", *Oncogene*, Vol. 18, No. 55, pp. 7860-7872, December.

Molinari, F., M. Rip, V. Meskenaite, F. Encha-Razavi, J. Auge, D. Bacq, S. Briault, M. Vekemans, A. Munnich, T. Attie-Bitach, P. Sonderegger and L. Colleaux, 2002, "Truncating Neurotrypsin Mutation in Autosomal Recessive Nonsyndromic Mental Retardation", *Science*, Vol. 289, No. 5599, pp. 1779-1781, November.

Moore, A. T., 1992, "Cone and Cone-Rod Dystrophies", *Journal of Medical Genetics*, Vol. 29, No. 5, pp. 289-290, May.

Morton, N. E., 1955, "Sequential Tests for the Detection of Linkage", *American Journal of Human Genetics*, Vol. 7, No. 3, pp. 277-318, September.

Motazacker, M. M., B. R. Rost, T. Hucho, M. Garshasbi, K. Kahrizi, R. Ullmann, S. S. Abedini , S. E. Nieh, S. H. Amini, C. Goswami, A. Tzschach, L. R. Jensen, D. Schmitz, H. H. Ropers, H. Najmabadi and A. W. Kuss, 2007, "A Defect in the Ionotropic Glutamate Receptor 6 Gene (*GRIK2*) is Associated with Autosomal Recessive Mental Retardation", *American Journal of Human Genetics*, Vol. 81, No. 4, pp. 792-798, October.

Nadeau, J. H., 2003, "Modifier Genes and Protective Alleles in Humans and Mice", *Current Opinion in Genetics and Development*, Vol. 13, No. 3, pp. 290-295, June.

Najmabadi, H., M. M. Motazacker, M. Garshasbi, K. Kahrizi, A. Tzschach, W. Chen, F. Behjati, V. Hadavi, S. E. Nieh, S. S. Abedini, R. Vazifehmand, S. G. Firouzabadi, P. Jamali, M. Falah, S. M. Seifati, A. Grüters, S. Lenzner, L. R. Jensen, F. Rüschendorf, A. W. Kuss and H. H. Ropers, 2007, "Homozygosity Mapping in Consanguineous Families Reveals Extreme Heterogeneity of Non-Syndromic Autosomal Recessive Mental Retardation and Identifies 8 Novel Gene Loci", *Human Genetics*, Vol. 121, No. 1, pp. 43-48, March.

Naveed, M., S. K. Nath, M. Gaines, M. T. Al-Ali, N. Al-Khaja, D. Hutchings, J. Golla, S. Deutsch, A. Bottani, S. E. Antonarakis, U. Ratnamala and U. Radhakrishna, 2007, "Genomewide Linkage Scan For Split-Hand/Foot Malformation with Long-Bone Deficiency in a Large Arab Family Identifies Two Novel Susceptibility Loci on

Chromosomes 1q42.2-q43 and 6q14.1", *American Journal of Human Genetics*, Vol. 80, No. 1, pp. 105-111, January.

Niemann, S., C. Zhao, F. Pascu, U. Stahl, U. Aulepp, L. Niswander, J. L. Weber and U. Müller, 2004, "Homozygous *WNT3* Mutation Causes Tetra-Amelia in A Large Consanguineous Family", *American Journal of Human Genetics*, Vol. 74, No. 3, pp. 558-563, March.

Niswander, L., 2003, "Pattern Formation: Old Models out on a Limb", *Nature Reviews Genetics*, Vol. 4, No. 2, pp. 133-43, February.

Oprea, G. E, S. Kröber, M. L. McWhorter, W. Rossoll, S. Müller, M. Krawczak, G. J. Bassell, C. E. Beattie and B. Wirth, 2008, "Plastin 3 is a Protective Modifier of Autosomal Recessive Spinal Muscular Atrophy", *Science*, Vol. 320, No. 5875, pp. 524-527, April.

Perrault, I., J. M. Rozet, S. Gerber, I. Ghazi, D. Ducroq, E. Souied, C. Leowski C, M. Bonnemaison, J. L. Dufier, A. Munnich and J. Kaplan, 2000, "Spectrum of retGC1 Mutations in Leber's Congenital Amaurosis", *European Journal of Human Genetics*, Vol. 8, No. 8, pp. 578-582, August.

Risch, N., 1992, "Genetic Linkage: Interpreting Lod Scores", *Science*, Vol. 255, No. 5046, pp. 803-804, February.

Roscioli, T., P. J. Taylor, A. Bohlken, J. A. Donald, J. Masel, I. A. Glass and M. F. Buckley, 2004, "The 10q24-linked Split Hand/Split Foot Syndrome (SHFM3): Narrowing of the Critical Region and Confirmation of the Clinical Phenotype", *American Journal of Medical Genetics Part A*, Vol. 124, No. 2, pp. 136-141, January.

Rose, R. A. and W. R. Giles, 2008, "Natriuretic Peptide C Receptor Signaling in the Heart and Vasculature", *Journal of Physiololgy*, Vol. 586, No. 2, pp. 353-366, January.

Ross, S. E, N. Hemati, K. A. Longo, C. N. Bennett, P. C. Lucas, R. L. Erickson and O. A. MacDougald, 2000, "Inhibition of Adipogenesis by Wnt Signaling", *Science*, Vol. 289, No. 5481, pp. 950-953, August.

Rozet, J. M., I. Perrault, S. Gerber, S. Hanein, F. Barbet, D. Ducroq, E. Souied, A. Munnich and J. Kaplan, 2001, "Complete Abolition of the Retinal-Specific Guanylyl Cyclase (retGC-1) Catalytic Ability Consistently Leads to Leber Congenital Amaurosis (LCA)", *Investigative Ophthalmology and Visual Science*, Vol. 42, No. 6, pp. 1190-1192, May.

Rüschendorf, F. and P. Nürnberg, 2005, "ALOHOMORA: A Tool for Linkage Analysis Using 10K SNP Array Data", *Bioinformatics*, Vol. 21, No. 9, pp. 2123-2125, May.

Scherer, S. W., P. Poorkaj, T. Allen, J. Kim, D. Geshuri, M. Nunes, S. Soder, K. Stephens, R. A. Pagon and M. A. Patton, 1994, "Fine Mapping of the Autosomal Dominant Split Hand/Split Foot Locus on Chromosome 7, Band q21.3-q22.1", *American Journal of Human Genetics,* Vol. 55, No. 1, pp. 12-20, July.

Schiffmann, R. and M. S. van der Knaap, 2004, "The Latest on Leukodystrophies", *Current Opinion in Neurology*, Vol. 17, No. 2, pp. 187-192, April.

Sidow, A., M. S. Bulotsky, A. W. Kerrebrock, B. W. Birren, D. Altshuler, R. Jaenisch, K. R. Johnson and E. S. Lander, 1999, "A Novel Member of the F-box/WD 40 Gene Family, Encoding Dactylin, is Disrupted in the Mouse Dactylaplasia Mutant", *Nature Genetics*, Vol. 23, No. 1, pp. 104-107, September.

Small, K. W., R. Silva-Garcia, N. Udar, E. V. Nguyen and J. R. Heckenlively, 2008, "New Mutation, P575L, in the *GUCY2D* Gene in a Family with Autosomal Dominant Progressive Cone Degeneration", *Archives of Ophthalmology*, Vol. 126, No. 3, pp. 397-403, March.

Stumpf, E., H. Masson, A. Duquette, F. Berthelet, J. McNabb, A. Lortie, J. Lesage, J. Montplaisir, B. Brais and P. Cossette, 2003, "Adult Alexander Disease with

Autosomal Dominant Transmission: A Distinct Entity Caused by Mutation in the Glial Fibrillary Acid Protein Gene", *Archives of Neurology*, Vol. 60, No. 9, pp. 1307-1312, September.

Terwilliger, J. D. and J. Ott, 1994, *Handbook of Human Genetic Linkage*, Johns Hopkins University, Baltimore.

Thompson, D. K. and D. L. Garbers, 1995, "Dominant Negative Mutations of the Guanylyl Cyclase-A Receptor. Extracellular Domain Deletion and Catalytic Domain Point Mutations", *The Journal of Biological Chemistry*, Vol. 270, No. 1, pp. 425-430, January.

Tickle, C., 2006, "Making Digit Patterns in the Vertebrate Limb", *Nature Reviews Molecular Cell Biology*, Vol. 7, No. 1, pp. 45-53, January.

Toniolo, D. and P. D'Adamo, 2000, "X-Linked Nonspecific Mental Retardation", *Current Opinion in Genetics and Development*, Vol. 10, No. 3, pp. 280-285, June.

Toydemir, R. M., A. Rutherford, F. G. Whitby, L. B. Jorde, J. C. Carey and M. J. Bamshad, 2006, "Mutations in Embryonic Myosin Heavy Chain (MYH3) Cause Freeman-Sheldon Syndrome and Sheldon-Hall Syndrome", *Nature Genetics*, Vol. 38, No. 5, pp. 561-565, May.

Tucker, C. L., V. Ramamurthy, A. L. Pina, M. Loyer, S. Dharmaraj, Y. Li, I. H. Maumenee, J. B. Hurley and R. K. Koenekoop, 2004, "Functional Analyses of Mutant Recessive *GUCY2D* Alleles Identified in Leber Congenital Amaurosis Patients: Protein Domain Comparisons and Dominant Negative Effects", *Molecular Vision*, Vol. 20, No. 10, pp. 297-303, April.

Ugur, S. A. and A. Tolun, 2008a, "Homozygous *WNT10b* Mutation and Complex Inheritance in Split Hand Foot Malformation", *Human Molecular Genetics*, doi: 10.1093/hmg/ddn164, May (electronic publication).

Ugur, S. A. and A. Tolun, 2008b, "A Deletion in *DRCTNNB1A* Associated with Hypomyelination and Juvenile Onset Cataract", *European Journal of Human Genetics*, Vol. 16, No. 2, pp. 261-264, October.

Van Bokhoven, H., B. C. Hamel, M. Bamshad, E. Sangiorgi, F. Gurrieri, P. H. Duijf, K. R. Vanmolkot, E. van Beusekom, S. E. van Beersum, J. Celli, G. F. Merkx, R. Tenconi, J. P. Fryns, A. Verloes, R. A. Newbury-Ecob, A. Raas-Rotschild, F. Majewski, F. A. Beemer, A. Janecke, D. Chitayat, G. Crisponi, H. Kayserili, J. R. Yates, G. Neri and H. G. Brunner, 2001, "p63 Gene Mutations in EEC Syndrome, Limb-Mammary Syndrome, and Isolated Split Hand-Split Foot Malformation Suggest a Genotype-Phenotype Correlation", *American Journal of Human Genetics*, Vol. 69, No. 3, pp 481-492, July.

Wang, J. and G. M. Shackleford, 1996, "Murine Wnt10a and Wnt10b: Cloning and Expression in Developing Limbs, Face and Skin of Embryos and in Adults", *Oncogene*, Vol. 13, No. 7, pp. 1537-1544, October.

Weatherbee, S. D., R. R. Behringer, J. J. Rasweiler and L. A. Niswander, 2006, "Interdigital Webbing Retention in Bat Wings Illustrates Genetic Changes Underlying Amniote Limb Diversification", *Proceedings of the National Academy of Sciences of the United States of America*, Vol. 103, pp. 15103-15107, October.

Weber, J. L. and K. W. Broman, 2001, "Genotyping for Human Whole-Genome Scans: Past, Present, and Future", *Advances in Genetics*, Vol. 42, No. 1, pp. 77-96.

Westendorf, J. J., R. A. Kahler and T. M. Schroeder, 2004, "Wnt Signaling in Osteoblasts and Bone Diseases", *Gene*, Vol. 341, pp. 19-39, October.

Willert, K., J. D. Brown, E. Danenberg, A. W. Duncan, I. L. Weissman, T. Reya, J. R. Yates and R. Nusse, 2003, "Wnt Proteins Are Lipid-Modified and can Act as Stem Cell Growth Factors", *Nature*, Vol. 423, No. 6938, pp. 448-452, May.

Woods, C. G., S. Stricker, P. Seemann, R. Stern, J. Cox, E. Sherridan, E. Roberts, K. Springell, S. Scott, G. Karbani, S. M. Sharif, C. Toomes, J. Bond, D. Kumar, L. Al-Gazali and S. Mundlos, 2007, "Mutations in *WNT7A* Cause a Range of Limb Malformations, Including Fuhrmann Syndrome and Al-Awadi/Raas-Rothschild/Schinzel Phocomelia Syndrome", *American Journal of Human Genetics*, Vol. 79, No. 2, pp. 402-408, August.

Yang, A., M. Kaghad, Y. Wang, E. Gillett, M. D. Fleming, V. Dötsch, N. C. Andrews, D. Caput and F. McKeon, 1998, "p63, a p53 Homolog at 3q27-29, Encodes Multiple Products with Transactivating, Death-Inducing, and Dominant-Negative Activities", *Molecular Cell*, Vol. 2, No. 3, pp. 305-16, September.

Yang, A., R. Schweitzer, D. Sun, M. Kaghad, N. Walker, R. T. Bronson, C. Tabin, A. Sharpe, D. Caput, C. Crum and F. McKeon, 1999, "p63 is Essential for Regenerative Proliferation in Limb, Craniofacial and Epithelial Development", *Nature*, Vol. 398, No. 6729, pp. 714-718, April.

Yang, R. B., D. C. Foster, D. L. Garbers and H. J. Fülle, 1995, "Two Membrane Forms of Guanylyl Cyclase Found in the Eye", *Proceedings of the National Academy of Sciences of the United States of America*, Vol. 92, No. 2, pp. 602-606, January.

Yang, R. B. and D. L. Garbers, 1997, "Two Eye Guanylyl Cyclases are Expressed in the same Photoreceptor Cells and Form Homomers in Preference to Heteromers", *The Journal of Biological Chemistry*, Vol. 23, No. 21, pp. 13738-41472, May.

Yang, X. R., K. Jacobs, K. F. Kerstann, A. W. Bergen, A. M. Goldstein and L. R. Goldin, 2006, "Linkage Analysis of the GAW14 Simulated Dataset with Microsatellite and Single-Nucleotide Polymorphism Markers in Large Pedigrees", *BioMed Central Genetics*, Vol. 6, No. 1, pp. 1-5, December.

Yang, Y., 2003, "Wnts and Wing: Wnt Signaling in Vertebrate Limb Development and Musculoskeletal Morphogenesis", *Birth Defects Research Part C Embryo Today*, Vol. 69, No. 4, pp. 305-317, November.

Yasue, A., H. Tao, T. Nohno, K. Moriyama, S. Noji and H. Ohuchi, 2001, "Cloning and Expression of the Chick p63 Gene", *Mechanisms of Development*, Vol. 100, No. 1, pp. 105-108, January.

Zara, F., R. Biancheri, C. Bruno, L. Bordo, S. Assereto, E. Gazzerro, F. Sotgia, X. B. Wang, S. Gianotti, S. Stringara, M. Pedemonte, G. Uziel, A. Rossi, A. Schenone, P. Tortori-Donati, M. S. van der Knaap, M. P. Lisanti and C. Minetti, 2006, "Deficiency of Hyccin, a Newly Defined Membrane Protein, Causes Hypomyelination and Congenital Cataract", *Nature Genetics*, Vol. 38, No. 10, pp. 1111-1113, October.

Zernant, J., M. Külm, S. Dharmaraj, A. I. den Hollander, I. Perrault, M. N. Preising, B. Lorenz, J. Kaplan, F. P. Cremers, I. Maumenee, R. K. Koenekoop and R. Allikmets, "Genotyping Microarray (Disease Chip) for Leber Congenital Amaurosis: Detection of Modifier Alleles", *Investigative Ophthalmology and Visual Science*, Vol. 46, No. 9, pp. 3052-3059, September.

Zhang, G., Y. Liu, J. Qin, B. Vo, W. J. Tang, A. E. Ruoho and J. H. Hurley, 1997, "Characterization and Crystallization of a Minimal Catalytic Core Domain From Mammalian Type II Adenylyl Cyclase", *Protein Science*, Vol. 6, No. 4, pp. 903-908, April.

Zhang, Z. F., C. Ruivenkamp, J. Staaf, H. Zhu, M. Barbaro, D. Petillo, S. K. Khoo, A. Borg, Y. S. Fan and J. Schoumans, 2008, "Detection of Submicroscopic Constitutional Chromosome Aberrations in Clinical Diagnostics: A Validation of the Practical Performance of Different Array Platforms", *European Journal of Human Genetics*, doi: 10.1038/ejhg.2008.14, February (electronic publication).

Zlotogora, J. and N. Nubani, 1989, "Is There an Autosomal Recessive Form of the Split Hand and Split Foot Malformation?" *Journal of Medical Genetics*, Vol. 26, No. 2, pp. 138-140, February.

Zou, H. and L. Niswander, 1996, “Requirement for BMP Signaling in Interdigital Apoptosis and Scale Formation”, *Science*, Vol. 272, No. 5262, pp. 738-741, May.